Effective Hamiltonians for Undoped and Hole-Doped Antiferromagnetic Spin-$\frac{1}{2}$ Ladders by Self-Similar Continuous Unitary Transformations in Real Space

Dissertation

vorgelegt von

Sebastian Duffe

angefertigt am

Lehrstuhl Theoretische Physik I

der Fakultät Physik

der Technischen Universität Dortmund

Juni 2010

Contents

1 Introduction

The theory of strongly correlated electrons is of great importance for solid state physics or in general condensed matter physics. For instance, conductivity and magnetic properties are strongly influenced by electronic correlations. Materials with strongly correlated electrons exhibit many interesting phenomena that can only be understood in consideration of quantum physics. The usual approach is to reduce the exhaustive many-body problems with a multitude of interactions to simple paradigmatic models that include the decisive physical properties.

One of the most challenging issues in modern solid state physics is the search for an appropriate theoretical description for high-temperature superconductivity. While conventional low-temperature superconductivity is well-understood and very accurately described on the microscopic level by the BCS theory [1], the mechanisms behind the superconductivity based on cuprate or iron pnictide compounds are subjects of ongoing research. The critical temperature T_c for cuprate superconductors (first discovered by Bednorz and Müller in 1986 [2]) is up to 138 K [3] and hence relevant for technical applications. The understanding of the underlying processes could also help finding materials with even higher T_c.

The crucial point for conventional superconductivity is the phonon mediated combination of two electrons to a Cooper pair with integer spin as described by the BCS theory. The bosonic Cooper pairs can form a collective quantum state which is responsible for the effects of superconductivity. In essence these are: (i) a current flow without resistance and (ii) the Meissner-Ochsenfeld effect. The current approaches to a theory for high-T_c superconductivity in cuprate compounds assume similar conditions. Fermionic charge carriers, which can be either holes or electrons depending on the material and doping, are supposed to be combined into pairs via attractive interactions. However, these interactions are likely not to be due to a barely phononic mediation [4].

A model system consisting of spins that interact magnetically with positive coupling constants and mobile charge carriers is called a doped antiferromagnet.

Its theoretical description is achieved by the so called t-J-model[1] [5, 6]. From a strong coupling perspective such a model in 2D is expected to incorporate the essential features of the high-T_c superconductors based on cuprates. This model captures the main effect because the superconduction takes place in two-dimensional cuprate layers separated from each other by the other constituents of the compound. The coupling between the cuprate planes is so weak that it can be neglected [7].

The schematic phase diagram for a typical hole-doped high-T_c cuprate superconductor in dependence on the temperature T and the hole concentration δ is shown in Figure 1.1. There is a phase characterised by a long-range commensurate antiferromagnetic order (AF), which occurs for small δ. The superconducting phase (SC) can be found at low T in the region $0.05 \lesssim \delta \lesssim 0.25$. It is also called "superconducting dome" because of its form in the phase diagram. Optimal doping is achieved when T_c becomes maximal. In the regime between antiferromagnet and superconductor various forms of disordered and incommensurate magnetism occur. The remaining regimes, which are not separated by phase transitions but by crossovers, are in the order of increasing δ: The pseudogap regime (PG), the non-Fermi liquid regime (NFL) and the Fermi liquid regime (FL).

Different theories have been developed as possible descriptions for high-T_c cuprate superconductivity: The resonating valence bond state and spin-charge separation respectively [4, 8, 9], stripe-like inhomogeneous spin and charge ordering [7, 10–13] and quantum criticality [14, 15] are the most important concepts. Certainly magnetic fluctuations and their interactions with the charge carriers play a key role.

In this thesis a quasi one-dimensional model system for cuprate superconductors is considered, which is the antiferromagnetic two-leg spin-$\frac{1}{2}$ ladder (discussed in Chapters 4 and 5). The assumed importance of the antiferromagnetic spin interaction within the cuprate layers for the attraction of the electrons or holes respectively is expected also to be featured by the spin ladder as an analogous one-dimensional effect. We expect that magnetic excitations, which are dominated by a local triplet state on a rung of the ladder, mediate an attractive interaction between the hole excitations.

The spin ladder model is not a purely theoretical toy model, the system is realised in the so called telephone number compounds (see Section 1.1). For these systems superconductivity can be detected under high pressure [16]. CaV_2O_5

[1] t denotes the hopping constant for the charge carriers and J the magnetic coupling constant.

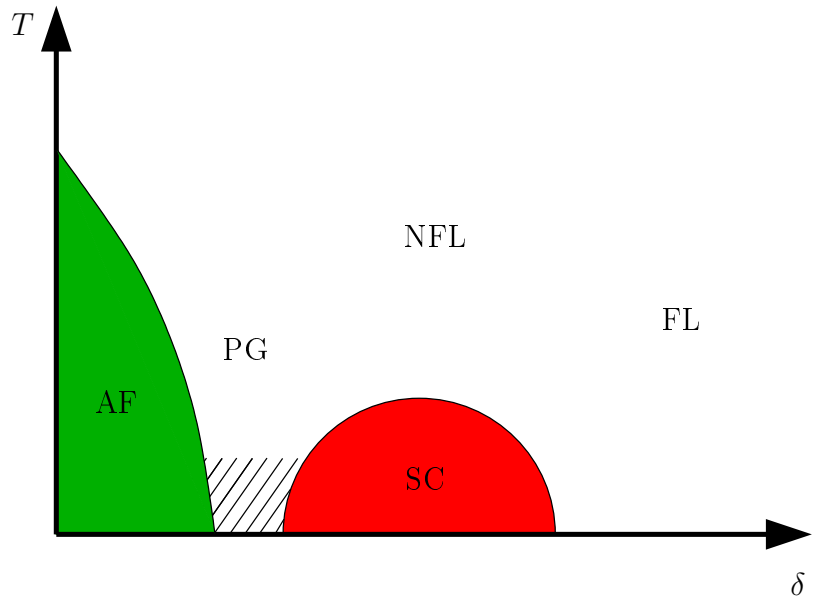

Figure 1.1: Schematic phase diagram for a typical hole-doped high-T_c cuprate superconductor [7]: The parameters are the temperature T and the hole concentration δ. The true phases are the long-range commensurate antiferromagnetic order AF and the superconducting phase SC. The pseudogap regime PG, the non-Fermi liquid regime NFL and the Fermi liquid regime FL are not strictly separated. In the shaded area various forms of disordered and incommensurate magnetism occur.

[17] and $SrCu_2O_3$ [16, 18] are further systems in which spin ladders can be found. Within the isolating regime the spin ladder is very well understood. The behaviour of magnetic excitations in spin ladders already examined in Ref. [19] is resumed in Chapter 4 and augmented by additional results. The ladder is effectively treated as a one-dimensional chain with sites populated by hardcore bosons. These particles obey a specific algebra (see Section 2.4).

The subject of Chapter 5 are hole-doped ladders, i.e. an extension of the model by insertion of charge carriers in the form of holes. The challenge of this extension consists in the combined appearance of fermionic and bosonic particles with hardcore properties. The concerning algebra is also discussed in Section 2.4. Including both algebras in the calculations at the same time is a rather demanding task. Furthermore the Hamiltonian contains a multitude of terms.

Our method of choice to derive effective Hamiltonians for the considered models

is the continuous unitary transformation (CUT). The CUT technique is introduced in Chapter 2. The general issue of diagonalising a Hamiltonian (or at least to achieve a form that is closer to diagonality) can be performed with this technique introduced by Wegner [20] as well as independently by Wilson and Głazek [21, 22]. Instead of applying only one single constant unitary transformation that diagonalises the Hamiltonian at once or several constant unitary transformations successively, a unitary transformation depending on a continuous parameter is applied to the Hamiltonian. This transformation adjusts itself permanently during its application. Discrete transformations must be known explicitly before we can apply them, whereas for the continuous transformation it is sufficient to set up the infinitesimal generator of the transformation. The choice of this generator determines which properties the transform exhibits and in which way the sorting of the eigenvalues is carried out. The generators used for the calculations in this thesis are based on the ideas of Mielke [23] as well as Knetter and Uhrig [24, 25], who designed a generator that induces an effective model that preserves the number of excitations (or quasiparticles respectively) and enables an easy classification of the resulting eigenenergies concerning this number. We do not only use this generator in its original form but also modifications introduced in Ref. [26]. These modifications enable the treatment of new parameter regimes, for which the original generator is not applicable.

The CUT can be performed in either a perturbative (PCUT) or a self-similar (SCUT) fashion. Both ways are discussed and compared. In this thesis the SCUT is applied to the spin ladder Hamiltonians and compared to established PCUT results [27] if available. Because infinite systems are considered, an adequate truncation has to be implemented. The chosen truncation scheme only restricts the operators and not the states of the system to which they are applied. Because the spin ladder is a gapful system, the correlation between the quasiparticles decreases exponentially depending on the real space distance. Hence a real space truncation is considered as the most suitable way of truncation.

Chapter 3 deals with the implementation of the SCUT on a computer. Readers interested in the technical aspects of the method will find a detailed description of the program and data structure within this chapter.

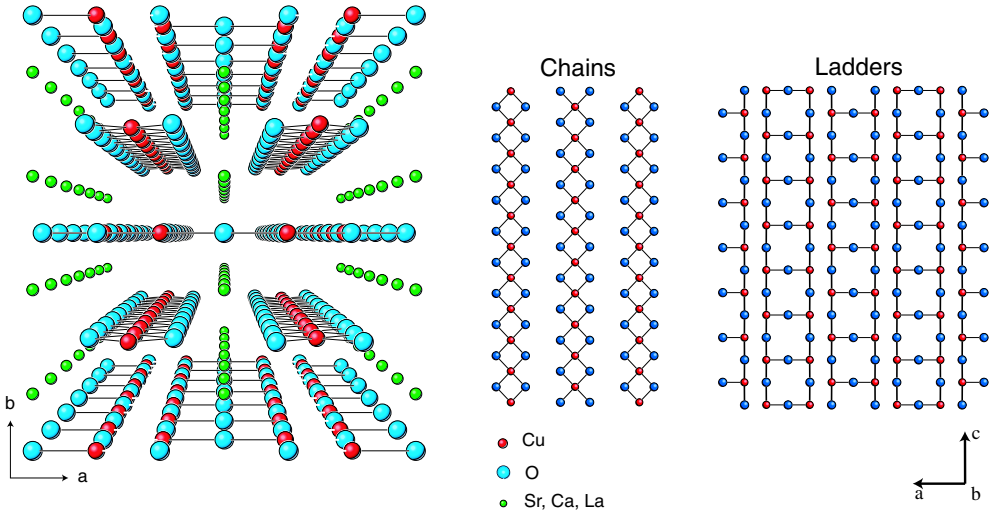

Figure 1.2: Schematic view of $(\mathrm{Sr,La,Ca,Y})_{14}\mathrm{Cu}_{24}\mathrm{O}_{41}$ taken from [28]. The coupling is illustrated by black lines. Left: A 3D view of the structure. Middle: A cuprate layer consisting of chains. Right: A cuprate layer consisting of ladders.

1.1 Telephone Number Compounds

The composite crystals $(\mathrm{Sr,La,Ca,Y})_{14}\mathrm{Cu}_{24}\mathrm{O}_{41}$ called telephone number compounds (a detailed survey of these interesting materials is given in Ref. [29]) are composed of cuprate layers alternated with (Sr, La, Ca, Y) layers. There are two kinds of cuprate layers: layers with CuO_2 chains and layers with $\mathrm{Cu}_2\mathrm{O}_3$ ladders (each aligned along the crystallographic c axis) (cf. Figure 1.2), which also alternate. The latter are of great interest in current research because the cuprate ladder can be considered as a model system for the 2D high-T_c superconducting cuprate square lattice.

The spin sites are the $3d_{x^2-y^2}$ orbitals of the copper atoms coupled via the $2p_x$ or $2p_y$ orbitals of the oxygen atoms, which hybridise with the copper $3d_{x^2-y^2}$ orbitals so that superexchange [30] is possible (see Figure 1.3). Interactions between the ladders are weak because they result from 90° exchange [31, 32]. Thus the ladders can be considered as isolated from each other. Even if the interladder coupling is taken into account, the strong frustration of the lattice causes the system to be effectively one-dimensional [33]. The dispersions of the magnetic excitations of the complete layer with interladder coupling are similar to those of a single spin

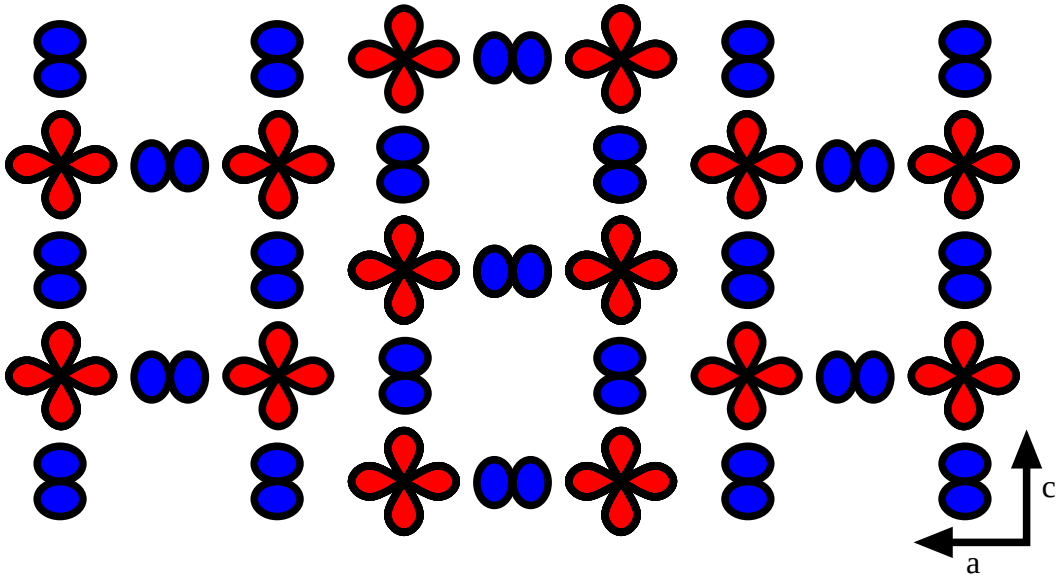

Figure 1.3: Schematic view of the Cu $3d_{x^2-y^2}$ (red) and O $2p_\sigma$ (blue) orbitals within the ladder layers of the telephone number compounds.

ladder. Important properties of the ladders are investigated in Refs. [34–38].

Typically the telephone number compounds are insulators with a temperature dependent DC conductivity, but by increasing the doping level of Ca a metal-insulator transition occurs [39]. The charge carrier density can be adjusted by doping. Under high pressure the crystal becomes a superconductor for appropriate doping [16].

$Sr_{14}Cu_{24}O_{41}$ exhibits an intrinsic doping of six holes per unit cell. Only 0.8 of these holes per unit cell are allotted to the ladders; the remaining 5.2 holes are found in the chains [40] because the chains possess a higher electronegativity [41]. $La_6Ca_8Cu_{24}O_{41}$ features undoped ladders [32] and the ladders in $La_{5.2}Ca_{8.8}Cu_{24}O_{41}$, which are only slightly doped, can be considered as approximately undoped [42].

In this thesis the isolated spin ladder is investigated. Chapter 4 is concerned with the undoped ladder, which will be treated as a half-filled spin-$\frac{1}{2}$ model without electron hopping. So just magnetic interactions are present. In Chapter 5 the hole-doped ladder is examined. The according model includes electron hopping additionally to the magnetic interactions. Double occupancy is forbidden, i.e. electrons do not occur as charge carriers but only holes. This can be justified by the fact that the onsite Coulomb repulsion between the electrons is large.

2 Continuous Unitary Transformations

The diagonalisation of Hamiltonians is a central issue in theoretical quantum physics. The technique of continuous unitary transformations (CUT) also referred to as flow equation method and introduced by Wegner [20] as well as by Wilson and Głazek [21, 22] offers a general approach to diagonalise operators or at least to achieve a form which is closer to diagonality. The basic idea of the CUT is to implement a method that adjusts itself during the procedure of the diagonalisation depending on the current form of the Hamiltonian at this point of the continuous transformation: The change of the Hamiltonian induced by the transformation is determined by the current magnitude of the non-diagonal elements.

A unitary transformation U dependent on the continuous parameter l is applied to the operator H_0 that is to be diagonalised:

$$H(l) = U(l)H_0U^\dagger(l) \tag{2.1}$$

where $U(0) = \mathbb{1}$.

Due to the unitarity of the transformation the eigenvalues of every $H(l)$ are the same as the ones for H_0. The antihermitian[1] generator η of the transformation U is defined by

$$\eta(l) = \frac{\partial U(l)}{\partial l}U^\dagger(l) \tag{2.2}$$

so that the derivative of H with respect to l is given by the so-called flow equation

$$\frac{\partial H(l)}{\partial l} = [\eta(l), H(l)] \ . \tag{2.3}$$

This is actually a system of differential equations (generically highly coupled) for the coefficients of the operators appearing in H. Other operators A that are to

[1] The generator η must be antihermitian to ensure that U is unitary.

be considered (e.g. observables) are subjected to the same transformation as all operators have to be transformed in the same manner – like for every change of basis. For A the general flow equation

$$\frac{\partial A(l)}{\partial l} = [\eta(l), A(l)] \tag{2.4}$$

holds true.

Inserting H_0 into the flow equation (2.3) generally yields new kinds of contributions for H that were not part of the original H_0. Applying the flow equation for these resulting terms yields again new terms and so on. For an infinite system one usually obtains an infinite number of terms and for sizable finite systems an exponentially large number of differential equations. Thus a truncation is required that neglects contributions that do not affect the main physical effects of a Hamiltonian H to reach a manageable number of differential equations.

The choice of $\eta(l)$ determines the transformation $U(l)$ and therefore the form of $H(l)$. Formally the transformation can be expressed by

$$U(l) = \mathcal{L} e^{\int_0^l \eta(l')\mathrm{d}l'} \tag{2.5}$$

where $\mathcal{L}$ denotes the l-ordering operator, which orders the following expression from right to left according to increasing values of l. In general it is complicated to determine the explicit $U(l)$ due to the complexity arising from the application of $\mathcal{L}$. Usually the flow equation (2.3) is integrated numerically to calculate H for a certain value of l.

The original generator, which was introduced by Wegner [20], is defined by the commutator of the diagonal and the non-diagonal part of H

$$\eta_{\text{Wegner}}(l) = [H_{\text{diagonal}}(l), H_{\text{non-diagonal}}(l)]\,. \tag{2.6}$$

The intention of this choice is that for the effective Hamiltonian, i.e. for $l \to \infty$, the non-diagonal part $H_{\text{non-diagonal}}$ vanishes. The definition of H_{diagonal} is arbitrary and depends on the choice of the basis. Therefore H_{diagonal} can be defined as a structure that can be treated easily. However, if subspaces of H_{diagonal} are degenerate, they remain non-diagonal.

The disadvantage of the Wegner generator is that if H_0 can be written in the form of a band matrix, this feature is usually lost during the transformation for finite l and eigenvalues cannot necessarily be assigned to a concrete number of excitations (respectively particles) without further investigation.

The generator of our choice is the so-called pc (particle conserving) generator [23–25]

$$\eta_{\mathrm{pc},i,j}(l) = \mathrm{sign}(q_i - q_j) H_{i,j}(l) \tag{2.7}$$

defined in the eigenbasis of the operator Q counting the particle number. The indices i, j denote a transition from state j to state i and q_i is the eigenvalue of Q (i.e. the number of particles) for the state i. Inserting the pc generator into the flow equation (2.3) yields

$$\begin{aligned} \frac{\partial H_{i,j}(l)}{\partial l} = \quad & -\mathrm{sign}(q_i - q_j)(H_{i,i}(l) - H_{j,j}(l)) H_{i,j}(l) \\ & + \sum_{k \neq i,j} \left(\mathrm{sign}(q_i - q_k) + \mathrm{sign}(q_j - q_k)\right) H_{i,k}(l) H_{k,j}(l)\,. \end{aligned} \tag{2.8}$$

The eigenstates of Q can be ordered so that $q_k \geq q_i$ for $k > i$ without loss of generality. For the derivative of the sum over the first r diagonal elements of $H(l)$

$$\frac{\partial}{\partial l} \sum_{i=1}^{r} H_{i,i}(l) = 2 \sum_{i=1}^{r} \sum_{k>r} \mathrm{sign}(q_i - q_k) |H_{i,k}(l)|^2 \leq 0 \tag{2.9}$$

holds true due to $q_k \geq q_i$. Therefore the sum $\sum_{i=1}^{r} H_{i,i}(l)$ is monotonically decreasing. Because a Hamiltonian is usually bounded from below, this sum converges for $l \to \infty$ and

$$\lim_{l \to \infty} \frac{\partial}{\partial l} \sum_{i=1}^{r} H_{i,i}(l) = 2 \sum_{i=1}^{r} \sum_{k>r} \mathrm{sign}(q_i - q_k) |H_{i,k}(l)|^2 = 0\,. \tag{2.10}$$

Hence it follows that for $l \to \infty$ and for all i, j with $i \neq k$ either $q_i = q_k$ or $H_{i,k}(l) = 0$. The case $q_i = q_k$ is equivalent to degeneracy with respect to the particle number. Therefore all non-diagonal elements $H_{i,k}(l)$ that couple subspaces with different particle numbers tend to zero for $l \to \infty$. Thus the induced transformation results in a block-diagonal Hamiltonian conserving the particle number for $l \to \infty$, i.e. $[H(\infty), Q] = 0$. Also due to $H_{i,k}(l) \to 0$ the asymptotic behaviour for the derivative of the non-diagonal elements is dominated by the first part of Equation (2.8)

$$\frac{\partial H_{i,j}(l)}{\partial l} \approx -\mathrm{sign}(q_i - q_j)(H_{i,i}(l) - H_{j,j}(l)) H_{i,j}(l)\,. \tag{2.11}$$

Thus

$$\mathrm{sign}(q_i - q_j)(H_{i,i}(l) - H_{j,j}(l)) > 0 \tag{2.12}$$

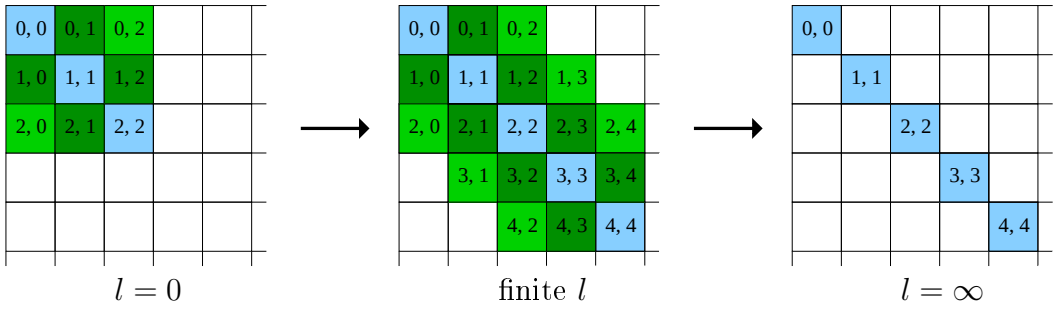

Figure 2.1: Schematic example for a transformation of $H(l)$ induced by the pc generator: Each coloured (n_c, n_a)-block represents contributions to H creating n_c particles after annihilating n_a particles.

holds for $i \neq j$ and for sufficiently large l because $H_{i,j}(l)$ tends to zero as well. This means that the transformation also sorts the eigenenergies according to the particle number if the corresponding subspaces of the Hilbertspace are coupled before the transformation, i.e. $H_{i,j}(l = 0) \neq 0$. For a detailed investigation of the asymptotic behaviour of the pc CUT see Refs. [23, 26, 43]. Note that for

$$\lim_{l \to \infty} \operatorname{sign}(q_i - q_j)(H_{i,i}(l) - H_{j,j}(l)) < 0 \tag{2.13}$$

convergence problems may occur if $H_{i,j}(l = 0) \neq 0$, i.e. an overlap of energies belonging to different particle numbers may hinder the convergence. We encounter this problem for the treatment of spin ladders (see Chapters 4 and 5). A possible remedy is a generator adaption (see Section 2.5).

An example for the structural change of $H(l)$ is depicted in Figure 2.1. In this example $H_0 = H(0)$ consists of terms affecting maximally two particles. For finite l terms affecting higher particle numbers occur. The truncation scheme has to be applied here to keep the number of terms finite for an infinite system[2]. The change of the particle number cannot be higher than in H_0. Hence the block-band structure is conserved [23, 25, 44]. For $l = \infty$ H is block-diagonal and conserves the particle number. Each block can be assigned to a concrete number of particles. Further information about the structure of the Hamiltonian and of the observables in the context of pc CUTs can be found in Ref. [44].

Note that the scheme in Figure 2.1 does not represent the form of a matrix corresponding to $H(l)$. A block in this representation contains all terms that

[2]The truncation is only applied to the operators but not to the Hilbert space.

create n_c particles after annihilating n_a particles. A (n_c, n_a)-block does not only affect states with n_a particles but also those with more than n_a particles. Therefore this representation is not identical with a matrix representation, for which the action of each block is restricted to the concerning subspace without overlaps.

If the flow equation (2.3) is numerically integrated (as usual in practice), the integration can be stopped at a certain finite l when the non-diagonal parts of H are small enough to be considered as negligible. For a comfortable handling the terms of H are expressed in second quantisation for the particles under study.

Three easily comprehensible examples for the application of CUTs are given in Ref. [45]. The differences between the pc and the Wegner generator are discussed by means of simple Hamiltonians. In particular the convergence behaviour is examined. The Wegner generator always leads to a fixed point, but degeneracies hinder the diagonalisation, whereas the pc generator is not sensitive to degeneracies, but the induced transformation does not always converge.

2.1 Perturbative CUT and Self-Similar CUT

Continuous unitary transformations can be performed in a perturbative or in a self-similar fashion. In this thesis the self-similar continuous unitary transformation (SCUT) was used exclusively. Nevertheless, this section also gives a brief description of the perturbative continuous unitary transformation (PCUT) because SCUT results were compared to PCUT results and the differences between the two approaches are an important issue. Both CUT procedures will be explained exemplarily for the pc generator (2.7). A detailed description of the PCUT with the pc generator is given in Ref. [25].

2.1.1 PCUT

For the PCUT the Hamiltonian H has to be split up into an unperturbed (particle conserving) part H_{u} and a perturbed part xV as usual in perturbation theory where x denotes the expansion parameter, which has to be small. Additionally the following conditions have to be fulfilled:

- The energy spectrum of H_{u} is equidistant with a lower boundary; the eigenenergies are proportional to the particle number.

- The perturbation term can be written as $V = \sum_{n=-N}^{N} T_n$ with $N \in \mathbb{N}$. The operator T_n changes the particle number by n.

Then $H(l)$ can be represented by the ansatz:

$$H(x,l) = H_\mathrm{u} + \sum_{k=1}^{\infty} x^k \sum_{|\underline{m}|=k} F(l,\underline{m}) T(\underline{m}). \tag{2.14}$$

$\underline{m}$ denotes a set of indices $m_i \in \{-N, -N+1, \ldots, N-1, N\}$ with $i \in \{1, 2, \ldots, k\}$ so that $T(\underline{m})$ is a product of the operators T_{m_i}. The number of components of $\underline{m}$ is denoted by $|\underline{m}|$. The coefficients $F(x,l)$ still have to be determined.

Now the chosen generator has to be depicted in the same representation. So the pc generator (2.7) reads in this representation

$$\eta(x,l) = \sum_{k=0}^{\infty} x^k \sum_{|\underline{m}|=k} \mathrm{sign}\left(M(\underline{m})\right) F(l,\underline{m}) T(\underline{m}). \tag{2.15}$$

Here $M(\underline{m}) := \sum_i m_i$ specifies the number of particles being created or annihilated by $T(\underline{m})$ in total.

Inserting H (2.14) and η (2.15) into the flow equation (2.3) yields a system of differential equations for the $F(l,\underline{m})$ via comparison of coefficients. The integration of this system for $l \to \infty$ results in the effective Hamiltonian

$$H_\mathrm{eff}(x) = H_\mathrm{u} + \sum_{k=1}^{\infty} x^k \sum_{|\underline{m}|=k} F(\infty,\underline{m}) T(\underline{m}), \tag{2.16}$$

which is particle conserving because all $F(\infty,\underline{m})$ with $M(\underline{m}) \neq 0$ are zero.

2.1.2 SCUT

For the SCUT the Hamiltonian H is represented by a sum of different operators $\hat{o}_i$ multiplied by the concerning prefactors g_i. At first a truncation scheme has to be defined that decides whether a term shall be neglected. The truncation scheme depends on the physical properties of the considered model. This is discussed in detail in Sections 2.1.3 and 2.2. The truncation scheme for the spin ladder models investigated in this thesis is discussed in Sections 4.2 and 5.2.

During the flow only the prefactors change while the operators remain constant

$$H(l) = \sum_i g_i(l) \hat{o}_i. \tag{2.17}$$

The operators serve as a fixed basis for $H(l)$. This is the reason why this fashion of CUT is called self-similar. The differential equations for the $g_i(l)$ are given via the flow equation (2.3) by performing the following steps:

1. Set up a Hamiltonian $H(l)$ with the operators $\hat{o}_i$ of the starting Hamiltonian $H(0)$ and variable prefactors $g_i(l)$.

2. Calculate the concerning pc generator $\eta(l)$ according to Equation (2.7) using the terms of $H(l)$ and insert $\eta(l)$ and $H(l)$ into the flow equation (2.3).

3. Compare the coefficients of the operators of the left and the right hand side of the flow equation (after having checked that the operator representation is unique[3]). This yields contributions that have to be added to the differential equations of the $g_i(l)$ in the form of $a_{i,j,k}g_j(l)g_k(l)$. The $a_{i,j,k}$ are prefactors depending on the result of the commutator $[\eta(l), H(l)]$. New operators $\hat{o}_i$ can emerge that do not appear in $H(l)$. The truncation scheme decides whether to keep them or not.

4. Take the new operators $\hat{o}_i$, which shall be kept, multiplied by variable prefactors $g_i(l)$ and attach them to $H(l)$.

Repeat steps 2 to 4 until no new non-negligible operators emerge. In the repetition of step 2 only new contributions to $[\eta, H]$ have to be calculated.

Then the differential equations for the $g_i(l)$ exhibit the form:

$$\frac{\partial g_i(l)}{\partial l} = \sum_{j,k} a_{i,j,k} g_j(l) g_k(l). \tag{2.18}$$

The formal solution for the effective Hamiltonian is

$$H_{\text{eff}} = \sum_i g_i(\infty)\hat{o}_i \,. \tag{2.19}$$

It is usually not feasible to achieve an analytically exact solution for $l \to \infty$. But the closed system of differential equations for the $g_i(l)$ can be solved numerically. The initial values $g_i(0)$ are given by the prefactors of H_0. The new terms arising during the calculation of $[\eta(l), H(l)]$ start with the intial prefactor zero. The prefactors belonging to operators that are not particle conserving are monitored

[3] We use normal ordered operators to have a unique representation (see Section 2.3).

during this integration because these terms are the ones that we want to eliminate. If their absolute values are sufficiently small for a certain large value $l = \tilde{l}$ so that they can be neglected, the integration is stopped and the effective Hamiltonian reads

$$H_{\text{eff}} = \sum_i g_i(\tilde{l})\hat{o}_i \,. \tag{2.20}$$

2.1.3 Comparison between PCUT and SCUT

The PCUT exhibits the typical advantages and disadvantages of perturbative approaches. The increase of the expansion parameter x leads relatively rapidly to poor results. Of course the quality of the results can be improved drastically by applying extrapolation techniques such as e.g. Padé approximation.

Comparatively large orders are easily achievable by PCUT. The actual integration has to be carried out only once for the general scheme which is applicable to variable models while the SCUT yields different systems of differential equations for each model. For SCUTs the differential equations have to be integrated whenever a new model is considered. Even if only the initial values are different, a new integration has to be carried out.

The PCUT has been successfully applied in the context of many different problems. Examples of such problems are the Hubbard model [46], many-particle systems [47], spin chains [25] and also spin ladders [27, 48]. The SCUT was also sucessfully used in a broad field of contexts – e.g. for the Anderson model [49–51], superconductivity [52–55], undoped antiferromagnetic spin chains and ladders [19], bosonic atoms in an optical lattice [19] and the derivation of an effective t-J-model from the Hubbard model [19, 56]. A general overview with many more examples for applications of both fashions is given in [57].

The overlap between energies of subspaces of the Hilbert space with different particle numbers hinders the convergence of the integration of the differential equations for $l \to \infty$ because the pc generator sorts the eigenenergies according to the particle number. If states with more particles have a lower energy, a CUT using the pc generator is no longer adequate[4]. In this case an adaption of the generator [26] can be helpful (see Section 2.5).

However, the PCUT constitutes an expansion around the point where the expansion parameter x is zero and no overlap exists. Therefore an actual overlap

[4] In praxi the CUT can converge, nevertheless, if the truncation is very strict. This is discussed in the next section.

for $x > c > 0$ has no influence on the convergence of the PCUT. The effects of an overlap are not captured by the PCUT. Also approaching continua, which do not overlap yet, pose a problem for the PCUT. Approaching continua are sensitive to each other, which results in a deformation of the continua. The PCUT results have to be corrected by rather sophisticated extrapolation techniques to reflect the physical properties of approaching continua. A clear advantage of the SCUT is that such properties are included directly in the resulting effective models.

While the PCUT results exhibit the typical problems of series-expansions increasing with the perturbation parameter, the errors of the SCUT results stem from the truncation of the Hamiltonian. To find a suitable truncation scheme is still a difficult task. The optimal truncation is usually determined a posteriori: If the results converge concerning the expansion of the truncation parameters, the results are expected to reflect the physical properties of the Hamiltonian and the effective model is considered to be valid and reliable (cf. Section 4.3.1). An a priori determination of the truncation error is an objective of current research [58].

The truncation for the SCUTs treated in this thesis is based on a real space representation. The reasons for this choice are discussed in the next section.

2.2 Real Space Representation and Truncation

A multitude of the problems treated in theoretical solid state physics is formulated using localised states (e.g. Wannier states) and local Hamiltonians in second quantisation [59]. This does of course not imply that the physics of these systems is restricted to local effects. The excitations of the spin ladder are known to have a gapful dispersion as long as the four-spin interactions are small enough (see Sections 4.1 and 5.4). The correlation length ξ and the energy gap Δ satisfy the relation $\Delta \propto \xi^{-z}$ where z denotes the dynamic critical exponent [60]. Thus the correlations are local and long-range interactions are less important. The truncation needed for the SCUT to keep the number of differential equations finite can hence appropriately be implemented by omitting longe-range terms.

We have to keep in mind that this truncation is a crucial point as it is essential to keep the number of differential equations finite for an infinite system (or to keep the number of differential equations manageable for a large finite system). Except for the numerical error of the integration the only step causing errors is the truncation. The most obvious truncation for a system dominated by local

correlations is to omit long-range interactions.

Another characteristic which has to be considered for the truncation is the number of particles involved in a certain interaction. This aspect is of course correlated with the locality of the interaction because the more hardcore particles are involved the less local is the concerning term. For the spin ladder the crucial physics of the parameter regime in which we are interested is covered by terms affecting one and two particles [61].

It should also be noted that the truncation is only restricted to operators. There is no truncation of the Hilbert space of the states. Thus although operators affecting higher numbers of particles are omitted, the number of particles that can be treated can be arbitrarily large. To illustrate this we consider the action of a term in second quantisation, e.g. $a_i^\dagger a_j^\dagger a_k$, which annihilates one particle and creates two. This term acts not only on the one-particle subspace, but also on the subspaces with more than one particle, e.g. it changes a four-particle into a five-particle state.

The concrete truncation scheme used for the spin ladders is discussed in detail in Sections 4.2 and 5.2.

The truncation also affects the convergence of the flow. In case of a diverging flow the truncation of terms that hinder the convergence can suppress the divergence. This is illustrated by an example for which the eigenenergies shall be known a priori. For convenience we assume that terms affecting more than two particles are negligible. Moreover, the only terms that do not conserve the particle number are of the form $a_n^\dagger a_{n+\Delta n}^\dagger a_m$ or $a_m^\dagger a_{n+\Delta n} a_n$, where the indices denote the site on which the operator acts. These terms are the non-diagonal ones in our example.

Let us consider a simple case first, in which the one-particle dispersion and the two-particle continuum do not overlap (see left panel in Figure 2.2). Because of the asymptotic behaviour of the non-diagonal elements (2.11) the convergence is hindered only if energies of subspaces with different quasiparticle numbers overlap, while the flow of an SCUT with the pc generator always converges. This was shown in the introduction of the present chapter.

If an overlap is present like in the middle and in the right panel in Figure 2.2, the flow may diverge. The difference between the panel in the middle and the panel on the right is the influence of different truncations. It depends on the truncation which two-particle states are reached by the non-diagonal terms. The real space distance between the two particles is decisive. The terms $a_n^\dagger a_{n+\Delta n}^\dagger a_m$

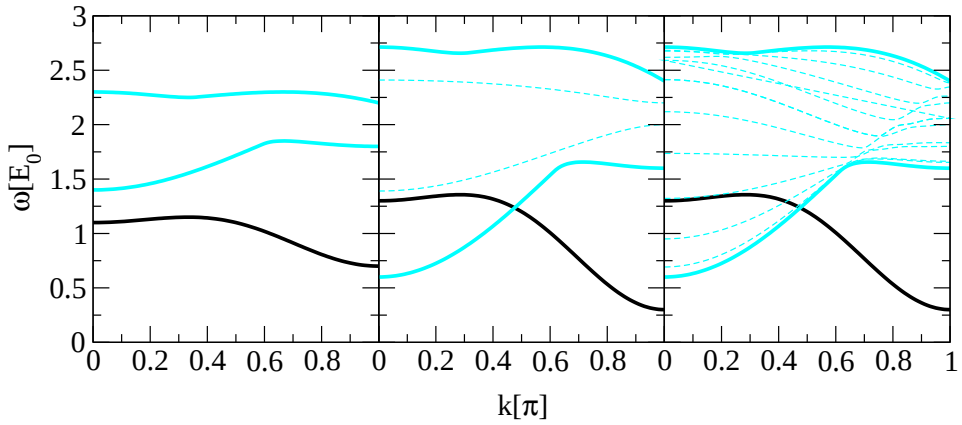

Figure 2.2: Schematic examples for one- and two-particle energies. The black line is the one-particle dispersion, the solid cyan lines are the boundaries of the two-particle continuum and the dashed cyan lines are the energies of the two-triplon states which are actually affected by the non-diagonal terms. In the left panel the one- and two-particle energies do not overlap and no convergence problems occur. In the middle and right panel an overlap is present. If this overlap actually causes divergence, a stricter truncation in real space may yield convergence. The energies of the two-particle states affected by the non-diagonal terms are discrete due to this truncation. Further information can be found in the text.

convert one particle into two particles with a real space distance $|\Delta n|$ between the particles, the Hermitian conjugate terms $a_m^\dagger a_{n+\Delta n} a_n$ convert two particles with a real space distance $|\Delta n|$ into one particle. The truncation restricts $|\Delta n|$ to a maximal distance $\Delta n_{\max}$. Hence not the whole continuum is affected by the non-diagonal terms but only $\Delta n_{\max}$ two-particle states with discrete energies lying within the continuum. These discrete energies are depicted as dashed lines in Figure 2.2. In the middle panel a stricter truncation ($\Delta n_{\max} = 2$) is considered than in the right one ($\Delta n_{\max} = 10$). Therefore the number of two-particle states with discrete energies, which are affected by the non-diagonal terms, is different. If the discrete two-particle energies do not overlap with the one-triplon dispersion (like in the middle panel), the SCUT is less sensitive to the actual overlap and the flow converges. Hence a stricter truncation can yield convergence in case of an overlap that would actually cause divergence. For $\Delta n_{\max} \to \infty$ the discrete energies merge into the continuum.

Note that the one-particle dispersion that lies within the two-particle continuum can only be exact if there is no coupling between their subspaces. In case of

possible transitions between the one- and two-particle subspace the one-particle dispersion is only defined outside the continuum. Nevertheless, the one-particle dispersion can still be tall in the two-particle continuum as a a resonance, which can be observed in the two-particle spectral density.

2.3 Reference State and Normal Order

The definition of a reference state is necessary for the implementation of a normal ordering scheme. The normal ordering is of great importance as a unique representation is needed for comparing operators during the setup of the differential equations. We also single out the relevant processes based on the normal ordering.

In the following n will denote the lattice site. In case of the spin ladder the global reference state $|0\rangle$ is composed of the local reference states $|0\rangle_n$ as follows

$$|0\rangle = \bigotimes_n |0\rangle_n \ . \tag{2.21}$$

This state will be mapped onto the quasiparticle vacuum by the CUT. For other models it is not always reasonable to compose $|0\rangle$ of local states. However, entangled reference states are less tractable.

The concrete choice of $|0\rangle_n$ and therefore $|0\rangle$ is physically motivated. The state $|0\rangle$ in its form before the transformation should be already close to the ground state, i.e. the quasiparticle vacuum. Usually we consider a solvable limit of the Hamiltonian. The ground state of this limit is a suitable choice for $|0\rangle$ as long as the parameters of the Hamiltonian are close to this limit. Then we expect $|0\rangle$ to be close to the actual ground state.

This actual ground state is usually very complex and not explicitly determinable. The same is true for the quasiparticles, i.e. excitations. Figure 2.3 illustrates the mapping of a CUT onto a state describing a single excitation if the correlation decreases exponentially with spatial range (cf. preceding section).

For the normal order we employ a definition that is somewhat different from the usual one because the reference state is a product state in our case (2.21). According to our definition, a local operator $\hat{o}_n$ is normal ordered if

$$\langle 0| \hat{o}_n |0\rangle = 0. \tag{2.22}$$

Accordingly a product of local operators $\hat{o} = \prod_n \hat{o}_n$ is normal ordered if each of its local factors $\hat{o}_n$ is normal ordered.

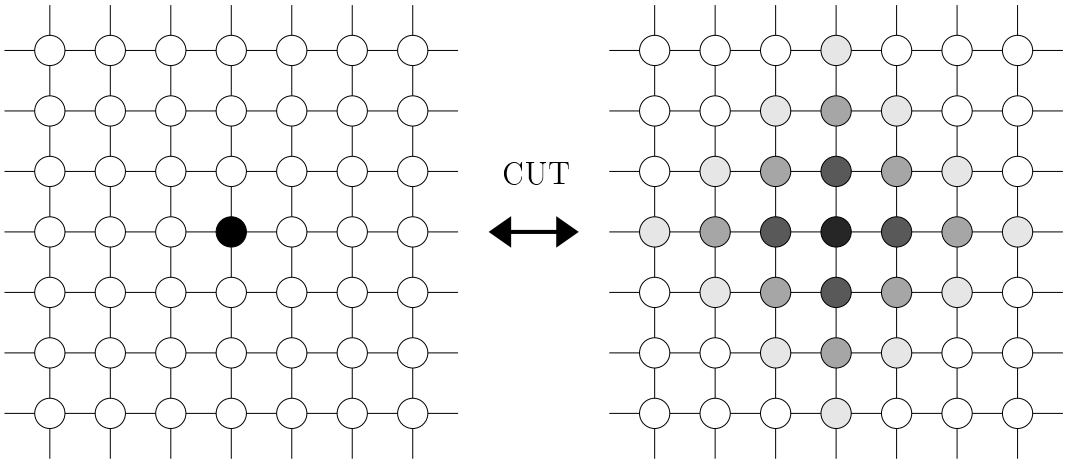

Figure 2.3: Illustration of the transformation of a state that is mapped onto a single quasiparticle in case of an exponentially decreasing correlation. On the left hand side the situation before the transformation is depicted: The state is a product state of local reference states (white circles) and another local state (black circle); this state is an excitation with respect to the solvable limit of the Hamiltonian for which the reference state is the ground state. The right hand side shows the state after the transformation: The actual excitation is dominated by the state on one site (black circle), but it polarises its environment (shaded circles). This polarisation decreases exponentially with the distance from its center (illustrated by different shadings).

In the case of a degenerate ground state a single reference state is not sufficient. A reference ensemble is needed instead, which is, however, not the case for the spin ladder. An example for a reference ensemble can be found in Ref. [56].

2.4 Hardcore Particle Algebra

The quasiparticles populating the spin ladder, which are introduced in Sections 4.1 and 5.1, are hardcore particles, i.e. if a site is occupied by such a quasiparticle no other quasiparticle can be created there. The magnetic exciations of the spin ladder are bosonic hardcore particles, which are dominated by a local triplet state. Due to the threefold degeneracy of the triplet these particles come in three flavours. The hole excitations are fermionic hardcore particles, which are dominated by a local state consisting of a hole and a spin $\frac{1}{2}$. This particle has four flavours because the spin has two possible positions and two possible orientations. Note that for the fermions the hardcore property is stronger than

the Pauli exclusion principle because a fermionic hardcore particle on a site also excludes bosons as well as fermions in different states.

We introduce operators $b^\dagger_{n,\alpha}$ and $b_{n,\alpha}$ creating and annihilating respectively a bosonic quasiparticle, i.e. a particle with integer spin. The index n denotes the site to which the operator is applied and the index α the state of the quasiparticle. In analogy we define fermionic creation operators $f^\dagger_{n,\alpha}$ and fermionic annihilation operators $f_{n,\alpha}$ for quasiparticles with half-integer spin.

The algebra for the hardcore bosons is given by the commutation relation

$$[b_{n,\alpha}, b^\dagger_{m,\beta}] = \delta_{n,m}\left(\delta_{\alpha,\beta}\left(\mathbb{1}_n - \sum_\gamma e^\dagger_{n,\gamma} e_{n,\gamma}\right) - b^\dagger_{n,\beta} b_{n,\alpha}\right) \tag{2.23}$$

where $e^\dagger_{n,\alpha}$ and $e_{n,\alpha}$ denote all possible creation and annihilation operators (bosonic and fermionic). The sum over γ goes over all possible states for the quasiparticles. Note that $\mathbb{1}_n - \sum_\gamma e^\dagger_{n,\gamma} e_{n,\gamma}$ is one for an empty state and zero otherwise. This operator is not normal ordered due to the identity operator (see Section 3.5). In products of local operators the identity operator can be neglected because only the operators affecting the quasiparticles are relevant. The operator product in the Hamiltonian consisting of identity operators only for all sites yields a constant energy (infinite for an infinite system), which can be omitted by an appropriate offset. In the effective particle conserving model, i.e. for $l \to \infty$, this constant energy is the groundstate energy of the system at hand.

Concerning different sites the operators behave like usual bosonic operators: they commute accommodated by the $\delta_{n,m}$ in Equation 2.23. Acting on the same site the hardcore property comes into play. According to its definition the commutator yields

$$[b_{n,\alpha}, b^\dagger_{n,\beta}] = b_{n,\alpha} b^\dagger_{n,\beta} - b^\dagger_{n,\beta} b_{n,\alpha}. \tag{2.24}$$

The action of the first term $b_{n,\alpha} b^\dagger_{n,\beta}$ depends on whether α is equal to β or not. It can be easily seen that $b_{n,\alpha} b^\dagger_{n,\beta} = 0$ for $\alpha \neq \beta$ due to the fact that multiple occupation of one site is not allowed. In the case $\alpha = \beta$ the term $b_{n,\alpha} b^\dagger_{n,\beta} = b_{n,\alpha} b^\dagger_{n,\alpha}$ acts like the operator which counts the empty states because it is zero for an occupied site and one for an empty one. Incorporating these relations one gets the form of Equation 2.23.

For the hardcore fermions the following anticommutation relation holds true

$$\{f_{n,\alpha}, f^\dagger_{m,\beta}\} = \delta_{n,m}\left(\delta_{\alpha,\beta}\left(\mathbb{1}_n - \sum_\gamma e^\dagger_{n,\gamma} e_{n,\gamma}\right) + f^\dagger_{n,\beta} f_{n,\alpha}\right). \tag{2.25}$$

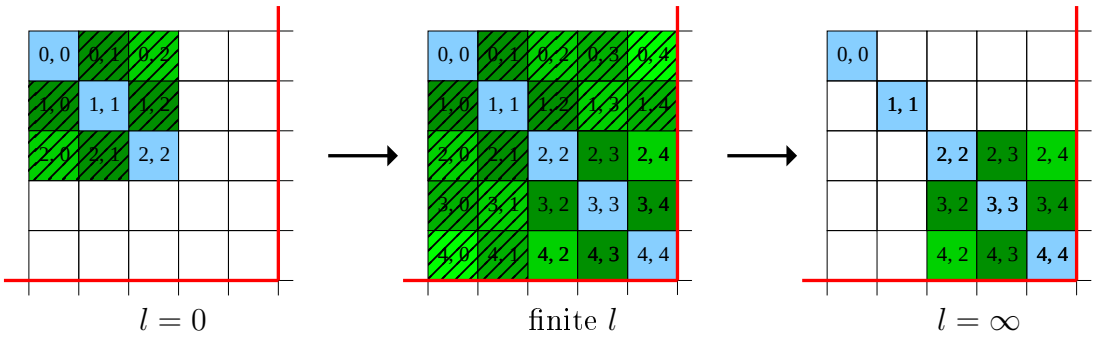

Figure 2.4: Schematic example for a transformation of $H(l)$ induced by the gs,1p generator: Each coloured (n_c, n_a)-block represents contributions to H creating n_c particles after annihilating n_a particles. The red line indicates that all operators affecting more than four particles are truncated. The generator contributions are depicted as shaded blocks.

In analogy to the bosonic operators the fermionic ones behave like usual fermionic operators if they act on different sites, i.e. they anticommute. For operators on the same site only the hardcore property is relevant.

Commutators with fermionic and bosonic operators belonging to hardcore particles yield

$$[b_{n,\alpha}, f^\dagger_{m,\beta}] = -\delta_{n,m} f^\dagger_{n,\beta} b_{n,\alpha} \tag{2.26}$$

and

$$[f_{n,\alpha}, b^\dagger_{m,\beta}] = -\delta_{n,m} b^\dagger_{n,\beta} f_{n,\alpha} \tag{2.27}$$

because bosonic and fermionic operators commute acting on different sites.

2.5 Adapted Generators

2.5.1 Exclusion of Terms from the Generator

If transitions between particle spaces with overlapping energies are possible, the pc generator (which is based on the idea that more present particles always correspond to a higher energy of the system) is only partly appropriate because the resulting SCUT usually shows problems with the convergence for $l \to \infty$. Actually the SCUT diverges in this case if the truncation scheme is made less strict. Because the divergence is induced only by long range terms for small overlaps, the truncation of these terms can restore convergence (see Section 2.2). But this

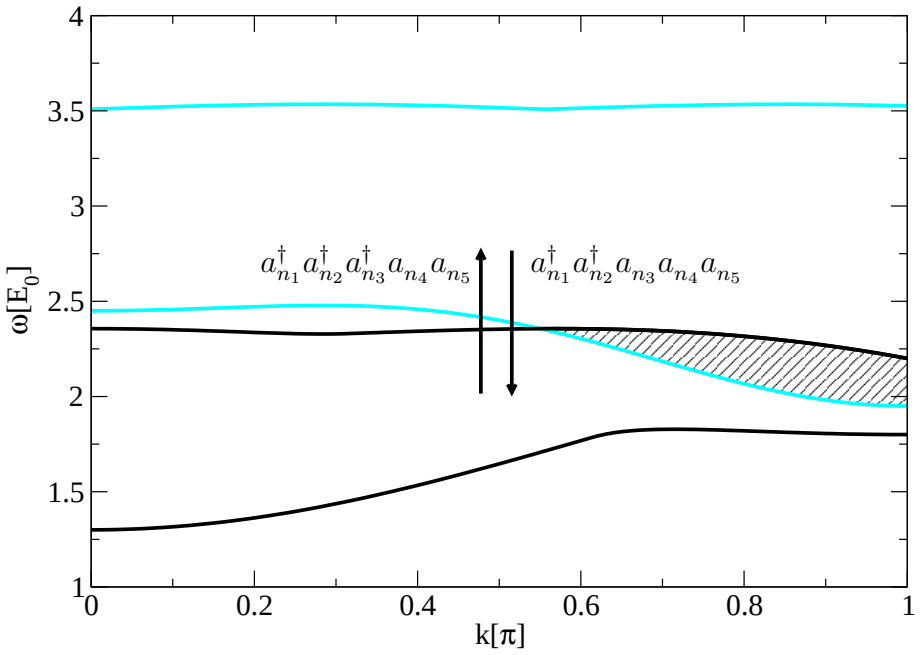

Figure 2.5: Schematic representation of an overlap between a two-particle continuum (boundaries in black) and a three-particle continuum (boundaries in cyan). The overlap is present for $k \gtrsim 0.55\pi$ and depicted by the black shaded area. The terms $a^\dagger_{n_1}a^\dagger_{n_2}a^\dagger_{n_3}a_{n_4}a_{n_5}$ induce a transition from the two- to the three-particle continuum and the hermitian conjugate terms a transition vice versa.

convergence is accompanied by the neglect of physical properties. Therefore the resulting eigenenergies reflect the assumptions implied by the generator. The concerning overlapping energies are separated by the transformation, i.e. the effective Hamiltonian does not exhibit this actual overlap.[5]

Nevertheless, if the continua have a strong overlap, the integration of the SCUT differential equations for the prefactors of the Hamiltonian diverges for $l \to \infty$. The exclusion of the terms responsible for the transition between the overlapping continua from the pc generator is a remedy for this problem. For instance, if an overlap between the two- and the three particle continuum (see Figure 2.5) hinders the convergence, terms of the form $a^\dagger_{n_1}a^\dagger_{n_2}a^\dagger_{n_3}a_{n_4}a_{n_5}$ and the hermitian conjugate terms are excluded from the generator.

[5]Note that the approach of non-overlapping continua results in a deformation of the energy bands as an actual physical effect. This effect is captured by the pc SCUT. However, if an overlap is present, the pc generator encounters problems (cf. Equation (2.13)).

The consequence of this exclusion is that the concerning particle spaces remain coupled. In contrast to the application of the pc generator the Hamiltonian loses its block-band form during the flow then. Of course the diagonalisation of the parts of the Hamiltonian concerning the according particle spaces still has to be done if the corresponding continua shall be calculated. But regarding all other particle numbers the Hamiltonian will be block-diagonal after the SCUT, which now converges for $l \to \infty$.

In Figure 2.4 an example for an SCUT adapted in the manner described here is depicted. We use again the (n_c, n_a)-block representation introduced in Section 2. In this example the generator contains only the $(0, n)$- and $(1, n)$-blocks as well as the conjugate terms. We use the term gs,1p generator for this generator, which decouples only the ground state and the one-particle state from the rest. We start from a Hamiltonian exhibiting the same structure as in the example for the pc generator in Figure 2.1. Conferring both examples the differences between both generators with respect to the structure of the Hamiltonian during the flow and for $l \to \infty$ become clear.

If the continua belonging to certain particle numbers are not of interest, the terms of the Hamiltonian connecting the concerning subspaces can be excluded for the sake of performance. Although terms appear during the flow that would not be induced by the pc generator, the right hand side contributions to the flow equation (2.3) are reduced which simplifies the problem considerably.

Generally all problematic terms can be excluded from the generator at the expense of the decoupling of the corresponding subspaces. A detailed discussion of generator adaptions by excluding terms from the pc generator can be found in [26] where quasiparticle decay is examined by means of SCUT.

2.5.2 Additional Sign Changes in the Generator

If the local behaviour in the model suggests that certain processes increasing the particle number are lowering the energy, the concerning terms can also be provided with a minus sign in the generator instead of being excluded. Then the Hermitian conjugate terms decreasing the particle number and raising the energy do not get the minus sign they would get in the pc generator. The advantage of sign change over exclusion is that these terms changing the particle number will not occur in the effective Hamiltonian since their contribution to the generator causes their decrease for large l. Thus all subspaces corresponding to certain par-

ticle numbers will be decoupled from each other producing a particle conserving effective model.

In the context of the hole-doped spin ladders this idea of adapting the sign of the generator terms becomes interesting. Increasing the number of magnetic excitations corresponding to quasiparticles is not necessarily accompanied by raising the energy because the presence of a hole permits new processes in which the generation of additional magnetic excitations implies the reduction of the energy of the hole. Analogous processes decreasing the number of excitations and enhancing the hole energy are also possible. A detailed discussion of this issue will be given in Section 5.3.

Both possibilities of adapting the generator for the SCUT described here – exclusion of terms and sign change – can of course be combined to achieve optimal results.

Nevertheless, the computation of the sign of the energy change in advance is not a simple task because this sign is actually one of the properties of the effective model which still has to be calculated. If this property depends on the momentum, the ansatz of truncating in real space depending on extensions of operators is not feasible. The effects of a generator based on a wrong estimation are discussed in Section 5.3.

2.5.3 Real Space Restriction of the Generator

Many terms that remain after the real space truncation of the Hamiltonian act on states with discrete energies within the continua (see Section 2.2). The divergence of the SCUT in case of an overlap is not induced by all terms that mediate between overlapping continua, but only by a part of these terms (see Figure 2.6). It was also shown in Section 2.2 that a stricter real space truncation of the Hamiltonian can induce convergence.

However, a stricter truncation causes a larger error for the results of the SCUT. Therefore we do not apply a stricter truncation to the Hamiltonian but we choose a stricter generator. We emphasize that a restriction of the generator does not imply an approximation. It only changes the direction of the unitary rotation. This restriction of the generator is not based on the total extension of the terms, but on the extension of the creation operators and the extension of the annihilation operators. Let us consider the example of an overlap between one- and two-particle energies shown in Figure 2.6. The terms $a_n^\dagger a_{n+\Delta n}^\dagger a_m$ and $a_m^\dagger a_{n+\Delta n} a_n$

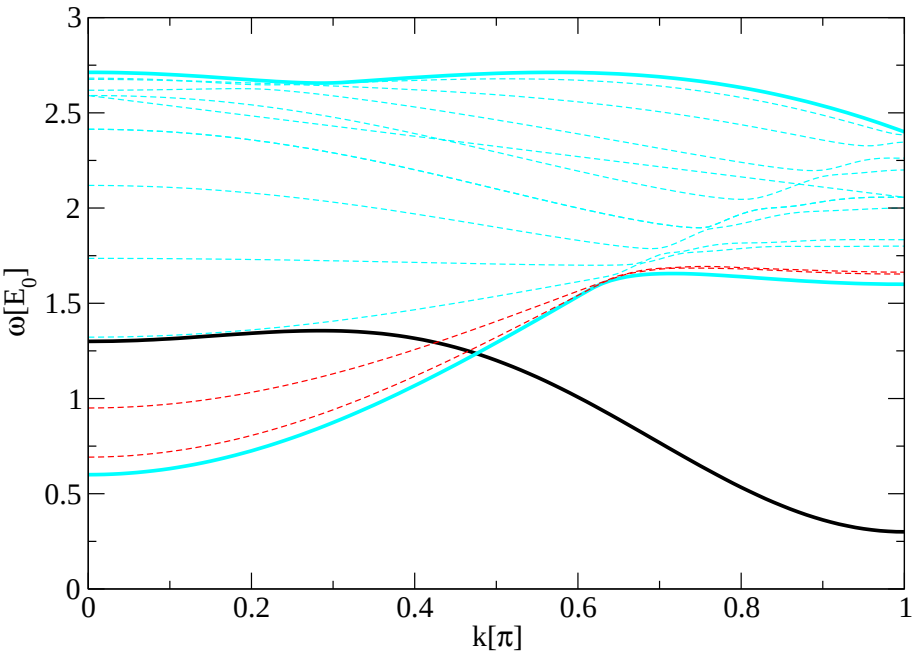

Figure 2.6: Schematic example for an overlap between one- and two-particle energies. The black line is the one-particle dispersion, the solid cyan lines are the boundaries of the two-particle continuum and the dashed lines are the energies of the two-triplon states which are actually affected by the terms $a_n^\dagger a_{n+\Delta n}^\dagger a_m$ and $a_m^\dagger a_{n+\Delta n} a_n$. The cyan dashed lines do not pose a problem because they do not cross the one-particle dispersion. The convergence problem is induced by the terms that act on the states with the red dashed dispersions, which cross the one-particle dispersion.

are responsible for transitions between the one- and the two-particle subspace. We choose to restrict the generator based on $|\Delta n|$, which is the distance between the two particles which are created or annihilated. Because the one-particle state does not have an extension, it is not relevant for the restriction of the generator. All terms that have a larger $|\Delta n|$ than a certain $\Delta n_{\max}$ are excluded from the generator. Note that they are still part of the Hamiltonian as long as they meet the truncation criteria for the Hamiltonian.

The transformation induced by this restricted generator does not try to sort all eigenenergies (cf. Equation 2.12), but only those which are captured by the terms in the generator. Therefore the flow may also converge in case of overlapping energies. The price to be paid is that the subspaces affected by the omitted terms are not completely decoupled from the remaining Hilbertspace. Thus either an

additional diagonalisation has to be applied to the effective Hamiltonian from this SCUT or the results have to be considered as upper limit for the actual results. The restriction of the generator can be applied to the pc generator or to any of its adaptions. A concrete example for such a restriction is introduced and discussed in Section 5.3.

3 SCUT Implementation on a Computer

For the realisation of an SCUT it is essential to implement a program tailored to the particular purpose. The special features of such a calculation have to be optimized for the computing performance. These technical aspects are discussed within this chapter.

Because the SCUT consists of two different parts, it is advisable to use two separate programs. The first one sets up the differential equations arising from the Hamiltonian to be diagonalised in consideration of the algebra of the underlying operators. The second one integrates the differential equations set up by the first one. The advantage of the separation of these two steps consists in the possibility to apply the second step with different initial values independently from the first one because setting up the differential equations is very demanding concerning memory and time.

3.1 Data Structure

To implement the first part of the SCUT, which sets up the differential equations for the prefactors of the Hamiltonian, the programming language C++ is used. For the sake of performance we do not use a computer algebra system like Mathematica or Maple because up to several hundred thousands of terms have to be treated for the systems considered within this thesis.

A class for the operator terms is an essential part of our program. The objects of this class have the following attributes.

The prefactor for these terms is a common fraction consisting of a sign, an integer numerator and an integer denominator. In this thesis only integer prefactors are actually needed. But for other algebrae fractions cannot be avoided, which should remain common fractions as long as possible to minimise the rounding

errors. Only the numerical integration in the second part of the SCUT requires floats.

A boolean variable determines whether the prefactor is real or imaginary. The terms appearing in the models of this thesis are either purely real or purely imaginary. However, complex prefactors can be represented using these attributes by splitting a number into its real and its imaginary part.

The main part of the term is an array of local operators. For these operators a particular class is implemented. It is advisable to use a matrix representation for the local operators as the commutators and the combinations of local operators are easier to calculate by means of matrix products. Also the site which is affected by the local operator has to be an attribute. The models of this thesis are quasi one-dimensional so that the site can be represented by an integer scalar. For higher dimensions it has to be a vector.

A large number of terms is generated during the setup of the differential equations and each resulting term of a commutator has to be compared to the terms of the Hamiltonian to check if it contributes to already existing terms in the Hamiltonian or to new terms to be established. To simplify this comparison a hash value is attributed to each term depending on the operators included. A hash function assigns a unique hash value to a certain combination of local operators. Terms with the same hash value are combined to a group. Then the search for equal terms can be restricted to the group with the same hash value. The more possible hash values there are the smaller the groups are and the faster the search can be done. The hash function should also assign the values evenly so that the sizes of the groups do not differ too much. If terms are similar, a search for a certain term is more difficult and therefore slower. Hence similar terms should get different hash values. The hash function should rather be implemented in a way that terms with equal hash values differ distinctly so that it is easier to distinguish them and the search becomes faster. An appropriate hashing can speed up the program significantly. We have chosen a simple hash function based on the modulo operation. The hash value v is given by

$$v = (\ldots(i_0 a + i_1) \mathrm{mod} M) a + i_2) \mathrm{mod} M) a + i_3) \mathrm{mod} M) a + \ldots i_n) \tag{3.1}$$

where i_k denotes the index that characterises the k-th local operator of the term. The number of local operators is n, the of possible hash values is M and a denotes the number of possible local operators. To avoid an integer overflow the modulo operation is applied after each addition.

It is also convenient to use an attribute "multiplicity", which appears in the context of the utilisation of the symmetries, which are discussed in the next section. The time needed to determine this number can be reduced if it is only calculated once and stored as an attribute instead of caculating it numerous times. Of course other properties that are needed frequently can be attributed to the terms as well if their calculation is time-consuming.

The terms in the sum of the Hamiltonian should be stored as a dynamical array because the size of the final Hamiltonian is not known in advance. Because the terms of the pc generator are all part of the Hamiltonian except for possible signs 2.7, the generator does not have to be stored additionally to the Hamiltonian. If a term has to be used as a generator term, the potential additional sign is added during the calculation if necessary. For the adaptions of the pc generator introduced in Section 2.5 we proceed in the same way.

Arbitrary operators are transformed according to Equation (2.4). Because Hamiltonians are the only operators that were transformed in this thesis, this aspect of the SCUT is not treated here. A detailed description of the implementation of general operator transformations can be found in Ref. [19].

3.2 Utilisation of Symmetries

The utilisation of symmetries given by the Hamiltonian of the model saves time and memory and it is therefore essential for complex problems. For infinitely extended systems the SCUT is even theoretically infeasible without the utilisation of at least one symmetry that reduces the Hamiltonian to a finite number of representative terms. Normally this symmetry is the translation symmetry. Terms that emerge from each other via translations in real space can be represented by one exemplary term. In a one-dimensional system in which the sites are labelled by integers one can use the term with the smallest site number equal to zero as the representative for the whole group, which contains an infinite number of terms.

Other generic symmetries that can be utilised are the remaining symmetries of the lattice, symmetries in spin space or particle-hole symmetries. Also the hermiticity of the Hamiltonian, which is no symmetry in the usual sense, can be utilised. It is discussed here how to calculate the complete commutator using the representative terms for discrete symmetries exemplarily.

The Hamiltonian H represented by a sum of the terms h_i with their prefactors

f_i can be written as a sum over the whole symmetry group G (with l_G elements) comprising all symmetries to be used:

$$H = \sum_{i=1}^{N} f_i h_i = \sum_{G} \sum_{j=1}^{N_s} \tilde{f}_j \tilde{h}_j \tag{3.2}$$

where N denotes the number of all terms of the Hamiltonian without consideration of the symmetries and N_s the number of representatives. The actual representatives $\tilde{h}_j$ carry the prefactors $\tilde{f}_j$ which are in general not equal to the f_i.

The relation

$$\mathrm{abs}(f_i) = \mathrm{abs}(s_j \tilde{f}_j) \tag{3.3}$$

holds true for the absolute value of the corresponding coefficients if there is a one-to-one correspondence between single operator monomials under the group transformations. The factor s_i is the multiplicity of $\tilde{h}_i$ in the sum over G. If the application of different symmetry operations to a representative generates terms multiple times so that the sum over G contains them multiple times as well, the prefactor of the concerning representative has to be reduced by the multiplicity in the sum over G. The simplest example for a nontrivial multiplicity, i.e. a multiplicity not equal to one, is the multiplicity of the unity operator. Because the unity operator remains unchanged by the application of every symmetry operation, its multiplicity is equal to the number of all possible symmetry operations, i.e. l_G.

For another simple example consider the symmetry operation R which reflects a term with respect to a certain plane. If a term does not change under R, but under all remaining symmetry operations, its multiplicity is 2.

Note that some symmetry operations change the sign of the coefficient. Hence the sign has to be taken into account as well for the $\tilde{f}_j$ and Equation (3.3) is only valid for the absolute values. For instance, the application of the parity operator to a term affecting a state with odd parity yields an additional minus sign.

Due to the multiplicities the number of terms in the Hamiltonian usually can not be reduced by the factor l_G. But especially for a large number of terms the reduction usually comes close to it. There are cases where the reduction can actually be larger than l_G if the utilisation of the symmetry avoids the emergence of certain terms [62].

The calculation of the commutator, however, cannot be restricted to the representatives only. As the generator consists of terms that are also part of the

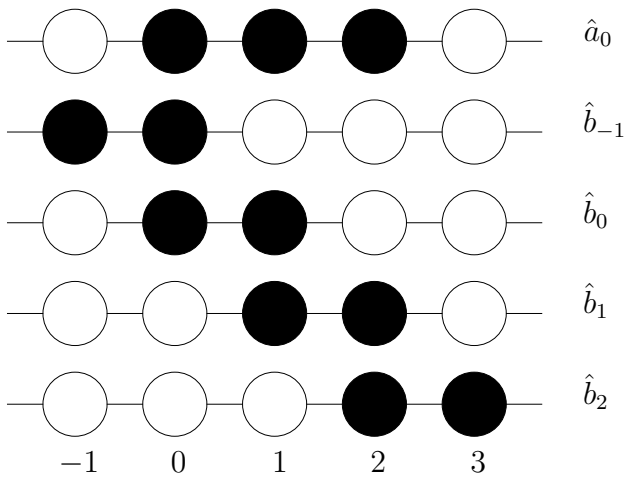

Figure 3.1: The example for the use of the translation symmetry in the commutator explained in the text is illustrated. The action of the terms a_0, b_{-1}, b_0, b_1 and b_2 on a one-dimensional chain, whose sites are depicted as circles, is shown. The sites affected by an operator are depicted by filled circles. The commutator $\left[\hat{a}_0, \sum_n \hat{b}_n\right]$ yields the representative terms for the complete commutator $\left[\sum_n \hat{a}_n, \sum_n \hat{b}_n\right]$. In contrast the commutator $\left[\hat{a}_0, \hat{b}_0\right]$ considered in isolation misses the relative translations of the operators that are present for $\left[\hat{a}_0, \hat{b}_{-1}\right]$, $\left[\hat{a}_0, \hat{b}_1\right]$ and $\left[\hat{a}_0, \hat{b}_2\right]$.

Hamiltonian, the commutator on the right hand side of the flow equation (2.3) can be calculated by commutators of the form $[h_i, h_j]$.

The symmetries can be used by

$$\left[\sum_G \tilde{f}_i \tilde{h}_i, \sum_G \tilde{f}_j \tilde{h}_j\right] = \sum_G \left[\tilde{f}_i \tilde{h}_i, \sum_G \tilde{f}_j \tilde{h}_j\right] \tag{3.4}$$

so that one sum of the commutator can be restricted to the representatives and only for the other sum the full symmetry group must be taken into account.

This is illustrated for the translational symmetry in a one-dimensional example. The example considers the commutator of a term $\hat{a}_n$ acting on three neighbouring sites and a term $\hat{b}_n$ acting on two neighbouring sites where n denotes the smallest site index (see Figure 3.1). The representative terms are a_0 and b_0 without loss of generality.

The complete commutator $\left[\sum_n \hat{a}_n, \sum_n \hat{b}_n\right]$ incorporates an infinite number of nontrivial terms for an infinite chain. The commutator $\left[\hat{a}_0, \sum_n \hat{b}_n\right]$ omitting the

first sum and taking into account the representative $\hat{a}_0$ only yields the representative terms for the result of the complete commutator because the omitted sum causes the translation of the whole term.

The commutator of the representatives $\left[\hat{a}_0, \hat{b}_0\right]$ is only a partial contribution to the representative terms of the result because omitting both sums neglects the possible relative translations of the operators $\hat{a}_n$ and $\hat{b}_n$.

In the present case the sum over n for the $\hat{b}_n$ can be restricted to n from -1 to 2 because all other $\hat{b}_n$ have no overlap with the representative $\hat{a}_0$ and the corresponding commutators are zero for bosonic operators[1].

Note that the resulting representatives do not match the form defined in the beginning and still have to be adapted to this definition. In our example this means that the smallest site index of the resulting representatives is not zero in general so that the terms have to be translated appropriately.

3.3 Setup of the Flow Equation

The essential part of the program that calculates the flow equation (2.3), which is actually a system of differential equations for the coefficients of the Hamiltonian (2.18), features two for loops running over the terms of the Hamiltonian. The terms originating from the first loop represent the generator terms. Therefore, still outside the second loop, it has to be checked whether the first term matches the criteria for the generator. If it is not part of the generator, the second loop is skipped and the first one continues with the next term.

Due to the utilisation of the symmetries the step in which the term from η and the term from H are identical must not be skipped. The application of the symmetry operations, which takes place inside the loops, generates terms from the H term that are different from the η term.

Figure 3.2 shows a structure diagram for the program that sets up the flow equation. The two for loops described in the preceding paragraph are embedded into a while loop that has the exit condition that no new terms arise inside.

In the case of a generator which conserves the block-band structure of the Hamiltonian the procedure inside the two for loops should start with a query if it can be concluded from the components of the two terms to be commuted whether the commutator yields terms outside the band of the Hamiltonian. These

[1] Terms consisting of an even number of fermionic operators behave like bosonic operators.

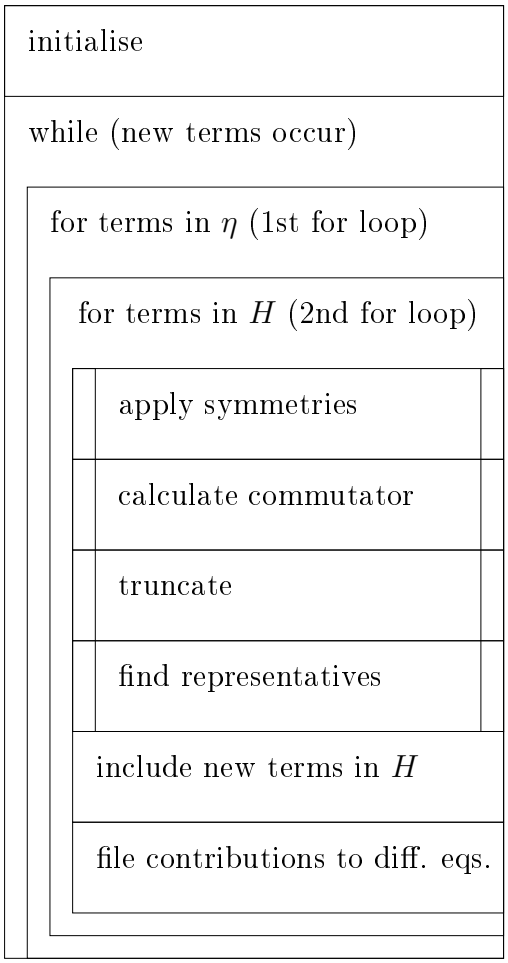

Figure 3.2: Structure diagram of the program for setting up the flow equation.

resulting terms are cancelled by other terms due to the properties of the generator. Hence they can be left out immediately and the commutator does not need to be calculated. Consider a starting Hamiltonian that changes the particle number maximally by N. All Hamiltonians $H(l)$ occurring during the flow inherit this property if a pc generator is employed. A commutator of a term that changes the particle number by n_1 and a term that changes the particle number by n_2 yields only terms that change the particle number by n_1+n_2 (with $n_1, n_2 \in \mathbb{Z}$). If $\mathrm{abs}(n_1+n_2) > N$, the results of the commutator violate the considered property and do not contribute to the flow equation.

The term representing a part of the generator is attributed the appropriate sign at this point. For the pc generator the sign is defined by Equation (2.7).

Because $\left[\tilde{f}_i\tilde{h}_i, \sum_G \tilde{f}_j\tilde{h}_j\right]$ has to be calculated (as explained in the last section), all possible symmetry operations are applied to the second term of the commutator. The arising terms are run over by a loop in which the commutator is calculated finally. The function carrying out this task resorts to an array in which all possible local commutators are stored[2] and to the distributive law for commutators which is the subject of the next section.

Afterwards the truncation is applied to the results of the commutator. The remaining terms are adapted to the definition of the representatives. Terms that are equivalent to the same representative have to be summed up.

The results of the commutator are now in the final form and have to be compared to the representative terms of the Hamiltonian. If they match an existing term, the program stores the information that the coefficients of the two terms which were inserted into the commutator contribute (including the resulting prefactor) to the derivative of the coefficient of the matching term (cf. Equation 2.18). If a commutator result is a new term, the term is added to the dynamical array of the Hamiltonian. Its initial value is set to zero because it is not present in the starting Hamiltonian. Then the contributions to the flow equation are stored like for an already existing term. This concludes the procedure inside the two for loops.

When all commutators are computed for the terms of the starting Hamiltonian, the for loops run over all combinations of the new terms among each other and of new terms and old terms. When all the concerning commutators are calculated, this procedure is repeated after each run as long as new terms emerge which are not truncated.

3.4 Calculation of the Commutator

A commutator of terms consisting of local operators[3]

$$\left[\left(\prod_{i=1}^{n_L}\hat{a}_i\right), \left(\prod_{j=1}^{n_R}\hat{b}_j\right)\right] \tag{3.5}$$

with n_L operators $\hat{a}_i$ in the first product and n_R operators $\hat{b}_j$ in the second product has to be calculated efficiently within the program. The operators $\hat{a}_i$ and $\hat{b}_j$ are

[2] The possible local commutators can be calculated via matrix products at the beginning of the program because the local operators can be represented by matrices (see Section 3.5).

[3] A local operator $\hat{a}_i$ acting on site i is here an abbreviatory notation for $\bigotimes_{j<i}\mathbb{1}_j \otimes \hat{a}_i \otimes \bigotimes_{j>i}\mathbb{1}_j$.

locally normal ordered[4] operators affecting only one site each.

The application of the commutator definition $[\hat{A}, \hat{B}] = \hat{A}\hat{B} - \hat{B}\hat{A}$ with subsequent combination of terms acting on the same sites is less efficient than the application of the distributive law for commutators. The commutator can be split into local commutators

$$\begin{aligned} & \left[\left(\prod_{i=1}^{n_L} \hat{a}_i\right), \left(\prod_{j=1}^{n_R} \hat{b}_j\right)\right] \\ = & \sum_{k=1}^{n_L}\sum_{l=1}^{n_R}\left(\left(\prod_{i=1}^{k-1} \hat{a}_i\right)\left(\prod_{j=1}^{l-1} \hat{b}_j\right)\left[\hat{a}_k, \hat{b}_l\right]\left(\prod_{j'=l+1}^{n_R} \hat{b}_{j'}\right)\left(\prod_{i'=k+1}^{n_L} \hat{a}_{i'}\right)\right) \end{aligned} \tag{3.6}$$

which is convenient for commutators of bosonic operators or mixed commutators with bosonic operators a_i and fermionic operators b_j or vice versa. If one of the parts of the generator consists of an even number of local operators, the commutator can be split into local anticommutators. Let n_R be even without loss of generality, then

$$\begin{aligned} & \left[\left(\prod_{i=1}^{n_L} \hat{a}_i\right), \left(\prod_{j=1}^{n_R} \hat{b}_j\right)\right] \\ = & \sum_{k=1}^{n_L}\sum_{l=1}^{n_R}\left((-1)^{l-1}\left(\prod_{i=1}^{k-1} \hat{a}_i\right)\left(\prod_{j=1}^{l-1} \hat{b}_j\right)\left\{\hat{a}_k, \hat{b}_l\right\}\left(\prod_{j'=l+1}^{n_R} \hat{b}_{j'}\right)\left(\prod_{i'=k+1}^{n_L} \hat{a}_{i'}\right)\right) \end{aligned} \tag{3.7}$$

which is convenient for fermionic operators. Because the fermion number is conserved within our models, in each term of the Hamiltonian the number of fermionic creation operators always equals the number of fermionic annihilation operators, i.e. there is an even number of fermionic operators in all of these terms.

The terms encountered in the commutator consist of both bosonic and fermionic local operators in general. These general terms can be dealt with by ordering the operators according to the algebra they obey, i.e. an operator $\hat{A}$ should be written as a product of $\hat{A}_b$ consisting of local bosonic operators and $\hat{A}_f$ consisting of local fermionic operators. Then each commuator to be calculated can be split up according to

$$\begin{aligned} & \left[\hat{A}, \hat{B}\right] = \left[\hat{A}_b\hat{A}_f, \hat{B}_b\hat{B}_f\right] \\ = & \left[\hat{A}_b, \hat{B}_b\right]\hat{B}_f\hat{A}_f + \hat{A}_b\left[\hat{A}_f, \hat{B}_b\right]\hat{B}_f + \hat{B}_b\left[\hat{A}_b, \hat{B}_f\right]\hat{A}_f + \hat{A}_b\hat{B}_b\left[\hat{A}_f, \hat{B}_f\right]. \end{aligned} \tag{3.8}$$

[4]The normal order used in this context is described in Section 2.3.

The first three parts of this sum can be evaluated via Equation 3.6 and the last part via Equation 3.7.

The advantage of this approach of relying on the distributive law is that the commutator is reduced to a small number of terms close to the desired form because most terms in the sums in Equations 3.6 and 3.7 are zero[5].

Now the operators in the remaining products outside the commutator or anticommutator respectively have to be combined until each site is related to just one local operator. The results of all possible local products can be stored in an array like the results for the local commutators. To be able to compare the resulting terms with the terms of the Hamiltonian, the defined order concerning bosonic and fermionic operators as well as concerning the sites has to be established; additional minus signs occur by swapping fermionic operators.

3.5 Matrix Representation for Local Operators

The local commutators, anticommutators and products of local operators needed for the calculation are calculated at the beginning of the program. This is conveniently done in matrix representation. For a local basis consisting of N states[6] there are N^2 linearly independent local operators, which can be represented by $N \times N$ matrices. One of the states is the local reference state $|0\rangle_n$ introduced in Section 2.3. The other states of the local basis shall be referred to as $|r\rangle_n$ with $r \in \{1, 2, \ldots, N-1\}$. The pc CUT maps $|0\rangle_n$ onto the empty site and the other states onto the site occupied by one quasiparticle, which can have $N-1$ different flavours r.

The corresponding vectors are defined to be

$$|0\rangle_n = \begin{pmatrix} 1 \\ 0 \\ 0 \\ \vdots \end{pmatrix}_n \quad |1\rangle_n = \begin{pmatrix} 0 \\ 1 \\ 0 \\ \vdots \end{pmatrix}_n \quad |2\rangle_n = \begin{pmatrix} 0 \\ 0 \\ 1 \\ \vdots \end{pmatrix}_n \quad \ldots \quad . \tag{3.9}$$

The operators $e^\dagger_{n,r}$ creating quasiparticles with the flavour r on site n are repre-

[5] The commutator for local bosonic operators acting on different sites vanishes and so does the anticommutator for local fermionic operators. Furthermore, many local products $a_i b_j$ or $b_j a_i$ yield zero.

[6] For the undoped ladder $N = 4$ holds (see Section 4.1). We consider $N = 8$ for the doped ladder neglecting the double hole state (see Section 5.1).

sented by the matrices

$$e^\dagger_{n,1} = \begin{pmatrix} 0 & 0 & 0 & \dots \\ 1 & 0 & 0 & \\ 0 & 0 & 0 & \\ \vdots & & & \ddots \end{pmatrix}_n \qquad e^\dagger_{n,2} = \begin{pmatrix} 0 & 0 & 0 & \dots \\ 0 & 0 & 0 & \\ 1 & 0 & 0 & \\ \vdots & & & \ddots \end{pmatrix}_n \qquad \dots \tag{3.10}$$

from which the local operators $e_{n,r}$ and $e^\dagger_{n,r}e_{n,r'}$ can be formed easily. Together with the unity operator $\mathbb{1}_n$ these N^2-1 operators $e^\dagger_{n,r}$, $e_{n,r}$ and $e^\dagger_{n,r}e_{n,r'}$ constitute a local basis. The operator

$$\begin{pmatrix} 1 & 0 & 0 & \dots \\ 0 & 0 & 0 & \\ 0 & 0 & 0 & \\ \vdots & & & \ddots \end{pmatrix}_n \tag{3.11}$$

is not chosen as an element of the basis because it is not normal ordered concerning $|0\rangle_n$. This operator is therefore represented by the linear combination

$$\mathbb{1}_n - \sum_{r=1}^{N-1} e^\dagger_{n,r}e_{n,r} \tag{3.12}$$

which was already used in Section 2.4. The unity operator $\mathbb{1}_n$ is also not normal ordered concerning $|0\rangle_n$, but it is not taken into account in products of local operators as usual in second quantisation because it acts only trivially. The overall unity operator $\mathbb{1} = \bigotimes_n \mathbb{1}_n$ yields only a constant energy contribution and does not appear on the right hand side of the flow equation (2.3) because it commutes with every term.

The matrices obey the hardcore algebra introduced in Section 2.4. The quasiparticles can be bosonic or fermionic since the local algebra is only given by the hardcore property. For bosonic particles (or mixed combinations of one bosonic and one fermionic particle) only the local commutators and for the fermionic particles only the local anticommutators are needed. So in total N^4 relations have to be calculated. Also N^4 different local products are possible. The results achieved via the matrices are stored in an array for further use.

Although it is not obligatory to store all results due to the antisymmetry of the commutator $[A,B] = -[B,A]$ and the symmetry of the anticommutator $\{A,B\} = \{B,A\}$, the program is faster if we can recall all results directly from the memory without further operations.

3.6 Numerical Integration of the Flow Equation

The second part of the SCUT – the solution of the flow equation – is a rather straightforward numerical integration. A system of ordinary first order bilinear differential equations (2.18) depending on the continuous variable l has to be solved. For instance, a fifth order Runge-Kutta method can be applied, which is our algorithm of choice. An adaptive step size control is advisable because most of the changes take place at the beginning of the integration while the coefficients $g_i(l)$ remain almost constant from a certain l on if the transformation converges for large l. So the size of the steps of the numerical integration can be increased during the calculation. The program code for the Runge-Kutta method can be found in Ref. [63].

The convergence is monitored during the integration. Since all contributions to the generator decrease exponentially in case of convergence, the concerning coefficients are squared and summed up. This sum is defined as residual off-diagonality (ROD). It is a measure for the convergence. The ROD is expected to tend to zero for $l \to \infty$. Note that the term "off-diagonality" is meant in the broadest sense, i.e. the definition of the generator determines which elements shall be kept for $l \to \infty$ and these elements are defined as diagonal parts of the Hamiltonian. The RODs depicted within this thesis are always normalised to the initial ROD.

With the decrease of the ROD the designated effective Hamiltonian is approached. If the ROD falls below a certain threshold specifying the precision of the result (usually $\approx 10^{-15}$), the integration can be considered as completed. The origin of divergencies is discussed in Section 2.5 in the context of the adaption of the generator. The number of coefficients is of the order of magnitude of up to 10^5 for the models considered in this thesis.

4 Undoped Antiferromagnetic Spin-$\frac{1}{2}$ Ladders

4.1 Model

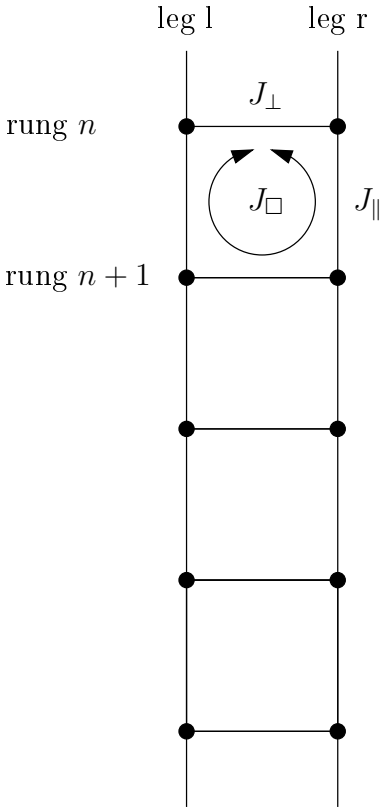

Figure 4.1: Undoped spin ladder.

An undoped ladder consists of two Heisenberg spin chains coupled to each other (see Figure 4.1). The ladder will be treated as a half-filled spin-$\frac{1}{2}$ model without electron hopping but only with magnetic spin interactions. If we just take into account nearest neighbour interactions (with the coupling $J_\perp$ along the rungs of the ladder and the coupling $J_\parallel$ parallel to the legs of the ladder), the Hamiltonian reads

$$H = J_\perp \sum_n \vec{S}_{n,\mathrm{l}} \cdot \vec{S}_{n,\mathrm{r}} + J_\parallel \sum_{n,\alpha} \vec{S}_{n,\alpha} \cdot \vec{S}_{n+1,\alpha} \quad (4.1)$$

where $\vec{S}_{n,\alpha}$ denotes the spin vector for the site on rung $n \in \mathbb{Z}$ and on leg $\alpha \in \{\mathrm{l}, \mathrm{r}\}$. In the following the spin will be $\frac{1}{2}$ and we will consider the antiferromagnetic case that $J_\perp$ and $J_\parallel$ are both positive. This model describes a subsystem of the telephone number compounds $(\mathrm{Sr}, \mathrm{La}, \mathrm{Ca}, \mathrm{Y})_{14}\mathrm{Cu}_{24}\mathrm{O}_{41}$ (see Section 1.1). The influence of the couplings $J_\perp$ and $J_\parallel$ is also illustrated in Figure 4.1. The coupling $J_\square$ also appearing in this figure is discussed later within this section.

Usually the spin ladders within the telephone number compounds are hole-doped. However, in this chapter the undoped spin ladder is discussed, which

does not consider the charge carriers. This case is realised in $La_6Ca_8Cu_{24}O_{41}$ [32] and approximately realised in $La_{5.2}Ca_{8.8}Cu_{24}O_{41}$ [42]. The doped ladder including the charge carriers in form of holes is discussed in Chapter 5.

If the ratio $x = \frac{J_\parallel}{J_\perp}$ goes to infinity for bounded $J_\parallel$, the two legs are decoupled and can be treated as two independent Heisenberg chains.

In the case $x = 0$ the rungs are decoupled and form independent dimers. Then the ground state for the antiferromagnetic case is composed of rung singlet states

$$|0\rangle = \bigotimes_n |\text{singlet}\rangle_n = \bigotimes_n \frac{1}{\sqrt{2}} \left(|\uparrow\downarrow\rangle - |\downarrow\uparrow\rangle\right)_n . \tag{4.2}$$

The excitations are rung triplet states for $x = 0$.

The state $|0\rangle$ is a suitable reference state for the CUT as it exhibits the properties required according to Section 2.3. For $x > 0$ this state is no longer the ground state and the actual ground state is unknown since the explicit operator that performs the SCUT cannot be determined. Yet as long as x is not too large the singlet is the dominant part and this reference state is reasonable. The elementary excitations are triplons, i.e. triplet states dressed with the magnetic interactions with their environment. We do not want to use the term "magnon" for these magnetic excitations because this term is usually associated with quasiparticles in systems that exhibit long-range magnetic order (which is not the case for the triplons). Moreover triplons feature a threefold degeneracy based on their $S = 1$ character [64].

For the triplet states we choose the so-called bond operator representation [65]. The creation operators $t^\dagger_{\alpha,n}$ with $t^\dagger_{\alpha,n} |\text{singlet}\rangle_n = |t_\alpha\rangle_n$ and the according annihilation operators $t_{\alpha,n}$ correspond to the states

$$|t_x\rangle_n = \frac{-1}{\sqrt{2}} \left(|\uparrow\uparrow\rangle - |\downarrow\downarrow\rangle\right)_n \tag{4.3a}$$

$$|t_y\rangle_n = \frac{\mathrm{i}}{\sqrt{2}} \left(|\uparrow\uparrow\rangle + |\downarrow\downarrow\rangle\right)_n \tag{4.3b}$$

$$|t_z\rangle_n = \frac{1}{\sqrt{2}} \left(|\uparrow\downarrow\rangle + |\downarrow\uparrow\rangle\right)_n . \tag{4.3c}$$

These states are aligned along the x-, y- and z-axis of the spin space. Due to the SU(2) symmetry of the spins this basis is advantageous. Its benefit is seen in the

representation of the Hamiltonian:

$$\begin{aligned}\frac{H}{J_\perp} &= H_\perp + xH_\parallel = \sum_{n,\alpha} t^\dagger_{n,\alpha} t_{n,\alpha} \\ &+\frac{x}{2}\sum_n \Bigg[\sum_\alpha t^\dagger_{n,\alpha} t_{n+1,\alpha} + t^\dagger_{n+1,\alpha} t_{n,\alpha} - \sum_{\alpha\neq\beta} t^\dagger_{n,\alpha} t^\dagger_{n+1,\alpha} t_{n,\beta} t_{n+1,\beta} \\ &+ \sum_{\alpha\neq\beta} t^\dagger_{n,\alpha} t^\dagger_{n+1,\beta} t_{n,\beta} t_{n+1,\alpha} + \sum_\alpha t^\dagger_{n,\alpha} t^\dagger_{n+1,\alpha} + t_{n,\alpha} t_{n+1,\alpha}\Bigg] .\end{aligned} \tag{4.4}$$

The invariance under rotations in spin space by $\frac{\pi}{2}$ about the principal axes S_x, S_y and S_z is manifest in this representation in contrast to the usual representation based upon the S_z component of the concerning triplet state. For instance, a clockwise rotation by $\frac{\pi}{2}$ about the z-axis, which changes $|t_x\rangle_n$ into $|t_y\rangle_n$, $|t_y\rangle_n$ into $-|t_x\rangle_n$ and does not change $|t_z\rangle_n$, leaves H unchanged. Note that the energy of the reference state $|0\rangle$ was set to zero in this Hamiltonian by adding the energy $\frac{3}{4}J_\perp$ to the local operator $J_\perp \vec{S}_{n,\mathrm{l}} \cdot \vec{S}_{n,\mathrm{r}} = J_\perp \left(-\frac{3}{4}\mathbb{1}_n + \sum_\alpha t^\dagger_{n,\alpha} t_{n,\alpha}\right)$, which is the diagonal part of the Hamiltonian in our representation.

The effects of the spin symmetries are discussed in Appendix A. An obvious consequence is the saving of memory and time, but also numerical improvements are implied.

Because the hybridization path around the Cu_4O_4 square plaquettes (cf. Figure 1.3) is strong, the influence of the four-spin interactions belonging to these plaquettes (i.e. two neighbouring rungs) is not negligible [66]. These interactions are referred to as ring exchange (also cyclic exchange) and can be expressed by the operators Π_p and Π_p^{-1}, which permutate the spins of the plaquette p clockwise and counterclockwise respectively. The complete ring exchange Hamiltonian reads

$$J_\square H^c_\square = \frac{J_\square}{4}\sum_p \left(\Pi_p + \Pi_p^{-1}\right) . \tag{4.5}$$

The action of this term is illustrated in Figure 4.1. In the spin operator representation the ring exchange Hamiltonian is expressed by

$$\begin{aligned}J_\square H_\square &= J_\square \sum_n \left(\vec{S}_{n,\mathrm{l}} \cdot \vec{S}_{n+1,\mathrm{l}}\right)\left(\vec{S}_{n,\mathrm{r}} \cdot \vec{S}_{n+1,\mathrm{r}}\right) \\ &+ \left(\vec{S}_{n,\mathrm{l}} \cdot \vec{S}_{n,\mathrm{r}}\right)\left(\vec{S}_{n+1,\mathrm{l}} \cdot \vec{S}_{n+1,\mathrm{r}}\right) - \left(\vec{S}_{n,\mathrm{l}} \cdot \vec{S}_{n+1,\mathrm{r}}\right)\left(\vec{S}_{n,\mathrm{r}} \cdot \vec{S}_{n+1,\mathrm{l}}\right) .\end{aligned} \tag{4.6}$$

Actually the complete ring exchange $H^c_\square$ also includes two-spin terms for all two-spin combinations of the four spins on two neighbouring rungs. Yet the

contributions from the terms coupling the spins along the rungs and parallel to the legs are merged with the terms $H_\perp$ and $H_\parallel$ so that the coupling constants $J_\perp$ and $J_\parallel$ include these contributions, whereas the terms coupling the spins diagonally can be neglected here because their prefactor is only of the order of 3% of $J_\perp$ [67]. The complete representation of the ring exchange using spin operators can be found in Ref. [68].

In analogy to x we define $x_\square = \frac{J_\square}{J_\perp}$. The term $H_\square$ is of importance for the quantitative comparison with the experimental data for both the two-dimensional Heisenberg lattice [66, 69–71] and the Heisenberg ladder [42, 68, 72–77]. Although one could fit the neutron scattering results for the spin ladders [68, 72, 73] to a model without ring exchange, this would imply that x was of the order of 2. But due to the fairly isotropic geometrical structure of the ladders no essential differences between $J_\perp$ and $J_\parallel$ are expected. An inclusion of the ring exchange yields $x \approx 1.2$ and $x_\square \approx 0.2$ [75]. The infrared absorption [42] and the Raman spectroscopy [74] also suggest that $x \approx 1.2$. For $La_4Sr_{10}Cu_{24}O_{41}$ inelastic neutron scattering determines $x = 1.5$ and $x_\square = 0.25$ [78].

Also the theoretical derivation of Heisenberg models for spin ladders from one-band [19, 79, 80] and three-band Hubbard models [67, 81–83] provides evidence that $x_\square$ is of the order of 0.2.

While the triplon gap Δ remains finite for all values of x without the ring exchange [34, 84], the gap closes with growing $x_\square$. Then the ground state is no longer dominated by singlets on the rungs and hence the reference state $|0\rangle$ no longer suits our purpose [85, 86]. Therefore the SCUT yields unphysical results approaching this phase transition and diverges finally (see Section 4.3.1).

In the bond operator representation the ring exchange term (except for a constant $\frac{9}{16}\mathbb{1}_n$ in the local term neglected here) reads

$$\begin{aligned} J_\square H_\square &= J_\square \sum_n \sum_\alpha \left[-\frac{3}{2} t^\dagger_{n,\alpha} t_{n,\alpha} + \frac{1}{4} \left(t^\dagger_{n,\alpha} t_{n+1,\alpha} + t^\dagger_{n+1,\alpha} t_{n,\alpha} \right) \right. \\ &\quad \left. - \frac{1}{4} \left(t^\dagger_{n,\alpha} t^\dagger_{n+1,\alpha} + t_{n,\alpha} t_{n+1,\alpha} \right) \right] + \sum_{\alpha,\beta} t^\dagger_{n,\alpha} t^\dagger_{n+1,\beta} t_{n,\alpha} t_{n+1,\beta}. \end{aligned} \tag{4.7}$$

All terms except the last one already appear in the Hamiltonian without ring exchange. This new term belongs to the diagonal part of the Hamiltonian because

it is a density-density term. The complete Hamiltonian divided by $J_\perp$ reads

$$\begin{aligned}\frac{H}{J_\perp} &= H_\perp + xH_\parallel + x_\square H_\square = \left(1-\frac{3}{2}x_\square\right)\sum_{n,\alpha} t^\dagger_{n,\alpha}t_{n,\alpha} \\ &+\sum_n\Bigg[\sum_\alpha\left(\frac{x}{2}+\frac{x_\square}{4}\right)\left(t^\dagger_{n,\alpha}t_{n+1,\alpha}+t^\dagger_{n+1,\alpha}t_{n,\alpha}\right) \\ &-\frac{x}{2}\sum_{\alpha\neq\beta} t^\dagger_{n,\alpha}t^\dagger_{n+1,\alpha}t_{n,\beta}t_{n+1,\beta}+\frac{x}{2}\sum_{\alpha\neq\beta} t^\dagger_{n,\alpha}t^\dagger_{n+1,\beta}t_{n,\beta}t_{n+1,\alpha} \\ &+\left(\frac{x}{2}-\frac{x_\square}{4}\right)\sum_\alpha\left(t^\dagger_{n,\alpha}t^\dagger_{n+1,\alpha}+t_{n,\alpha}t_{n+1,\alpha}\right) \\ &+x_\square\sum_{\alpha,\beta} t^\dagger_{n,\alpha}t^\dagger_{n+1,\beta}t_{n,\alpha}t_{n+1,\beta}\Bigg]\end{aligned} \tag{4.8}$$

and includes all terms which are relevant for an appropriate description of the spin ladder.

Note that H is invariant under the parity operation P, which is illustrated in Figure 4.2. The parity of a singlet state with respect to P is odd, whereas the parity of a triplon is even. Therefore the creation or annihilation of an odd number of triplons violates the parity, while the parity is conserved if the triplon number is changed by an even number. The terms of H either conserve the triplon number or change it by two. Hence the parity is conserved by H.

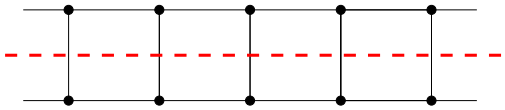

Figure 4.2: Illustration of the parity operator P, which reflects about the red axis.

4.2 Truncation

The finite energy gap Δ of the triplons [35, 36] is equivalent to a correlation between the triplons which is exponentially decreasing with respect to the distance. Hence a truncation in real space is feasible. The extension in real space shall be used as a measure for the physical importance of a term of the Hamiltonian. In our quasi one-dimensional spin ladder the extension of a term is defined as

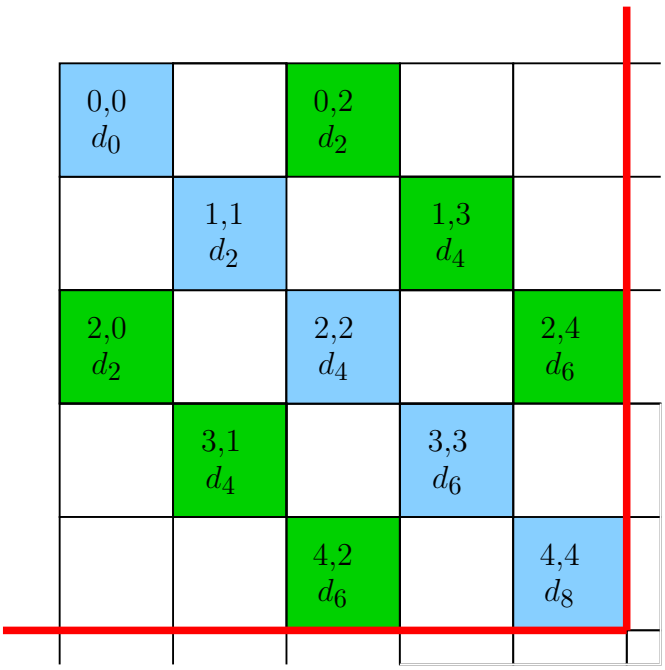

Figure 4.3: Schematic representation for a truncation of the undoped ladder Hamiltonian $H(l)$: Each coloured (n_c, n_a)-block represents contributions to $H(l)$ creating n_c particles after annihilating n_a particles. The d_n are the maximal extensions relevant for the blocks in which they appear. The red line indicates a maximal particle number $N = 4$, i.e. terms cut off by the red line are omitted. The blue blocks are the particle conserving terms that remain the only contributions for $l \to \infty$ in case of a converging pc CUT. The green blocks are the contributions to the pc generator, which go to zero for $l \to \infty$.

the difference between the smallest and the largest rung index of the local operators within the term. For higher-dimensional lattices an extension defined in the taxicab metric is easy to handle.

The simplest way of truncating would be one maximal extension in real space for all terms. Terms exceeding this limit would be omitted. But this approach is not reasonable in our case. The number of possible terms increases more strongly with the maximal extension for terms consisting of more local operators. However, terms consisting of less operators are usually more important in the sense that higher extensions should be taken into account for terms with less operators. For instance, the coefficient of a one-particle hopping term consisting of two local operators is usually larger than the coefficient of a two particle interaction term

consisting of four local operators if they both have the same extension. Therefore different maximal extensions d_n are defined in units of the rung distance where n is the number of local operators of the concerned term.

Additionally a maximal particle number N is defined for the operators, i.e. terms affecting higher particle numbers than N are completely omitted even if the corresponding d_n is larger than zero. Figure 4.3 shows the truncation for the undoped ladder schematically for $H(l)$. The restriction $N = 4$ rejects all terms outside the red line. Because only terms changing the particle number by two or conserving the particle number occur in the starting Hamiltonian (4.4) or (4.8) respectively, the number of local operators in a term is always even during the flow and the Hamiltonian only consists of the coloured blocks in the figure[1]. The total number of local operators is equal for the terms of the diagonals from left bottom to right top. Therefore all blocks of each of these diagonals share the same maximal extension d_n. The parameter d_0 for the (0, 0)-block is meaningless as this block contains only the non-local unity operator for the whole ladder, i.e. a constant energy contribution. This truncation scheme, which we use within this thesis, is not compulsory. Other schemes could be implemented, which use different classifications for the groups of terms sharing the same maximal extension.

An important point is that a truncation of the operators does not affect the Hilbert space. Actually we do not reduce the Hilbert space at all. A maximal particle number for the operators does not restrict the possible number of particles because we work in second quantisation on the infinite system. A (n_c, n_a)-block affects all states with n_a particles or more. Therefore the (1, 1)-block acts on all states that exhibit triplon excitations of arbitrary number larger than zero. Actually the multi-particle continua are mainly determined by the one-particle dispersion and can be made more accurate by including two-particle interactions.

[1] The conservation of the parity with respect to P, which was introduced in the preceding section, forbids the change of the triplon number by an odd value as the parity of one triplon is odd.

4.3 Results for the pc Generator

4.3.1 One-Triplon Dispersion

The dispersion for one triplon can be easily deduced from the effective Hamiltonian, which conserves the number of triplons. The (1, 1)-block has the structure

$$H_{1,1} = \sum_{d=-d_2}^{d_2} \sum_{n,\alpha} a_d t^\dagger_{n+d,\alpha} t_{n,\alpha} \tag{4.9}$$

where the hopping processes are restricted by the maximal extension d_2. The coefficients a_d are calculated by SCUT. A Fourier transformation diagonalises $H_{1,1}$ in the one-particle space. We consider a one-triplon-state with a concrete flavour $\alpha \in \{x, y, z\}$ because the three flavours are equivalent due to the SU(2) symmetry of the spins. The one-triplon dispersion $\omega_{1\mathrm{t}}(k)$, i.e. the one-triplon energy relative to the ground state, can be identified as the Fourier transform of $H_{1,1}$ applied to a one-triplon state, which is

$$\omega_{1\mathrm{t}}(k) = a_0 + \sum_{d=1}^{d_2} 2a_d \cos(dk) \tag{4.10}$$

with the rung distance set to one.

At first let us consider $x_\square = 0$. For small x the coefficients a_d with $d > 1$ are negligibly small and the one-triplon dispersion is

$$\frac{\omega_{1\mathrm{t}}(k)}{J_\perp} \approx 1 + x\cos(k). \tag{4.11}$$

Increasing x causes a growing dip in the dispersion at $k = 0$. This is illustrated by the one-triplon dispersions for $x = 0.5$, $x = 1$ and $x = 1.5$ shown in Figure 4.4 compared to the PCUT results. The dip at small momenta is due to the closeness of the three-triplon continuum which lies energetically above (cf. Section 4.3.2). The two-triplon continuum has no influence on the one-triplon dispersion as the triplon number can only be changed by even values. The lowering of the one-triplon energy observed here is included within the SCUT without further effort. In contrast the PCUT is in need of additional extrapolations to incorporate this feature [27]. The energy minimum is also located at $k = \pi$. The gap decreases with ascending x, but it stays finite when $x \to \infty$ for $J_\parallel = \text{const}$ where the ladder turns into two independent chains [34, 84].

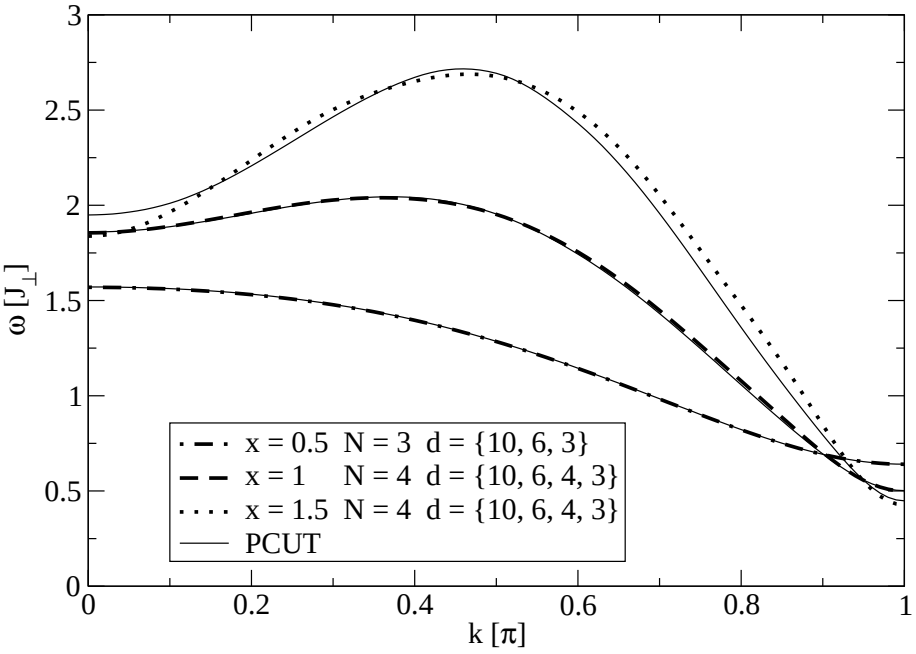

Figure 4.4: One-triplon dispersion for $x_\Box = 0$: Comparison between PCUT and SCUT with the maximal extension $d = \{d_2, d_4, d_6, d_8\}$.

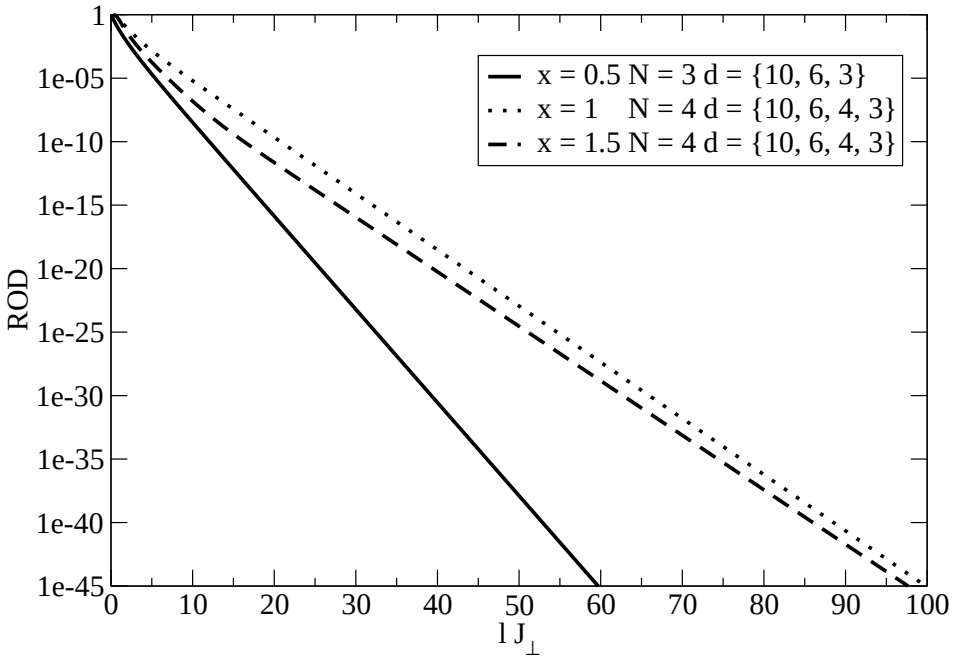

Figure 4.5: ROD for $x_\Box = 0$ and various values of x according to the dispersions of Figure 4.4.

The maximal extensions d_n have to be adjusted to the parameters of the model. For an accurate one-triplon dispersion result for $x = 0.5$, $x_\square = 0$ the truncation $N = 3$, $d_2 = 10$, $d_4 = 6$ and $d_6 = 3$ is necessary and sufficient. The relative deviation to the PCUT results [27] is less than 1%. Also the agreement with the results derived by series-expansion [87], exact diagonalisation [68] and DMRG [75] is very good. Thus increasing N or the d_n beyond these values is not requisite. As the two- and the four-triplon continuum already show a small overlap for $x = 0.5$, $x_\square = 0$ in the region $k \lesssim 0.6\pi$ (as shown in Section 4.3.2), a truncation scheme including more extended terms is expected to lead to divergence. If transitions between subspaces with different quasiparticle numbers are possible, the CUT created by the pc generator should theoretically diverge because the sorting of the eigenenergies with respect to the quasiparticle number is not possible [23, 26]. Truncating the terms responsible for the divergence, however, may yield convergence again (see Section 2.2). For the given example the actual divergence is caused by long-range terms, which are neglected by our truncation. Nevertheless, the crucial physical properties are retrieved by the short-range terms included.

The residual off-diagonality (ROD) defined as the sum over the squared matrix elements which are part of the generator[2] show an exponential decay (cf. Section 3.6). The ROD according to the three dispersions in Figure 4.4 are shown in Figure 4.5.

The case $x = 1$, $x_\square = 0$ is more interesting because the overlap between the two- and the four-triplon continuum is larger and it is present for all values of k (see Section 4.3.2). But for the truncations implemented within this thesis the SCUT still converges. The expected divergence would also be induced by terms of considerably larger extensions. Figure 4.6 depicts several one-triplon dispersion results generated by SCUT, which differ in their maximal extensions. The PCUT result is also shown for comparison. There are deviations between the methods for small momenta. The SCUT result seems to converge towards a dispersion which has a slightly less pronounced dip [3]. Nevertheless, this result is within the error bounds of the PCUT dispersion. We will come back to these deviations

[2] For the pc generator the ROD contributions consist of all the non-diagonal blocks of the Hamiltonian while for the adapted generators every term that is not part of the generator shall be considered as diagonal even if some terms are actually non-diagonal.

[3] The difference between the results for the truncations $d = \{10, 8, 6, 4\}$ (which is not shown here) and $d = \{10, 8, 6, 5\}$ is of the order of 0.01%.

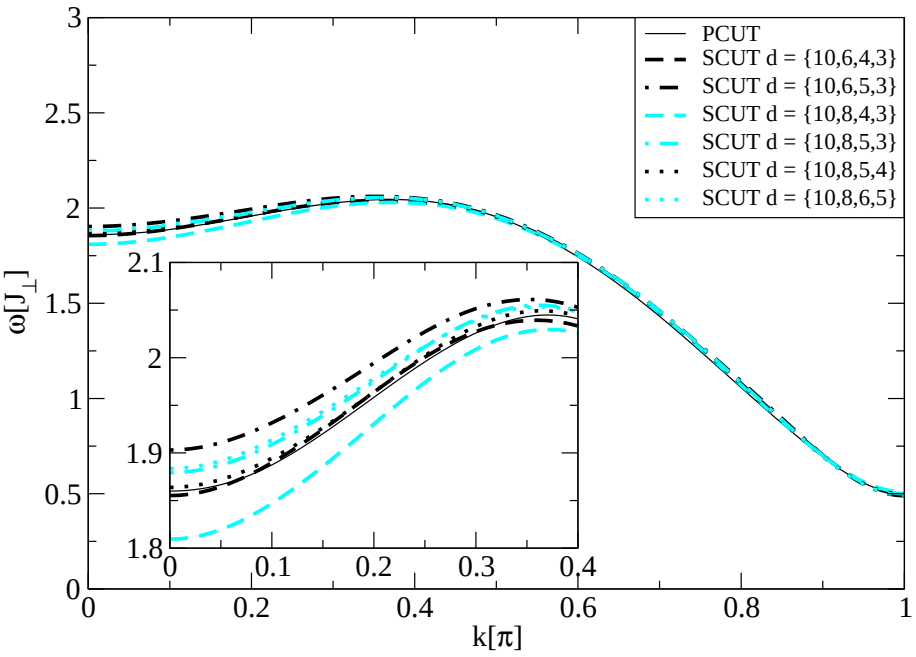

Figure 4.6: One-triplon dispersion for $x = 1, x_\square = 0$: Comparison between PCUT and SCUT with different truncations with $N = 4$ and maximal extension $d = \{d_2, d_4, d_6, d_8\}$.

and discuss the possibilities of their origin in the final discussion for the undoped ladder (see Section 4.5).

For $x = 1.5$ and $x_\square = 0$, it is not possible to obtain results for truncations distinctly higher than $N = 4$, $d_2 = 10$, $d_4 = 6$, $d_6 = 4$ and $d_8 = 3$ (shown in Figure 4.4). A further increase of the extensions leads to divergence. Thus the influence of the overlap between the two- and the four-triplon continuum is already noticeable. Yet an adaption of the generator can eliminate this influence on the convergence. This adaption is discussed in Section 5.3.

The ring exchange lowers the one-triplon dispersion. This is illustrated by the dispersions for $x = 1$ and various values for $x_\square$ in Figure 4.7. Once the one-triplon gap closes, a phase transition takes place. The ground state is no longer dominated by singlet states on the rungs but by singlet states staggered along the ladder [85]. For $x = 1$ this transition happens at $x_\square \approx 0.5$ (see Ref. [86][4]). Our representation, in which excitations are dominated by triplet states on the rungs, is no longer feasible for a real space truncation scheme because the correlations

[4]Note that within this reference $x_\square$ includes an additional factor $\frac{1}{2}$ and it is therefore half as large.

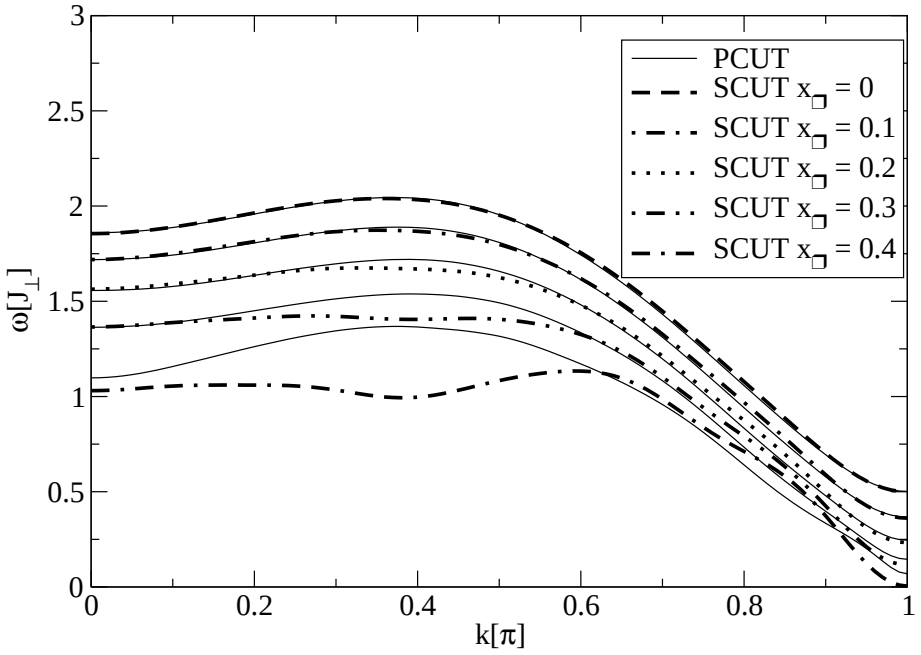

Figure 4.7: One-triplon dispersion for $x = 1$ and various values of $x_\square$: Comparison between PCUT and SCUT with $N = 4$ and maximal extensions $d_2 = 10, d_4 = 6, d_6 = 4, d_8 = 3$.

between excitations do not remain locally restricted for a gapless dispersion. The vicinity of the phase transition becomes noticeable in the quality of the SCUT result. Note that the decline of the quality is only due to the real space truncation. When the gap becomes less pronounced, terms with much larger extensions have to be taken into account.

While the agreement between PCUT and SCUT is good for $x_\square$ up to 0.2, already for $x_\square = 0.3$ deviations occur and the shape of the SCUT result begins to lose its smoothness. This effect is even more pronounced for $x_\square = 0.4$. For $x_\square = 0.5$ the flow diverges. The slowing down of the convergence with increasing ring exchange and its eventual loss can be seen in Figure 4.8 where the residual off-diagonality (ROD), which was defined in Section 3.6, is plotted.

4.3.2 Multi-Triplon Continua

The band edges of the multi-triplon continua can be determined from the one-triplon dispersions. For a complete n-triplon continuum the interactions of n and less triplons have to be included. However, only binding effects for two

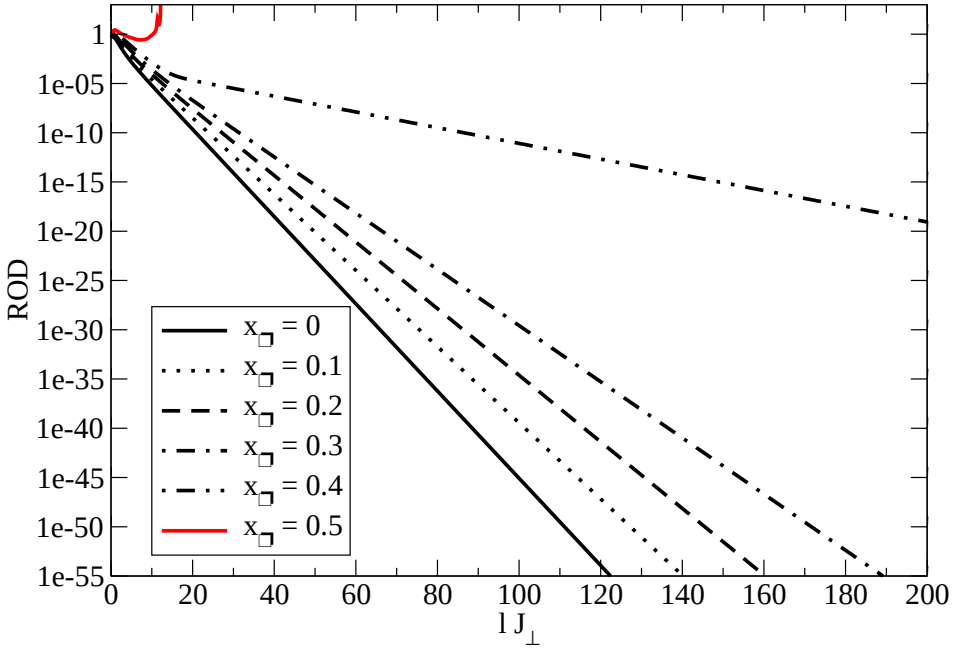

Figure 4.8: ROD for $x = 1$ and various values of $x_\square$ corresponding to the dispersions in Figure 4.7. For $x_\square \leq 0.4$ the SCUT converges, for $x_\square = 0.5$ it diverges.

triplons have a detectable influence on the boundaries of the continua [61]. In the following only the two-triplon bound states [42, 88–95], which correspond to these two-triplon binding effects, will be considered.

For the calculation of the two-triplon bound states the (2, 2)-block of the effective Hamiltonian

$$H_{2,2} = \sum_{\substack{n,\alpha,\beta,\gamma,\delta \\ d,r,d'}} a_{d,r,d'} t^\dagger_{n+r+d',\alpha} t^\dagger_{n+r,\beta} t_{n+d,\gamma} t_{n,\delta} \tag{4.12}$$

$$\text{with} \quad |d|, |d'|, |r|, |r+d'|, |r-d|, |r+d'-d| < d_4$$

has to be diagonalised in addition to the (1, 1)-block. The initial distance between the triplons d, the final distance d' and the displacement r are restricted by the maximal extension d_4. Due to spin conservation for each operator one of the following relations between α, β, γ and δ holds true

$$\alpha = \beta \quad = \quad \gamma = \delta \tag{4.13a}$$

$$\alpha = \beta \quad \neq \quad \gamma = \delta \tag{4.13b}$$

$$\alpha = \delta \quad \neq \quad \beta = \gamma \tag{4.13c}$$

$$\alpha = \gamma \quad \neq \quad \beta = \delta\,. \tag{4.13d}$$

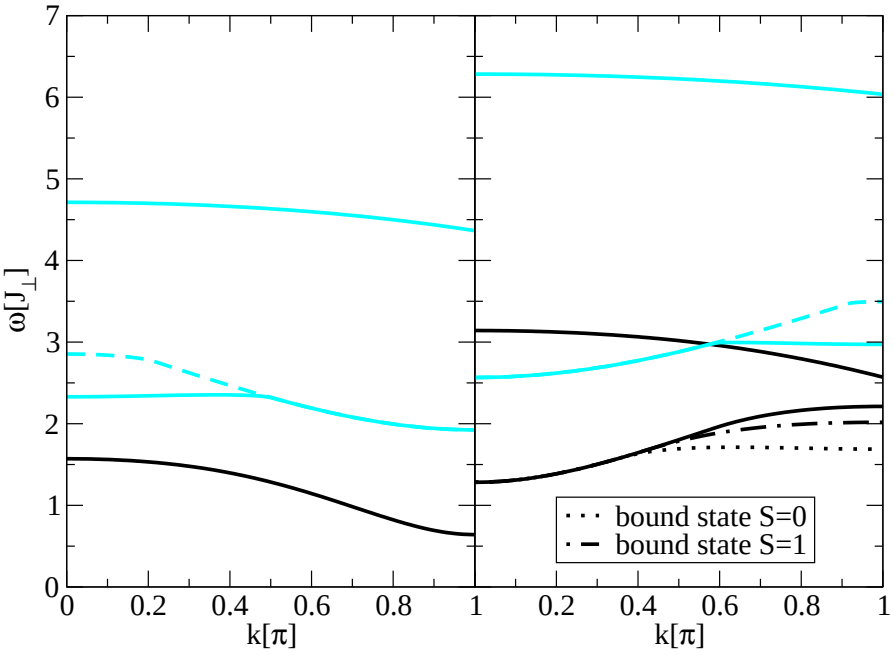

Figure 4.9: Triplon continua for $x = 0.5$, $x_\square = 0$: On the left side the one-triplon dispersion (black) and the boundaries of the three-triplon continuum (cyan) and on the right side the boundaries of the two-triplon continuum (black), the two-triplon bound states and the boundaries of the four-triplon continuum (cyan) are displayed. The dashed lines (in each panel) represent the boundaries of the continua without consideration of the two-triplon binding effects.

A two-triplon state $|K, d, S, m\rangle$ is characterised by the total momentum K, the distance between the triplons d, the total spin S and the magnetic quantum number m. The action of the (1, 1)-block

$$H_{1,1}\,|K, d, S, m\rangle = 2\sum_{d'\neq d} a_{d'} \cos\left(\frac{Kd'}{2}\right) (\mathrm{sign}(d-d'))^S\,|K, |d-d'|, S, m\rangle \quad (4.14)$$

and the action of the (2, 2)-block

$$H_{2,2}\,|K, d, S, m\rangle \quad (4.15)$$
$$= \left(\sum_{d'} a_{d,\frac{d-d'}{2},d'} + 2\sum_{r>\frac{d-d'}{2},d'} a_{d,r,d'} \cos\left(K\left(r-\frac{d-d'}{2}\right)\right)\right)|K, d', S, m\rangle$$

yield all matrix elements relevant for the two-particle subspace. Note that $a_{d,\frac{d-d'}{2},d'} = 0$ for $\frac{d-d'}{2} \notin \mathbb{Z}$. The part of H_{eff} acting on the two-particle space is still non-

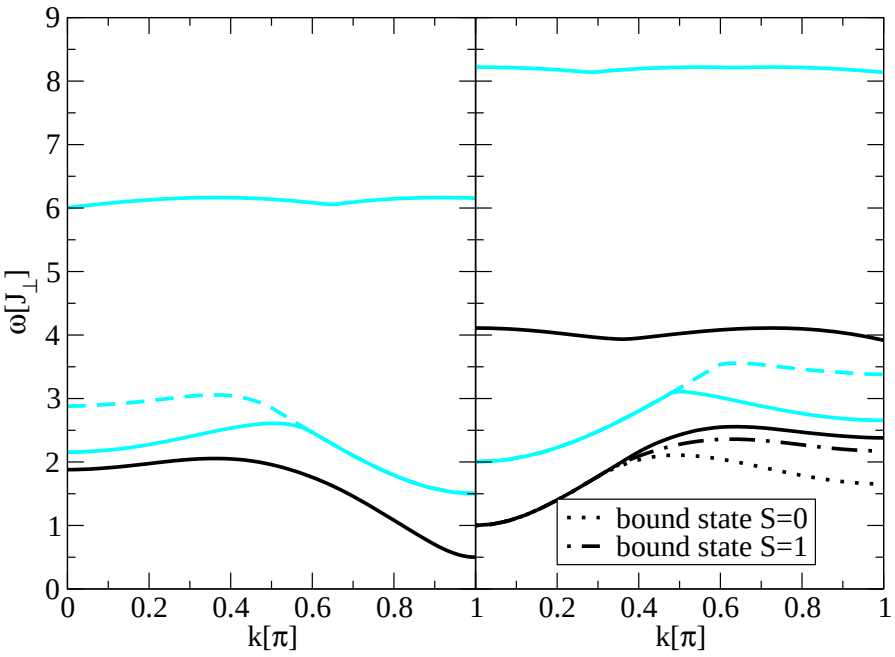

Figure 4.10: Triplon continua for $x = 1$, $x_\square = 0$: On the left side the one-triplon dispersion (black) and the boundaries of the three-triplon continuum (cyan) and on the right side the boundaries of the two-triplon continuum (black), the two-triplon bound states and the boundaries of the four-triplon continuum (cyan) are displayed. The dashed lines (in each panel) represent the boundaries of the continua without consideration of the two-triplon binding effects.

diagonal with respect to d in this representation. Therefore a Lanczos algorithm is applied to the matrix. A detailed description of the diagonalisation of H_{eff} can be found in Ref. [48].

For $x = 0.5$ and $x_\square = 0$, the overlap between the two- and the four-particle continuum is already present. In Figure 4.9 this case is depicted. The graphs for the odd and the even triplon numbers are separated because only transitions are allowed that change the particle number by two. In the region $0 < k \lesssim 0.6\pi$ the lower boundary of the four-particle continuum lies below the upper boundary of the two-particle continuum. In the preceding section it was shown that this overlap is weak enough that its hindering influence on the convergence can be excluded by the truncation while the decisive physical properties are included.

The dispersions of the two-triplon bound states are also presented in Figure 4.9. For small momenta these dispersions are absorbed by the two-triplon continuum

and hence no binding occurs. If the two-triplon binding effects are included in the calculation of the continua with more than two particles, the lower boundary of the three-triplon continuum is lowered for $k \lesssim 0.49\pi$ and the lower boundary of the four-triplon continuum is lowered for $k \gtrsim 0.58\pi$.

For $x = 0.5$ and $x_\square = 0$, the gap between the one-triplon dispersion and the three-triplon continuum is manifestly too large to produce an appreciable deviation from the dominating cosine shape of the one-triplon dispersion even if the two-triplon interactions are considered. This deviation in form of a dip at $k = 0$ caused by the approaching three-triplon continuum becomes relevant for increasing x only (cf. Section 4.3.1). For $x = 1$ and $x_\square = 0$ this dip is present and also the proximity of the three-triplon continuum to the one-triplon dispersion can be observed if the two-triplon interactions are included in the three-triplon continuum (see Figure 4.10). The results gained by the SCUT are again in very good agreement with the PCUT results [96].

Although the distinct overlap between the two- and the four-particle continuum ranges over all values of k for $x = 1$, it does not hinder the convergence of the transformation for the considered truncations. The two-triplon bound states also change their dispersion qualitatively with increasing x. For the $S = 1$ bound state the maximum of the dispersion moves away from $k = \pi$ (to $k \approx 0.63\pi$ for $x = 1$) and the maximum of the $S = 0$ dispersion increases distinctly in relation to the rest of the curve.

4.4 Generator Adaption

For $x > 1$ the SCUT with the pc generator is affected by the overlap of the two- and four-triplon continuum relatively rapidly when the maximal extensions are increased. The convergence worsens accordingly. To solve this problem a generator adaption is advisable. The idea of excluding terms from the generator introduced in Section 2.5 is the method of choice here. The CUT induced by the pc generator diverges because it is not able to sort the eigenenergies of the overlapping two- and the four-particle space according to the triplon number. The terms that are responsible for the transitions between these two subspaces are the terms with either four creation and two annihilation operators or vice versa. If these terms are excluded from the generator, we expect the CUT to converge despite the overlap (cf. Ref. [26]). The corresponding generator is referred to as gs,1p (ground state, one particle) generator because it decouples the vacuum and

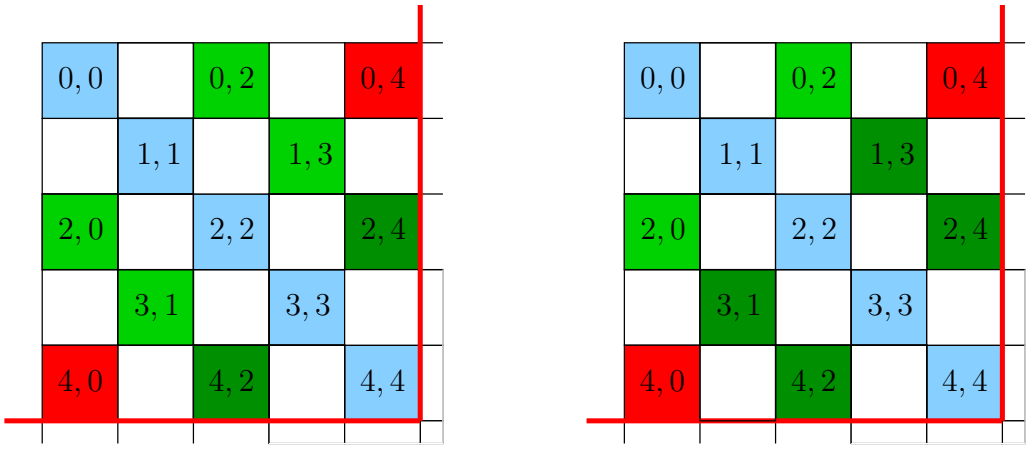

Figure 4.11: Schematic representation of the Hamiltonian $H(l)$ for the undoped ladder using a gs,1p generator and a gs generator: Each coloured (n_c, n_a)-block represents contributions to $H(l)$ creating n_c particles after annihilating n_a particles. The blue blocks contain the particle conserving terms. The light green blocks are the contributions to the generators. The generators do not include the dark green blocks in contrast to the pc generator. Thus these blocks contain finite contributions for $l \to \infty$. The red blocks occur during a CUT induced by the adapted generators. This is not the case for a pc CUT, which preserves the block-band diagonal structure [23, 25, 44]. However, the contributions of the red blocks go to zero for $l \to \infty$ if the transformation converges.

the one-triplon space from the rest while the spaces with higher particle numbers remain coupled. Actually the three particle space is also decoupled from the rest as it only couples to the one-particle space due to the truncation parameter $N = 4$ and the restriction that the particle number can only be changed by even numbers. Nevertheless, the name gs,1p generator will be used because the decoupling of the subspaces with low particle numbers are the essential feature. A schematic representation of the transformation of the Hamiltonian is depicted in Figure 4.11. The two-triplon bound state dispersions are not directly computable from an effective Hamiltonian based on the gs,1p generator because the two-triplon subspace has to be decoupled for this purpose. However, the one-triplon dispersion can be derived as before (see Section 4.3.1).

In analogy we define the gs generator which decouples only the ground state. This generator contains only (0, n)- and (n, 0)-blocks. The behaviour of the Hamiltonian during the flow induced by the gs generator is also illustrated in

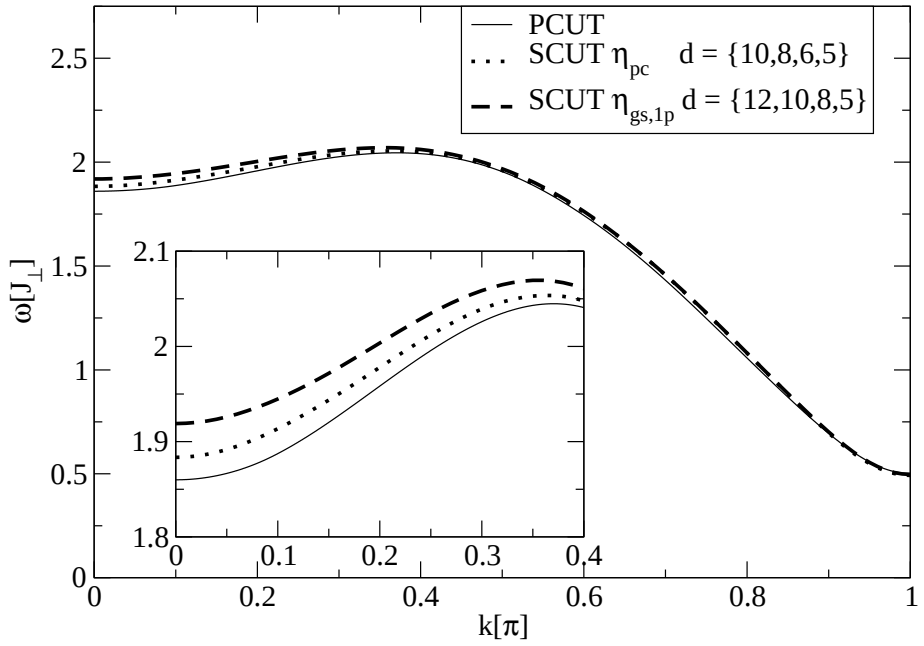

Figure 4.12: One-triplon dispersion for $x = 1, x_\square = 0$: Comparison between PCUT and SCUT with pc as well as gs,1p generator with $N = 4$ and maximal extension $d = \{d_2, d_4, d_6, d_8\}$.

Figure 4.11. The resulting effective Hamiltonian, however, yields no one-triplon dispersion if only its (1, 1)-block is taken into account because the one-triplon subspace is still coupled to the three-triplon subspace. Yet the Fourier transform of the (1, 1)-block yields an upper bound for the one-triplon dispersion due to the variational principle that a minimum in a restricted subspace is an upper bound to the minimum in an unrestricted subspace. At the end of this section we will present a gs result of the one-triplon dispersion for $x = 1.5$ that was achieved by an additional diagonalisation concerning the one- and three-triplon subspace using a Lanczos algorithm (cf. Ref [26]).

Before we consider the region $x > 1$ for which the generator adaption was designed, we compare the results of the pc and the gs,1p generator for $x = 1$, $x_\square = 0$ (see Figure 4.12). The gs,1p generator yields a one-triplon dispersion that deviates from the pc result in the region $k \lesssim 0.4\pi$. Although these deviations are small ($\approx 2\%$ at maximum), the difference is larger than numerical inaccuracies. The origin of these deviations is discussed in the next section.

In Figure 4.13 several one-triplon dispersion results for $x = 1.5$, $x_\square = 0$ are

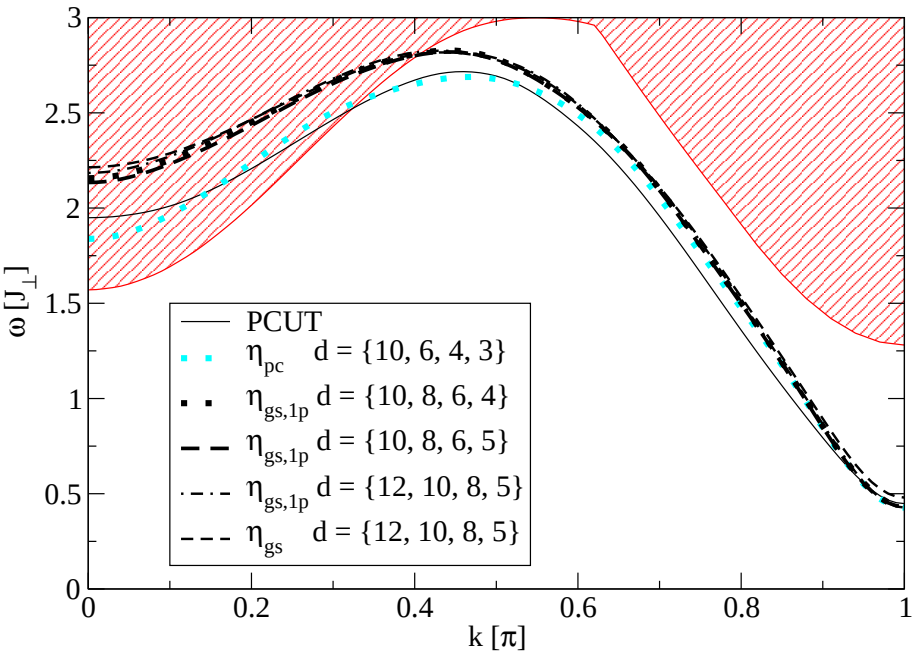

Figure 4.13: One-triplon dispersion for $x = 1.5$, $x_\square = 0$ with $N = 4$, $N_t = 2$, $d = \{d_2, d_4, d_6, d_8\}$: SCUT result for pc, gs,1p and gs generator compared to PCUT result. The red shaded area depicts the three-triplon continuum including two-triplon binding effects. This continuum was calculated from the pc result with $d = \{10, 6, 4, 3\}$.

compared. The SCUT was performed with the pc, the gs,1p and the gs generator. The PCUT results are also shown. All calculations yield the gap at $k = \pi$ in very good agreement. However, the deviations for the rest of the curve are significant for the different methods. While the SCUT results coincide for large k for both generators, the PCUT result already differs once k moves away from π. The different truncations for the gs,1p SCUT lead to similar results that only differ marginally at $k = 0$. Also the gs result is in very good agreement with the gs,1p result.

The lower boundary of the three-triplon continuum including two-triplon binding effects is also shown in Figure 4.13. The effective Hamiltonians from the gs,1p generator and from the gs generator yield no reliable result for the lower boundary of the three-triplon continuum because two-triplon binding effects cannot be considered due to the coupling to the four-triplon space, which is still present for $l \to \infty$. But the influence of the two-triplon binding effects is decisive for the closeness of one-triplon dispersion and three-triplon continuum (see Sec-

tion 4.3.2). Hence we used the pc result with $d = \{10, 6, 4, 3\}$. The one-triplon dispersion enters the three-triplon continuum for small momenta. This suggests that both the pc generator, which was also used for the PCUT, and the gs,1p encounter problems due to the sorting of the eigenenergies. In the next section we will discuss the reliability of the different one-triplon dispersion results in detail.

4.5 Discussion

For small x and $x_\square$ the SCUT and the PCUT yield results in very good agreement for the one-triplon dispersion and the boundaries of the multi-triplon continua. The overlap between the two- and the four-triplon continuum can be detected. Nevertheless, it does not hinder the convergence of the pc SCUT for the considered truncations as long as $x \lesssim 1.5$. The increase of x produces a growing dip at $k = 0$ in the one-triplon dispersion while the gap decreases yet remains finite and stays at $k = \pi$. Raising the ring exchange lowers the energy of the triplons until a phase transition to a ground state dominated by staggered singlets occurs.

With growing x also the deviations between SCUT and PCUT grow. The employment of the gs,1p generator, which is insensitive to the overlap between the two- and the four-triplon continuum and which allows the examination of higher values of x, leads to deviating results as well. However, the gap is still in good agreement for all CUT versions. In the PCUT results the dip at $k = 0$ is more pronounced than in the SCUT results. For the gs,1p SCUT the effect of the lowering of the one-triplon dispersion due to the approach of the three-triplon continuum in the region of small k is less pronounced.

The deviations between PCUT and SCUT for $x = 1.5$ have precursors at $x = 1$ (cf. Figure 4.6). For $x = 1$ the dip at $k = 0$ is already less pronounced for the SCUT result than for the PCUT result. Also the deviations for larger k are adumbrated for $x = 1$. The dispersions from the SCUT calculations lie all above the PCUT result in the k region from 0.55π to 0.91π. Even if this is hardly noticeable due to the slope of the curve, these deviations are of the order of 1% for the larger maximal extensions and slightly larger for the stricter truncations, i.e. for lower maximal extensions.

Although the extrapolations which estimate the effects of the approach of the energies of states with different triplon numbers are rather sophisticated, they become less precise when these effects increase. Thus a possible explanation for the deviations could be that the extrapolations for the perturbative ansatz

overestimate these effects. The SCUT could also underestimate the effect because operators affecting five triplons, which are excluded by the truncation, could cause an additional lowering. However, the influence of the five-triplon continuum is expected to be small because the spectral weight decreases with the number of quasiparticles [61]. The error bound of the extrapolated PCUT results is actually so large that it includes the SCUT results. In addition the results from the adapted generators seem to converge with increasing maximal extensions so that we conclude that the SCUT results induced by the adapted generators constitute an improvement over the PCUT result. Moreover, the one-triplon dispersion crosses the lower boundary of the three-triplon continuum. This also indicates that the pc results (including the PCUT result) are less reliable than the results from the adapted generators because this overlap leads to problems with respect to the sorting of the eigenvalues if the generator includes the (1, 3)- and the (3, 1)-block respectively. Although in principle the gs,1p generator can encounter such problems as well, in the present case its result is in very good agreement with the dispersion from the gs generator.

The regime $J_{\parallel} > J_{\perp}$ is still challenging for the CUTs although the generator adaption for the SCUT allows us to extend the calculations into this regime. As the gs,1p generator leaves the subspaces with two and four triplons coupled to each other, a subsequent transformation has to be found that allows the determination of the two-triplon bound states which yield an important contribution to the continua with more than two triplons. The Lanczos algorithm that was used to decouple the one- and the three-triplon subspace in case of the gs generator is not feasible for this purpose because it becomes too intricate if four-particle states are involved.

5 Hole-Doped Antiferromagnetic Spin-$\frac{1}{2}$ Ladders

5.1 Model

For the hole-doped ladder four additional rung states with one hole are possible:

$$|a_{\tau=1,\sigma=1}\rangle_n = \frac{1}{\sqrt{2}}\left(|\uparrow 0\rangle + |0 \uparrow\rangle\right)_n \tag{5.1a}$$

$$|a_{\tau=-1,\sigma=1}\rangle_n = \frac{1}{\sqrt{2}}\left(|\uparrow 0\rangle - |0 \uparrow\rangle\right)_n \tag{5.1b}$$

$$|a_{\tau=1,\sigma=-1}\rangle_n = \frac{1}{\sqrt{2}}\left(|\downarrow 0\rangle + |0 \downarrow\rangle\right)_n \tag{5.1c}$$

$$|a_{\tau=-1,\sigma=-1}\rangle_n = \frac{1}{\sqrt{2}}\left(|\downarrow 0\rangle - |0 \downarrow\rangle\right)_n \tag{5.1d}$$

where 0 denotes the hole. State (5.1a) and state (5.1b) have an S_z-spin of $+\frac{1}{2}$ while state (5.1c) and state (5.1d) have an S_z-spin of $-\frac{1}{2}$. The sign of the spin is indicated by σ. The parity with respect to P, which was introduced in Section 4.1, is denoted by τ. It is even for the states (5.1a), (5.1c) and odd for (5.1b), (5.1d). All these four states have fermionic properties regarding states on different rungs. They can be created from the local singlet by the application of the corresponding creation operators $a^\dagger_{\tau,\sigma,n}$ so that $a^\dagger_{\tau,\sigma,n}\,|\text{singlet}\rangle_n = |a_{\tau,\sigma}\rangle_n$.

A further possible rung state – the double hole state –

$$|d\rangle = |00\rangle \tag{5.2}$$

consists of a hole on each leg of the ladder. Hence $|d\rangle$ behaves like a boson in relation to the states of other rungs. However, in this thesis only one-hole states will be considered and hence this state $|d\rangle$ will be neglected. The local energy of $|d\rangle$ is also larger than the energy of the other states. Therefore $|d\rangle$ is expected to be also neglible for slightly doped ladders. So the local basis consists of eight

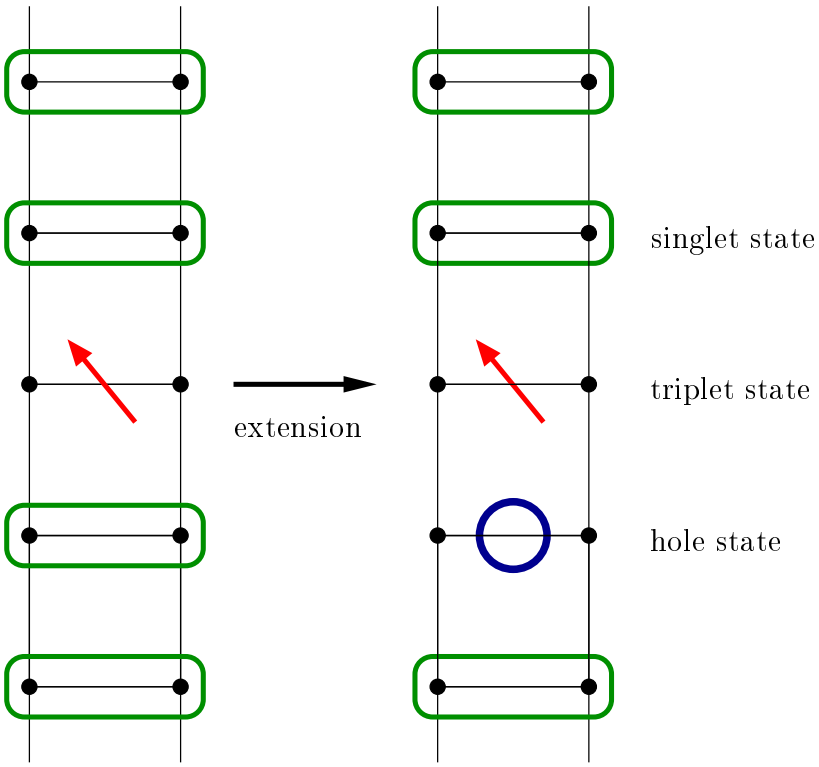

Figure 5.1: Extension of the spin ladder by inclusion of hole states in the basis of local states: While the undoped ladder (left hand side) has only singlet and triplet states (the latter with three possible flavours and total spin 1), the hole-doped ladder has four additional hole states which carry spin $\frac{1}{2}$. The difference between these four states consists in the sign of the spin z-component and the parity of the state.

states including the local reference state – i.e. the singlet. This reduction by one local state decreases the number of potential terms decisively[1].

The Hamiltonian incorporating the local one-hole states is extended by the next nearest neighbour electron hopping

$$H_{\text{hopping}} = -t_{\perp} \sum_{n,\alpha} c^{\dagger}_{\sigma,\alpha,n} c_{\sigma,\overline{\alpha},n} - t_{\parallel} \sum_{n,\alpha} c^{\dagger}_{\sigma,\alpha,n} c_{\sigma,\alpha,n\pm1} \tag{5.3}$$

with the constants $t_{\perp}$ for the hopping within the rung from one leg to the other and $t_{\parallel}$ for the hopping along the ladder from rung to rung. The electron creation and annihilation operators $c^{\dagger}_{\sigma,\alpha,n}$ and $c_{\sigma,\alpha,n}$ concerning an electron with spin $\sigma \in$

[1] If physical properties like charge or spin conservation did not forbid certain processes, the number of potential terms with a maximal extension of d would be exactly $s^{2d} - 1$ for a local basis with s states.

$\{-\frac{1}{2}, \frac{1}{2}\}$ act on leg $\alpha \in \{l, r\}$ and rung $n \in \mathbb{Z}$. These electron operators already contain hardcore properties as double occupancy is forbidden.

The Hamiltonian for the undoped ladder is extended by the hopping term and magnetic interaction terms affecting the hole states. Since the hole states $|a_{\tau,\sigma}\rangle_n$ also have spin $S = \frac{1}{2}$, they interact magnetically with the neighbouring states. The complete Hamiltonian reads

$$H = H_{\text{undoped}} + \sum_{j=0}^{9} H_j. \tag{5.4}$$

This Hamiltonian H is a t-J-model. The extension consists of the terms H_j given explicitly below. The terms are again divided by $J_\perp$ to obtain a dimensionless Hamiltonian. In analogy to $x = \frac{J_\parallel}{J_\perp}$ and $x_\square = \frac{J_\square}{J_\perp}$ the parameters $\lambda_\perp = \frac{t_\perp}{J_\perp}$ and $\lambda_\parallel = \frac{t_\parallel}{J_\perp}$ are used.

$$\frac{H_0}{J_\perp} = \sum_{\tau,\sigma,n} a^\dagger_{\tau,\sigma,n} a_{\tau,\sigma,n} \left(-\tau\lambda_\perp + \frac{3}{4}\right) \tag{5.5a}$$

$$\frac{H_1}{J_\perp} = \frac{\lambda_\parallel}{2} \sum_{\tau,\sigma,\langle n,m\rangle} a^\dagger_{\tau,\sigma,n} a_{\tau,\sigma,m} \tag{5.5b}$$

$$\frac{H_2}{J_\perp} = \frac{\lambda_\parallel}{2} \sum_{\tau,\sigma,\langle n,m\rangle} \sigma\, a^\dagger_{-\tau,\sigma,n} \left(t^\dagger_{z,m} + t_{z,n}\right) a_{\tau,\sigma,m} \tag{5.5c}$$

$$\begin{aligned} \frac{H_3}{J_\perp} &= \frac{\lambda_\parallel}{2} \sum_{\tau,\langle n,m\rangle} a^\dagger_{-\tau,1,n} \left(t^\dagger_{x,m} - i\, t^\dagger_{y,m} + t_{x,n} - i\, t_{y,n}\right) a_{\tau,-1,m} \\ &\quad + a^\dagger_{-\tau,-1,n} \left(t^\dagger_{x,m} + i\, t^\dagger_{y,m} + t_{x,n} + i\, t_{y,n}\right) a_{\tau,1,m} \end{aligned} \tag{5.5d}$$

$$\begin{aligned} \frac{H_4}{J_\perp} &= \frac{\lambda_\parallel}{2} \sum_{\tau,\langle n,m\rangle} a^\dagger_{\tau,1,n} \left[\left(t^\dagger_{x,m} - i\, t^\dagger_{y,m}\right) t_{z,n} + t^\dagger_{z,m} \left(-t_{x,n} + i\, t_{y,n}\right)\right] a_{\tau,-1,m} \\ &\quad + a^\dagger_{\tau,-1,n} \left[\left(-t^\dagger_{x,m} - i\, t^\dagger_{y,m}\right) t_{z,n} + t^\dagger_{z,m} \left(t_{x,n} + i\, t_{y,n}\right)\right] a_{\tau,1,m} \end{aligned} \tag{5.5e}$$

$$\begin{aligned} \frac{H_5}{J_\perp} &= \frac{\lambda_\parallel}{2} \sum_{\tau,\langle n,m\rangle} a^\dagger_{\tau,1,n} \left(t^\dagger_{x,m} t_{x,n} + t^\dagger_{y,m} t_{y,n} + t^\dagger_{z,m} t_{z,n}\right. \\ &\quad \left. - i\, t^\dagger_{x,m} t_{y,n} + i\, t^\dagger_{y,m} t_{x,n}\right) a_{\tau,1,m} + a^\dagger_{\tau,-1,n} \left(t^\dagger_{x,m} t_{x,n} + t^\dagger_{y,m} t_{y,n}\right. \\ &\quad \left. + t^\dagger_{z,m} t_{z,n} + i\, t^\dagger_{x,m} t_{y,n} - i\, t^\dagger_{y,m} t_{x,n}\right) a_{\tau,-1,m} \end{aligned} \tag{5.5f}$$

$$\frac{H_6}{J_\perp} = \frac{x}{4} \sum_{\tau,\sigma,\langle n,m\rangle} \sigma\, a^\dagger_{-\tau,\sigma,n} \left(t^\dagger_{z,m} + t_{z,m}\right) a_{\tau,\sigma,n} \tag{5.5g}$$

$$\begin{aligned} \frac{H_7}{J_\perp} &= \frac{x}{4} \sum_{\tau,\langle n,m\rangle} a^\dagger_{-\tau,1,n} \left(t^\dagger_{x,m} - i\, t^\dagger_{y,m} + t_{x,m} - i\, t_{y,m}\right) a_{\tau,-1,n} \\ &\quad + a^\dagger_{-\tau,-1,n} \left(t^\dagger_{x,m} + i\, t^\dagger_{y,m} + t_{x,m} + i\, t_{y,m}\right) a_{\tau,1,n} \end{aligned} \tag{5.5h}$$

$$\begin{aligned} \frac{H_8}{J_\perp} &= \frac{x}{4} \sum_{\tau,\langle n,m\rangle} a^\dagger_{\tau,1,n} \left[\left(t^\dagger_{x,m} - i\, t^\dagger_{y,m}\right) t_{z,m} + t^\dagger_{z,m} \left(-t_{x,m} + i\, t_{y,m}\right)\right] a_{\tau,-1,n} \\ &\quad + a^\dagger_{\tau,-1,n} \left[\left(-t^\dagger_{x,m} - i\, t^\dagger_{y,m}\right) t_{z,m} + t^\dagger_{z,m} \left(t_{x,m} + i\, t_{y,m}\right)\right] a_{\tau,1,n} \end{aligned} \tag{5.5i}$$

$$\begin{aligned} \frac{H_9}{J_\perp} &= \frac{x}{4} \sum_{\tau,\langle n,m\rangle} a^\dagger_{\tau,1,n} \left(-i\, t^\dagger_{x,m} t_{y,m} + i\, t^\dagger_{y,m} t_{x,m}\right) a_{\tau,1,n} \\ &\quad + a^\dagger_{\tau,-1,n} \left(i\, t^\dagger_{x,m} t_{y,m} - i\, t^\dagger_{y,m} t_{x,m}\right) a_{\tau,-1,n} \end{aligned} \tag{5.5j}$$

The terms H_0 to H_5 contain the electron hopping (5.3) while the terms H_6 to H_9 cover the magnetic interactions between the hole states caused by the spin interactions (4.1).

The local terms for the one-hole states constitute H_0. This term causes the splitting of the one-hole dispersion into two bands – one for each parity – due to the factor $-\tau\lambda_\perp$. Note that the terms H_1 to H_9 do not depend on the parity of the hole states as they are invariant under change of parity. Because the singlet is considered as the vacuum state defining the zero-point energy, the energy difference of $\frac{3}{4}$ has to be paid additionally for each hole state.

The term H_1 describes the pure nearest neighbour hopping of the hole states $|a_{\tau,\sigma}\rangle_n$. Note the additional factor $\frac{1}{2}$ in the coefficient $\frac{\lambda_\parallel}{2}$ of these terms in contrast to the coefficient for the electron hopping (5.3). The c operators in Equation (5.3) act on single-spin sites, while the a operators in H_1 act on rungs. The projection of the bare hopping onto the final state yields the factor $\frac{1}{2}$.

The terms H_2 and H_3 belong to processes creating or annihilating triplons associated with the hopping of a hole state. The prefactor is $\frac{\lambda_\parallel}{2}$ as well. The parity of the hole state has to change because the creation or annihilation of one triplon would violate parity. In H_2 the triplons are z-triplons, which do not carry an S_z spin, while the x- and y-triplons in H_3 are composed of states with an S_z spin of ± 1. So due to spin conservation the spin of the hole state does not change

in H_2 and it is altered in H_3. Single terms of the sum in H_3 violate the spin conservation, but the combination of terms with $t^\dagger_{x,m}$ $(t_{x,n})$ on the one hand and $t^\dagger_{y,m}$ $(t_{y,n})$ on the other conserves the spin.

H_4 and H_5 are correlated hopping terms for one hole state and one triplon state exchanging their places. Again the coefficient is $\frac{\lambda_\parallel}{2}$. The parity of the hole state is unchanged because the number of triplons is also unchanged. It depends on the alignment of the spin of the triplon before and after the interaction whether the spin of the hole state is altered or not. The former is the case for H_4, the latter for H_5. Concerning the spin conservation for the single terms of H_4 the same holds true as for H_3.

The magnetic interaction terms for the hole states, which all carry the prefactor $\frac{x}{4}$, have a similar structure like the hopping terms since the same conservation laws for spin and charge are valid. The difference is that the hole must not change its place for the magnetic interactions. The ring exchange does not affect the hole states because the concerning terms (4.6) are zero if one spin is missing.

The triplon creation and annihilation without spin flip is represented by H_6 in analogy to H_2. The term H_7 contains the triplon creation and annihilation with spin flip analogous to H_3. The correlated hopping of triplons and hole states is described by H_8 with spin flip (analogous to H_4) and by H_9 without spin flip (analogous to H_5). Note that there are less terms in H_9 than in H_5 because processes that do not change the spin alignment of the triplon can occur for hopping but not without hopping.

Because a hole does not change the magnetic degrees of freedom, the part H_{undoped} is not influenced by the terms with hole state operators H_j during the flow, i.e. the differential equations for the terms of H_{undoped} do not include contributions from the H_j terms. Therefore the dispersion and the continua for pure triplon states are independent of $\lambda_\perp$ and $\lambda_\parallel$. The energies do not differ from the results for the undoped ladder. This is straightforward because the dynamics of pure triplon states must be identical to the dynamics in an undoped ladder. In contrast the terms including hole operators are strongly affected by the terms of H_{undoped} dependent on the parameter x, which also enters the terms H_6 to H_9.

Due to charge conservation the subspaces of the Fock space with fixed hole numbers are already decoupled from each other. Only the number of magnetic excitations changes.

5.2 Truncation

The truncation for the hole-doped ladder includes many parameters for the fine tuning considering the multitude of possible terms with hole state operators. In addition to the remaining maximal extensions d_n for terms consisting only of n triplon operators and the maximal triplon number N we introduce the following restrictions.

The parameter N_h defines the maximal number of holes which is one for the case we want to consider here. By $h_{n'}$ we denote the maximal extension for n' hole state operators. It does not matter if the term concerned contains additional triplon operators. For terms with triplon and hole state operators, $h_{n'}$ affects only the hole state operators. The total maximal extension $t_{n''}$ for these mixed terms depends on the number of triplon operators n''. The parameter N_t denotes the maximal number of triplons interacting with holes. Note that $t_{n''}$ with odd n'' have to be taken into account because the triplon number is changed by an odd number if the hole state parity is altered.

Since the size of the system of differential equations for the doped ladder grows drastically with increasing extensions, the truncation is always very strict for our calculations. The parameters $N = 4$, $d_2 = 10$, $d_4 = 6$, $d_6 = 4$ and $d_8 = 3$ were used for the pure triplon terms because these maximal extensions are sufficient for the undoped case up to $x = 1$. For the terms including hole operators the truncation used for the SCUT is given by $N_t = 2$, $h_2 = 3$, $t_1 = 6$, $t_2 = 6$, $t_3 = 5$, $t_4 = 5$, $t_5 = 4$ and $t_6 = 4$. Only if other parameteres are used, they are given explicitly.

5.3 Generator Adaption

In this section the adapted generators are introduced that are used for the doped ladder besides the pc generator. Because the number of the flow equations becomes very large for physically reasonable extensions, a central issue is the reduction of this number. This can be achieved by the exclusion of terms from the generator. For general and for undoped systems in particular this strategy is comprehensively discussed in Ref. [26]. In the following we are only interested

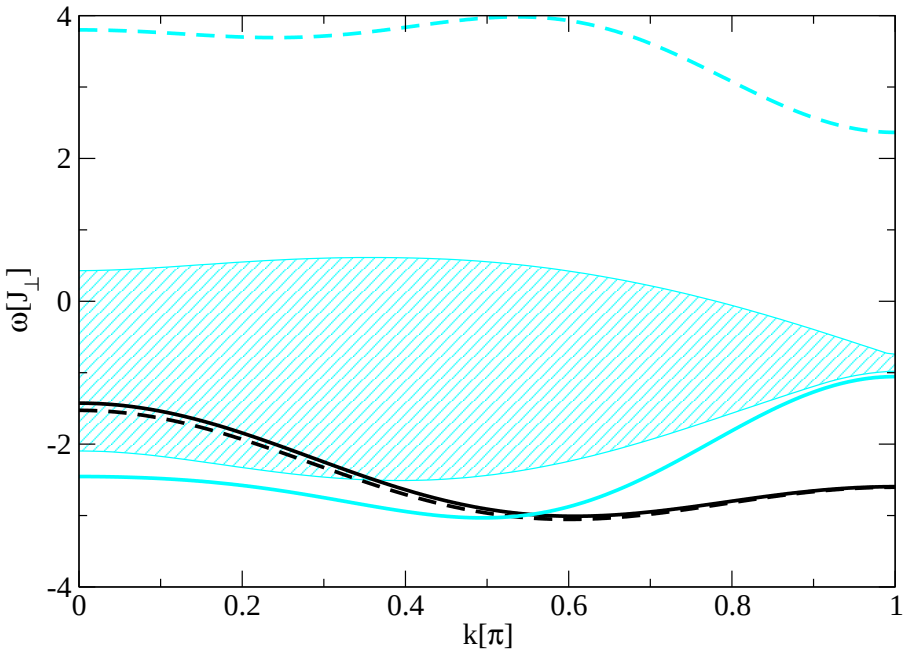

Figure 5.2: Comparison between the gs generator and the adapted generator described in the text for $x = 1$, $x_\square = 0$ and $\lambda_\perp = \lambda_\parallel = 2$. The even hole dispersion is almost identical for the gs generator (black solid) and the adapted generator (black dashed). The odd hole dispersion from the gs generator (cyan continuous) lies below the continuum formed by one even hole and one triplon (cyan shaded area), whereas the odd hole dispersion from the adapted generator (cyan dashed) lies above it.

in pure hole states. Hence the zero-triplon space[2] is the only subspace that has to be decoupled from the remaining Hilbert space. The terms in the generator that is restricted to performing just this task contain only triplon creation or only triplon annihilation operators apart from possible hole state operators. This is the gs generator already introduced in Section 4.4. This generator may induce converging transformations in the case of overlapping triplon continua[3].

Considering the local hole state terms of the Hamiltonian (5.5a) it seems likely that for sufficiently large $\lambda_\perp$ the process of creating or annihilating one triplon (under change of the parity of one hole) the energy change is dominated (or at least strongly influenced) by the band change. If this is actually the case, the pc

[2] A state without triplons can include holes. Because of charge conservation the number of holes is fixed. Thus after the CUT the zero-triplon state is the ground state for every spin ladder with a certain number of holes.

[3] These continua have to incorporate the hole energies for the doped case.

generator based on the idea that the change of the particle number dominates the energy change will no longer induce a converging transformation. If there is a distinctly dominating process for each term of the Hamiltonian, the adaption of the generator can take this into account by appropriate signs. But a pronounced gap between the hole bands with different parity is necessary to make the band change always dominating at least for processes involving the creation or annihilation of a single triplon. The system does not develop such a gap in the examined parameter space as the next section will show. In fact the bands exhibit a crossing if the hopping constants are increased. Therefore the triplon creation or annihilation either remains the dominant process or competes with the band change and an adaption of a sign change in the generator is not appropriate. Only if all other parameters are much smaller than $\lambda_\perp$, this adaption is suitable.

In the case that for certain terms it can not be determined in general whether they increase or decrease the energy a simple sign correction in the generator is not possible. This happens if the sign of the energy change depends on the momentum. Then the real space truncation scheme is not the optimal ansatz.

An implementation of a generator adaption according to Section 2.5.2 was also tested. If we use the adapted generator which considers the band change as the dominant process in the way that the even band is assumed to be the lower energy, we obtain unphysical results for the parameters examined within this thesis. The results for the even band are indeed the same as without the adaption (apart from small deviations for small momenta). However, the odd band is forced to lie above the continuum formed by one even hole and one triplon. This can be seen examplarily for $x = 1$, $x_\square = 0$ and $\lambda_\perp = \lambda_\parallel = 2$ in Figure 5.2.

In the regime $x = 1$, $x_\square = 0$ and $\lambda_\perp = \lambda_\parallel > 2$ we encounter convergence problems with both the pc and the gs generator. We will show this in Section 5.4.1. To preserve convergence a restricted generator η_{rs} was used (see Section 2.5.3). The problematic terms are the ones which couple the single-hole subspace to the subspace with one hole and one triplon

$$a^\dagger_{\tau,\sigma,n} t^\dagger_{\alpha,n+\Delta n} a_{\tau',\sigma',m} \quad \text{and} \quad a^\dagger_{\tau,\sigma,m} t_{\alpha,n} a_{\tau',\sigma',n+\Delta n}. \tag{5.6}$$

For η_{rs} we restrict $|\Delta n|$ to be smaller than or equal to a maximal value $\Delta n_{\max}$. This restriction indeed yields a converging flow for $x = 1$, $x_\square = 0$ and $\lambda_\perp = \lambda_\parallel > 2$, which will also be illustrated in Section 5.4.1.

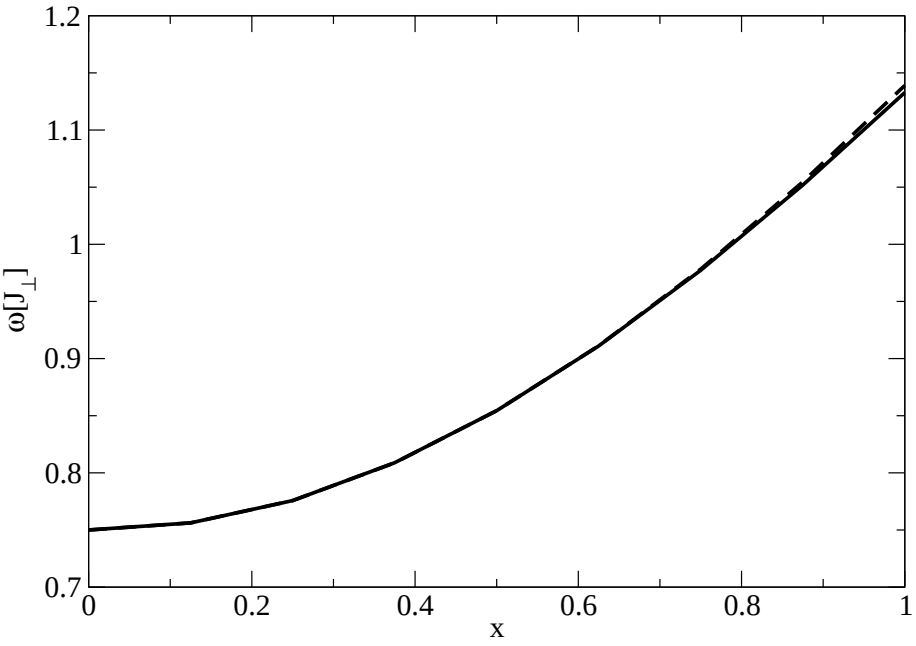

Figure 5.3: Fourfold degenerate one-hole energy for $\lambda_\perp = \lambda_\parallel = x_\square = 0$ in dependence of x calculated with the pc generator (solid) and with the gs generator (dashed).

5.4 One-Hole Dispersion

The dispersion of a single hole in the absence of triplons can be as easily derived from the effective Hamiltonian in the same manner as the one-triplon dispersion in Section 4.3.1. The part of the Hamiltonian to be diagonalised

$$H_{1\mathrm{h}} = \sum_{d=-h_2}^{h_2} \sum_{\tau,\sigma,n} b_d \, a^\dagger_{\tau,\sigma,n+d} a_{\tau,\sigma,n} \tag{5.7}$$

contains the one-hole terms restricted by h_2 and characterised by the coefficients b_d. The one-hole energy relative to the ground state

$$\omega_{1\mathrm{h},\tau}(k) = b_0 + \sum_{d=1}^{h_2} 2b_d \cos(dk) \tag{5.8}$$

only depends on the parity τ and is degenerate concerning the spin σ.

If $\lambda_\parallel$ and $\lambda_\perp$ are small while $x = x_\square = 0$, the dispersion is

$$\frac{\omega_{1\mathrm{h},\pm1}(k)}{J_\perp} = \frac{3}{4} \mp \lambda_\perp + \lambda_\parallel \cos(k) + \mathcal{O}(\lambda_\perp^2, \lambda_\parallel^2, \lambda_\perp \lambda_\parallel). \tag{5.9}$$

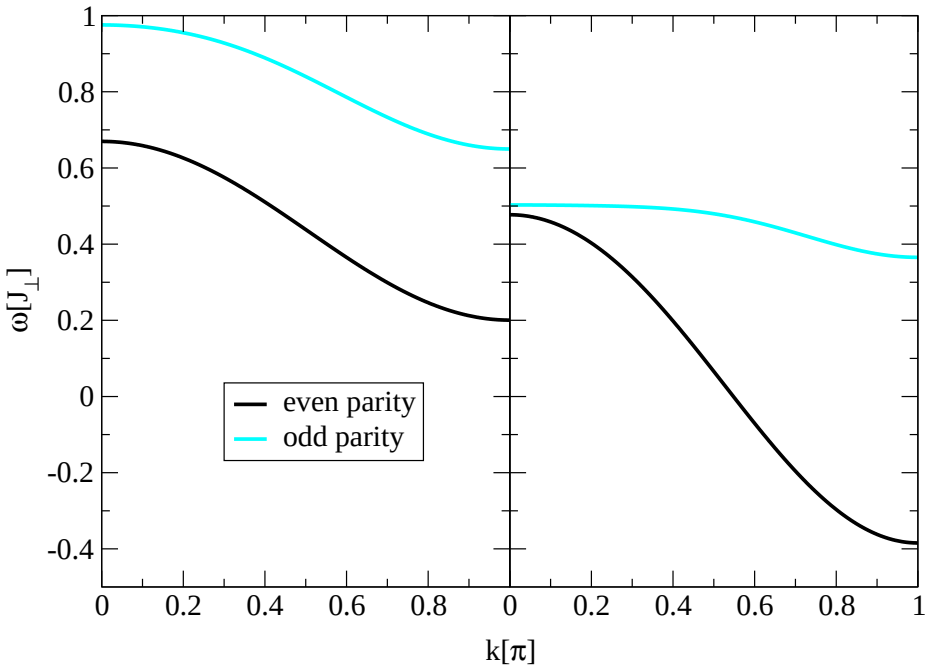

Figure 5.4: One-hole dispersion for $x = x_\square = 0$ calculated with the pc generator; left: $\lambda = 0.25$, right: $\lambda = 0.5$. The curves coincide well with the series expansion results from [97].

If $\lambda_\perp = \lambda_\parallel = 0$ the hole energy is a dispersionless constant and fourfold degenerate (concerning spin and parity). This energy increases with growing x due to the terms of the Hamiltonian that describe the magnetic interactions of the hole states with their environment (5.5g-5.5j). Figure 5.3 demonstrates this quantitatively for $x_\square = 0$. The deviations between the results from the pc generator and from the gs generator are growing with x. However, they are still marginal ($< 1\%$) for $x = 1$.

5.4.1 Isotropic Hopping

Let us at first consider the isotropic case $\lambda_\perp = \lambda_\parallel = \lambda$. For small values of the parameters x, $x_\square$ and λ the deviations from Equation (5.9) are actually small. In Figure 5.4 two values of λ are considered for $x = x_\square = 0$. The result for $\lambda = 0.25$ already exhibits deviations from the relation for small hopping constants. Both bandwidths are smaller than $2\lambda = 0.5$. The odd band is narrower than the even band. Moreover the odd band is shifted upwards by less than λ, while the even

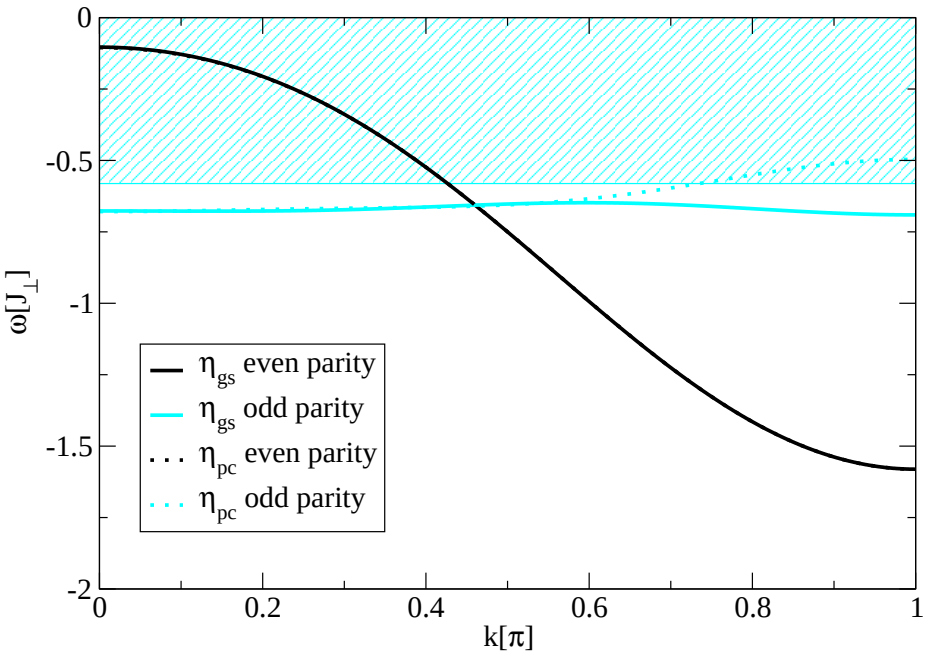

Figure 5.5: One-hole dispersion for $x = x_\square = 0$, $\lambda = 1$ calculated with the gs generator and the pc generator. The results for the even bands coincide so that the curves cannot be distinguished. The cyan shaded area is the continuum formed by one triplon and one even hole state.

band is shifted downwards by slightly more than λ.

The increase of λ to 0.5 yields a result with obvious deviations relative to 5.9. The odd band becomes lower and narrower with growing λ in this region. The cosine shape of both dispersions is – for $\lambda = 0.25$ as well as for $\lambda = 0.5$ – not deformed by higher harmonics. The results of the series expansion [97] exhibit the same behaviour for these parameters in good agreement with the SCUT results. However, it has to be pointed out that the convergence of the SCUT is much worse for $\lambda = 0.5$ than for $\lambda = 0.25$. The residual off-diagonality (ROD) which is defined as the sum over the squared coefficients contributing to the generator and used as a measure for the convergence (cf. Section 3.6) is decreasing very slowly for $\lambda = 0.5$. While the ROD is smaller than 10^{-13} at $lJ_\perp = 200$ for $\lambda = 0.25$, it is still $\approx 10^{-5}$ at $lJ_\perp = 200$ for $\lambda = 0.5$. Both RODs are decreasing exponentially for large l.

For $x = x_\square = 0$, $\lambda = 1$ the pc generator yields results for the even band that still agree very well with the series expansion. For the odd band there are

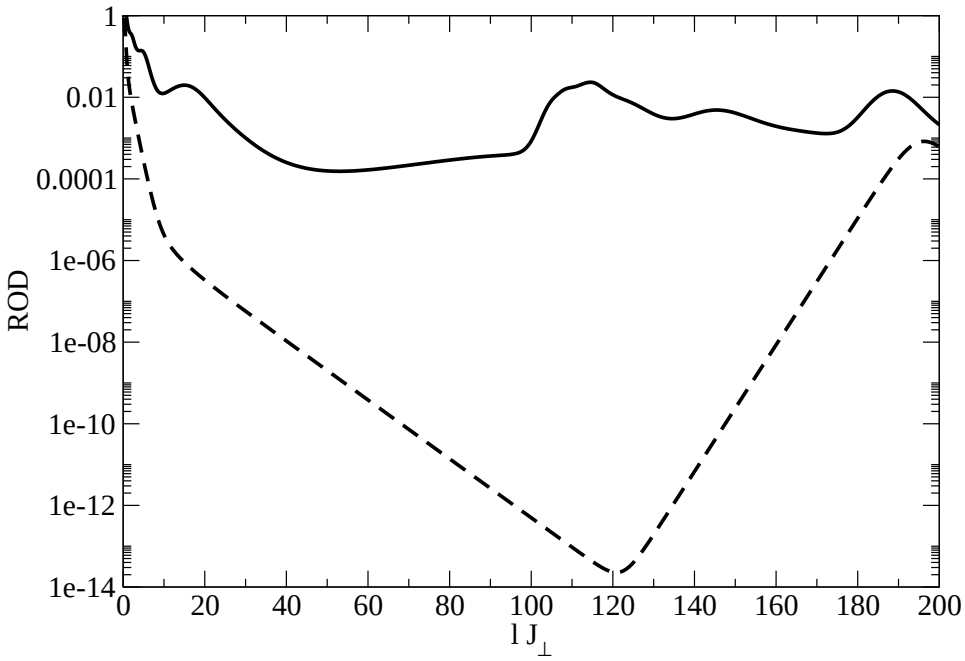

Figure 5.6: ROD for the SCUT for $x = x_\square = 0$, $\lambda = 1$ induced by the pc generator (solid line) and by the gs generator (dashed line).

no series expansion results available. Figure 5.5 shows the comparison between the results for the pc generator and for the gs generator. The even band results lie on top of each other, but the odd band exhibits deviations for $k \gtrsim 0.57\pi$. While the gs generator produces an almost featureless dispersion (compared to the even band), the pc generator causes a pronounced maximum at $k = \pi$. These differences are due to the position of the lower boundary of the continuum formed by one triplon and one even hole state[4] (see also Figure 5.5). An overlap between the odd dispersion and this continuum is present for the pc result. The deviating odd band from the gs generator avoids this overlap. For both generators the even and the odd band cross at $k \approx 0.46\pi$. While the even band keeps its cosine shape, for the odd band the second harmonic is no longer negligible for both the pc and the gs generator.

It is necessary to mention that for $x = x_\square = 0$, $\lambda = 1$ the transformation does not converge for the pc generator, while the gs generator induces convergence (see Figure 5.6). The overlap hinders the convergence for the pc generator. The kink

[4]The boundaries of this continuum are constant because the triplon dispersion is also constant for $x = x_\square = 0$.

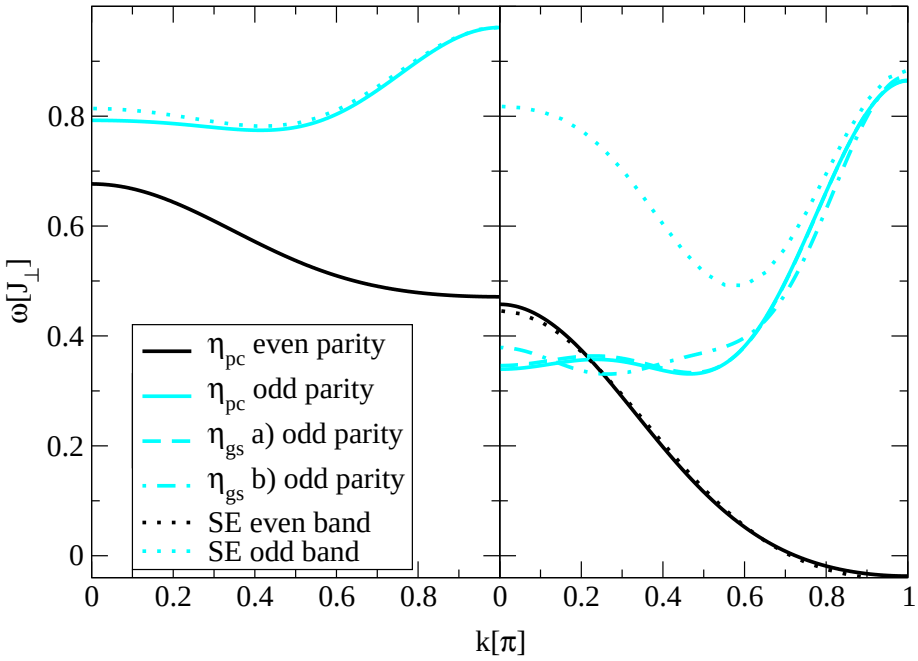

Figure 5.7: Left panel: One-hole dispersion for $x = 0.5$, $x_\Box = 0$, $\lambda = 0.25$ calculated with the pc generator. The series expansion result for the odd band is also shown, while the result for the even band is not available. Right panel: One-hole dispersion for $x = 0.5$, $x_\Box = 0$, $\lambda = 0.5$ calculated with the pc generator and the gs generator. For a) the usual truncation was used, for b) h_2 was increased to 4, t_1 and t_2 to 8 as well as t_3 and t_4 to 6. The dotted curves are extrapolations from the series expansion data.

at $lJ_\perp \approx 120$ in the gs ROD is probably due to numerical inaccuracies that are amplified via a feedback within the flow equation (cf. Appendix A). Since the ROD is already $< 10^{-13}$ at the kink we can stop the transformation at this point and neglect the remaining off-diagonal terms, i.e. we consider the transformation converged. For the calculation of the hole dispersions the pc SCUT was stopped at $lJ_\perp \approx 50$ where the ROD is still $\approx 10^{-4}$ and not negligible. Therefore the result from the gs generator is more trustable than the result from the pc generator. The parameters $x = x_\Box = 0$, $\lambda = 2$ lead to divergence for either generator.

Now we want to consider $x > 0$. For $\lambda = 0$ the energy of the hole states which is independent of k and τ decreases with increasing x due to the terms (5.5g-5.5j). For small finite λ the deviations from the simple cosine shape appear quite early in λ for the odd band. This can be seen in Figure 5.7 where the one-hole dispersions for $x = 0.5$ and $\lambda = 0.25$ are depicted. The odd band is in good

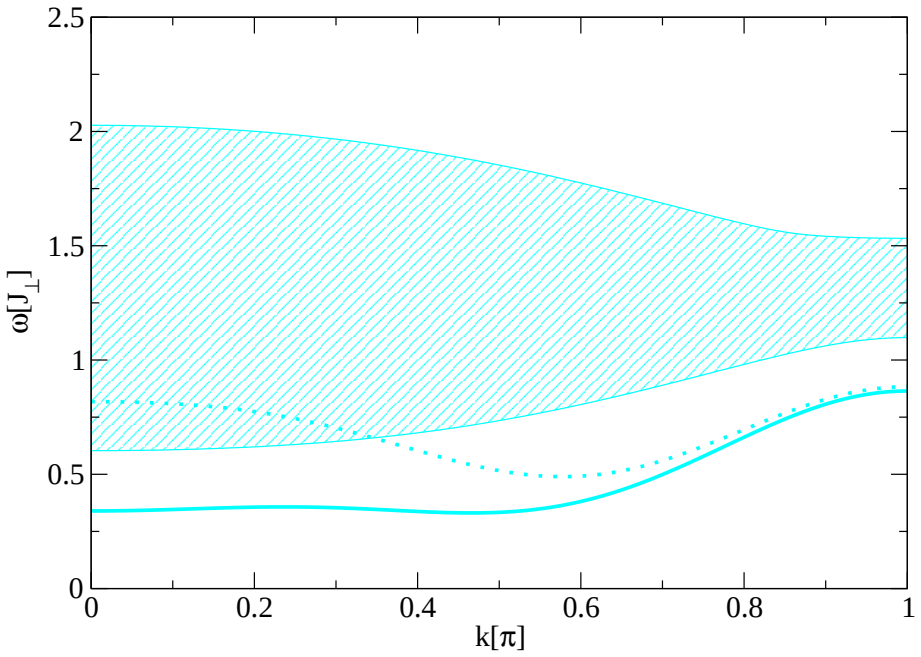

Figure 5.8: Comparison between the odd hole dispersion and the continuum formed by one triplon and one even hole state for $x = 0.5$, $x_\square = 0$, $\lambda = 0.5$. The odd hole dispersion was derived by SCUT using the pc generator (cyan solid) and by series expansion (cyan dotted). The cyan shaded area is the continuum (derived by the same SCUT calculation).

agreement with the series expansion (only slight deviations at $k = 0$ occur), for the even band no series expansion data are available.

For $x = 0.5$ and $\lambda = 0.5$ (see also Figure 5.7) the result for the even band is again in good agreement with the series expansion result, but the odd band behaves differently. Only for large k the behaviour is similar although also in this region the SCUT result is slightly lower. The series expansion result exhibits a local maximum at $k = 0$ and a global minimum at $k \approx 0.58\pi$, while the SCUT result hardly changes in the region $0 < k < \frac{\pi}{2}$. The gs generator yields the same result as the pc generator apart from minimal deviations ($< 2\%$) at $k = 0$. However, the gs generator allows us to extend the truncation scheme: h_2 was increased to 4, t_1 and t_2 to 8 as well as t_3 and t_4 to 6. In the result the shape of the odd band changes mainly for small k. Thus the odd dispersion still changes with increasing maximal extensions.

We can understand these differences between SCUT and series expansion by

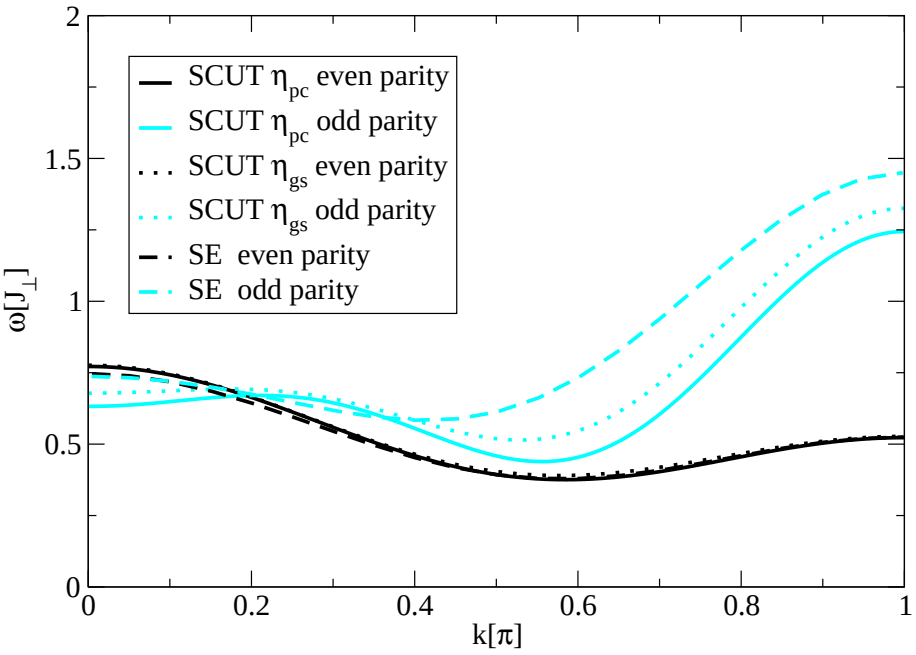

Figure 5.9: One-hole dispersion for $x = 1$, $x_\square = 0$, $\lambda = 0.5$ calculated with the pc generator and the gs generator. The dashed curves are extrapolations from the series expansion data.

looking at the position of the continuum formed by one triplon and one even hole state (see Figure 5.8). The series expansion result crosses the lower boundary of this continuum at $k \approx 0.34\pi$. Assuming that the series expansion yields a result near to the actual odd hole dispersion it is cogent that the SCUT based on the pc generator is not able to sort the eigenvalues properly for small k because creating one triplon does not necessarily increase the energy. Since the problematic overlap concerns the zero- and the one-triplon space, the exclusion of terms from the generator is no remedy here. Hence the gs generator yields mainly the same result. Although the odd dispersion still changes with increasing maximal extensions, due to the overlap an agreement with the series expansion result is not to be expected for small k. It is also possible that the extrapolation does not completely comprise the effect of the overlapping continuum.

For $x = 1$ and $\lambda = 0.5$ (see Figure 5.9) the SCUT results for the odd band again show distinct deviations from the series expansion results. While the even band exhibits its maximal deviation at $k = 0$ which is only $\approx 1\%$, the odd band deviates concerning the shape for small k (but the quantitative deviations are

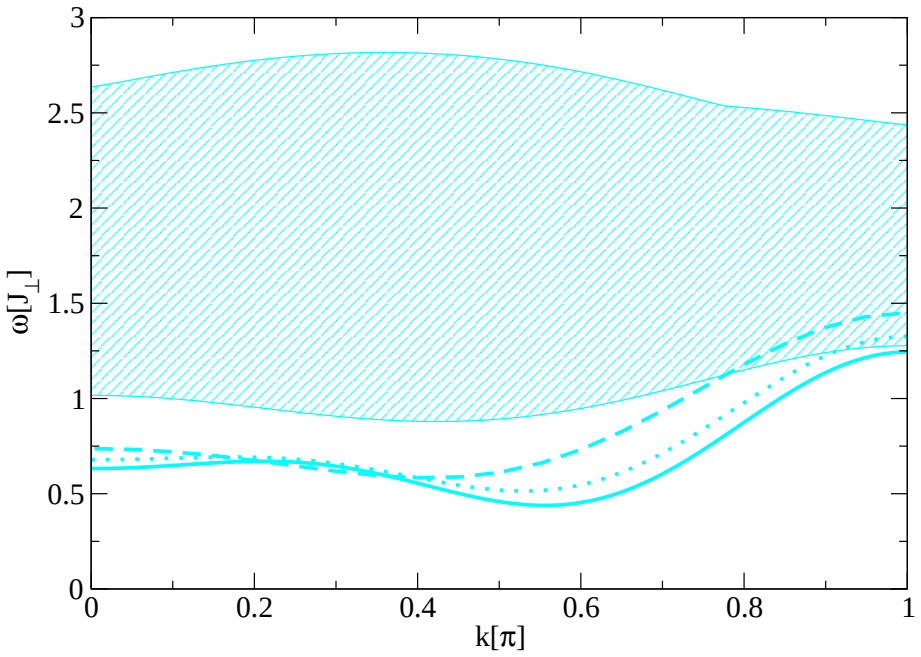

Figure 5.10: Comparison between the odd hole dispersion and the continuum formed by one triplon and one even hole state for $x = 1$, $x_\square = 0$, $\lambda = 0.5$. The odd hole dispersion was derived by SCUT using the pc generator (cyan solid), using the gs generator (cyan dotted) and by series expansion (cyan dashed). The cyan shaded area is the continuum (derived by the same pc SCUT calculation).

not very pronounced there) and is considerably lower for large k. All in all the deviations are not as pronounced as for $x = 0.5$ and $\lambda = 0.25$. A comparison with the continuum formed by one even hole and one triplon (see Figure 5.10) shows that an overlap exists around $k = \pi$ for the series expansion result and for the gs result. This explains again the deviations in this region. As this overlap is not as strong as the overlap for $x = 0.5$ and $\lambda = 0.5$ the deviations are accordingly smaller. Even if we cannot clearly state that there is an actual overlap, the continuum is at least very close. Hence it is to be expected that the odd hole dispersion is lowered for $k \approx \pi$ due to this reason.

Since for $x = 1$ and $\lambda = 1$ (see Figure 5.11) no one-hole dispersion result with odd parity is available from the series expansion, we can only compare the even band. But we also compare with exact diagonalisation results by Läuchli [98]. For the exact diagonalisation a finite ladder with 14 rungs was examined and the resulting eigenenergies were fitted by a series with three cosine terms for both

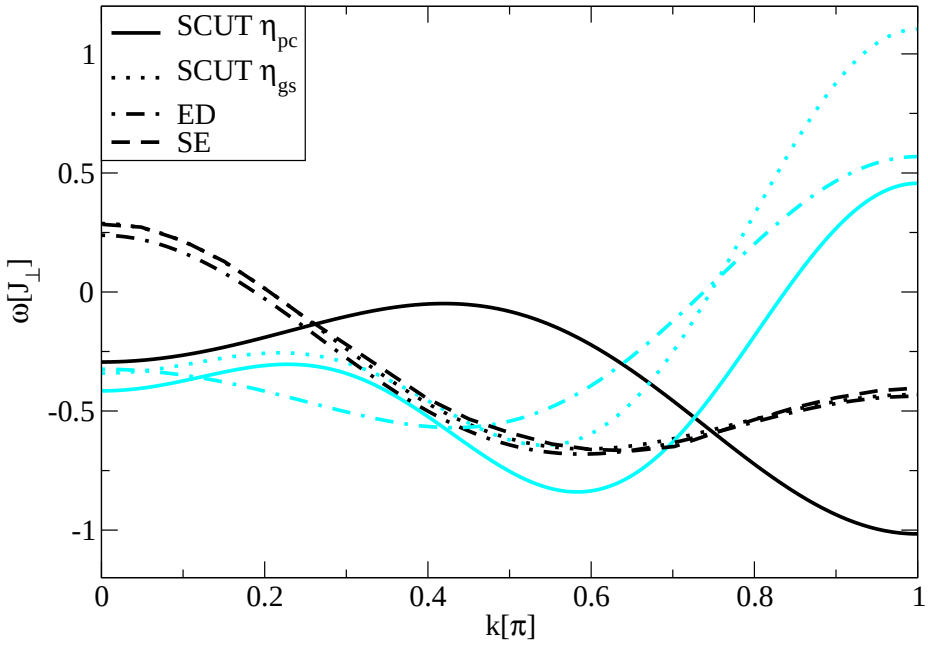

Figure 5.11: One-hole dispersion for $x = 1$, $x_\square = 0$, $\lambda = 1$ calculated with the pc generator and the gs generator. The dashed curve is the result from the series expansion, for which only the even band is available. The dashed-dotted curves are the exact diagonalisation results.

bands. The pc result for the even band exhibits a completely different behaviour than the gs result. For the odd band the pc result lies below the gs result and the deviations grow with increasing momentum. The comparison with the series expansion and with the exact diagonalisation suggests that the gs result is more reasonable because the deviations are smaller than 1% for the even band. Also for the odd band the gs result is closer to the exact diagonalisation result.

It should be noted that the diagrammatic approach from Ref. [99] yields bands that show qualitative deviations from the SCUT and from the exact diagonalisation concerning the shape for small k. But the authors say that in this regime they only provide an approximate description actually beyond their approach. The quantum Monte Carlo result from Ref. [100] is in good agreement with our result. For the even band the agreement is actually very good like the agreement between SCUT and exact diagonalisation.

The odd band result from the gs SCUT enters the continuum formed by one triplon and one even hole state for $k \gtrsim 0.83\pi$ (see Figure 5.12), while the pc

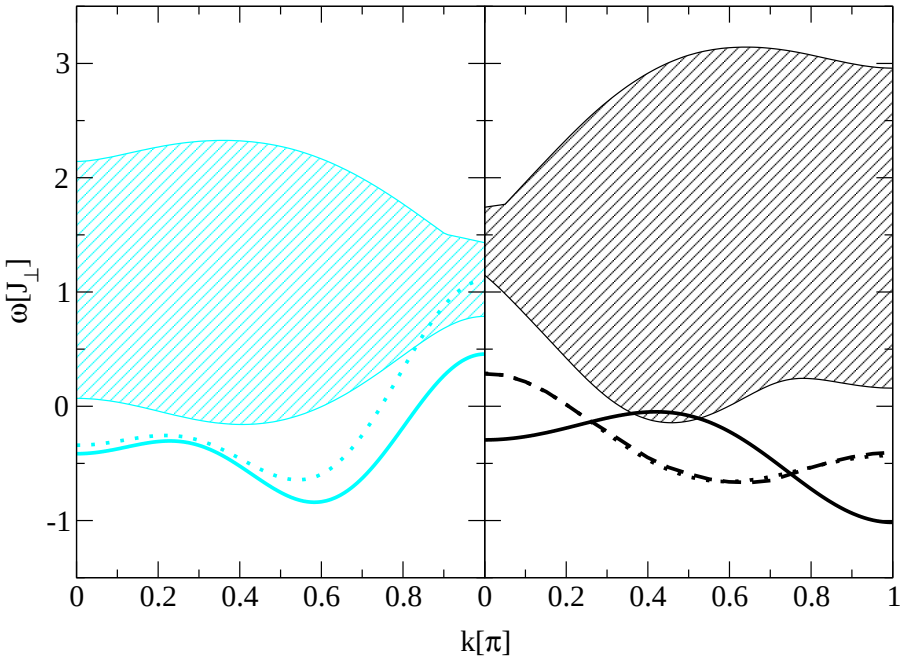

Figure 5.12: Comparison between the hole dispersions and the continua formed by one triplon and one hole state for $x = 1$, $x_\square = 0$, $\lambda = 1$. Left: The odd hole dispersion was derived by SCUT using the pc generator (cyan solid) and using the gs generator (cyan dotted). The cyan shaded area depicts the continuum with one even hole and one triplon (derived by the same gs SCUT calculation). Right: The even hole dispersion was derived by SCUT using the pc generator (black solid), using the gs generator (black dotted) and by series expansion (black dashed). The black shaded area depicts the continuum with one odd hole and one triplon (derived by the same gs SCUT calculation).

result lies always below the continuum. This overlap is also present in the exact diagonalisation result [98] and in the quantum Monte Carlo result [100]. A comparison between the even one-hole dispersion and the continuum formed by one triplon and one odd hole state (see also Figure 5.12) supports the assumption that the gs result is more reliable than the pc result because the dispersion induced by the gs SCUT exhibits a shape that appears as if it were formed by the lower boundary of the approaching continuum. The pc result, however, stays away from the continuum at $k = 0$ and at the boundary of the Brillouin zone, while it overlaps with the continuum around $k \approx 0.44\pi$.

At this point we compare the convergence behaviour for $x = 0.5$, $\lambda = 0.5$; $x = 1$, $\lambda = 0.5$ and $x = 1$, $\lambda = 1$ in case of the pc generator. The concerning

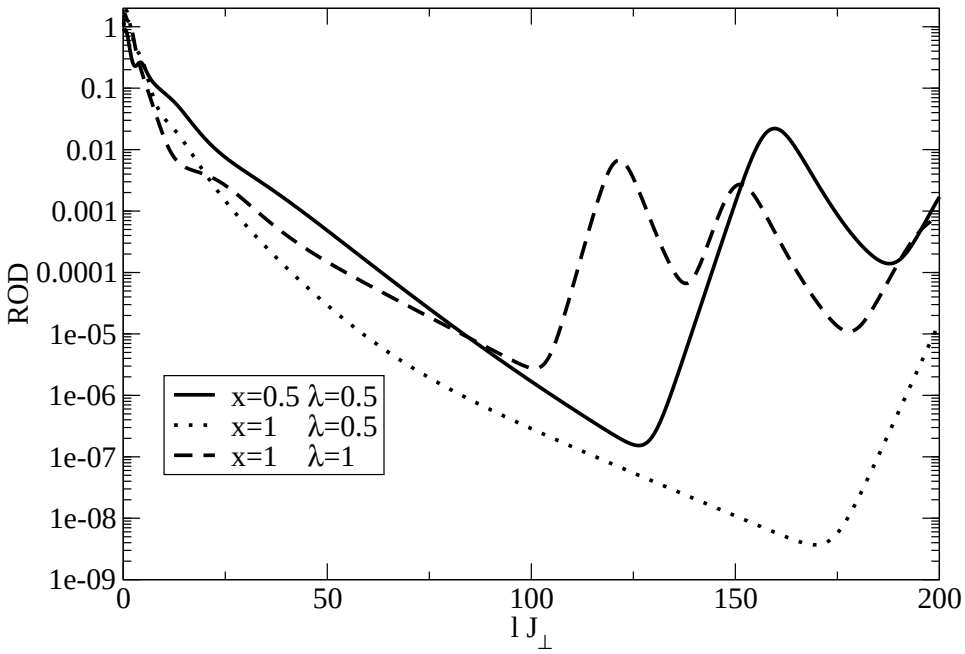

Figure 5.13: ROD for the SCUT calculated with the pc generator for different parameters.

RODs are depicted in Figure 5.13. All three curves exhibit a kink with non-converging behaviour afterwards. This is typical for cumulating rounding errors because of a symmetry breaking due to numerical inaccuracies (cf. Appendix A). Such a symmetry breaking is not unlikely because the spin symmetry could not be used explicitly. The problems of this utilisation are discussed in Section 5.5.

It is interesting that the ROD for $x = 1$, $\lambda = 0.5$ achieves the lowest value with less than 10^{-8}. However, if we consider the rate of decrease before the kink for all curves, it can be clearly seen that for $x = 0.5$, $\lambda = 0.5$ this rate is the largest. This is to be expected as these parameters are the smallest of the ones considered here and the corresponding unitary transformation is the least demanding.

For $x = 1$ and $\lambda > 1$ the parameters are entering a region which is expected to reflect realistic relations of the constants in the telephone number compounds. The results for $x = 1$ and $\lambda = 2$ are shown in Figure 5.14. Again we do not only compare with the series expansion (for which only the even band is available) but

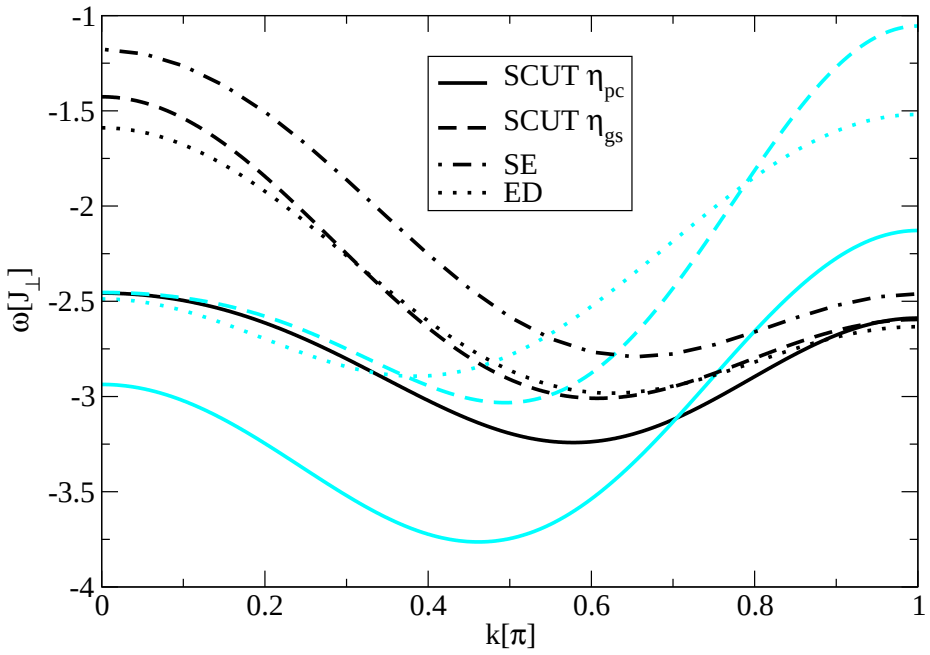

Figure 5.14: One-hole dispersion for $x = 1$, $x_\square = 0$, $\lambda = 2$ calculated with the pc generator and the gs generator. The graph also shows the exact diagonalisation data (ED) and the series expansion data (SE). For the latter only the even band is available. The even band results are black, the odd band results are cyan.

also with exact diagonalisation results for $L = 14$ by Läuchli [98].[5]

$$\omega_{1\mathrm{h},\tau}(k) = b_0 + \sum_{d=1}^{3} 2b_d \cos(dk). \tag{5.10}$$

Approximate analytic results were obtained in Ref. [102] by perturbation theory improved by a variational ansatz. These results lie even above the series expansion results but confirm the qualitative shape for the even band. The pc result for both the even and the odd band is again very distinct from the other results like for $x = 1$, $\lambda = 1$. The gs result, however, is in better agreement with the data from the series expansion and especially with the exact diagonalisation result in accordance with our previous observations.

Apart from the pc result the dispersions exhibit the same features. The even band has a global maximum at $k = 0$ and a local maximum at $k = \pi$, while it is vice versa for the odd band. Because both bands lie in the same energy range,

[5] For a finite ladder with 10 rungs results were published by Troyer, Tsunetsugu and Rice [101].

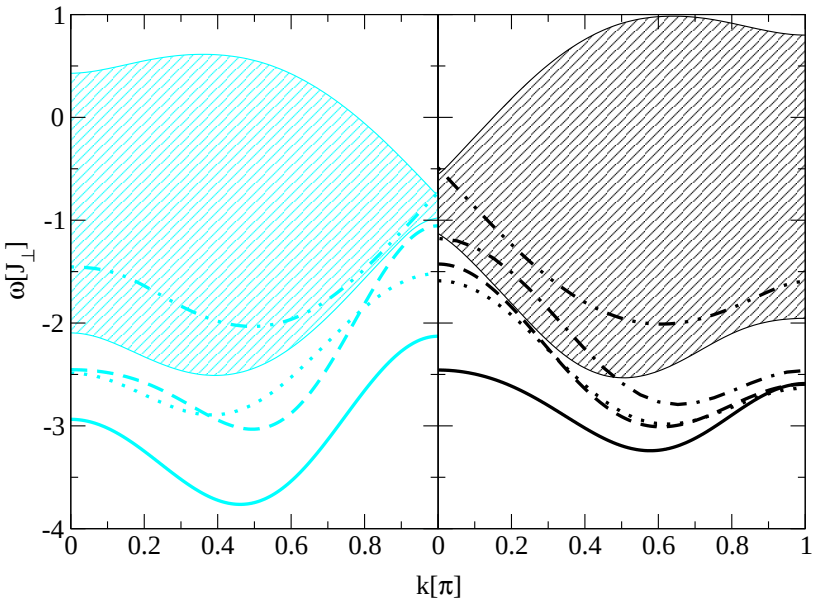

Figure 5.15: Comparison between the hole dispersions and the continua formed by one triplon and one hole state for $x = 1$, $x_\square = 0$, $\lambda = 2$. Left: The odd hole dispersion was derived by pc SCUT (cyan solid), gs SCUT (cyan dashed) and by exact diagonalisation (cyan dotted). The cyan shaded area depicts the continuum with one even hole and one triplon (derived by the same gs SCUT calculation). The cyan dash dot dot line is the lower boundary of the continuum formed by two triplons and one odd hole. Right: The even hole dispersion was derived by pc SCUT (cyan solid), gs SCUT (cyan dashed), by exact diagonalisation (cyan dotted) and by series expansion (cyan dashed-dotted). The black shaded area depicts the continuum with one odd hole and one triplon (derived by the same gs SCUT calculation). The black dash dot dot line is the lower boundary of the continuum formed by two triplons and one even hole.

they cross in the middle between $k = 0$ and $k = \pi$. The exact diagonalisation predicts the crossing to be at $k \approx 0.48\pi$, but the gs SCUT sees the crossing at $k \approx 0.55\pi$. The even band calculated by series expansion is located above both the series expansion and the gs SCUT result for all k. This is a further indicator that the extrapolation used to correct the bare series underestimates the lowering of the band induced by the hybridisation with the hole-triplon continuum.

Let us consider the continua formed by one hole and one triplon. The continua consisting of one hole and one triplon are compared to the one-hole dispersions in Figure 5.15. The continua do not overlap with the hole dispersions, but they are very close to each other. The only exception is the series expansion result for

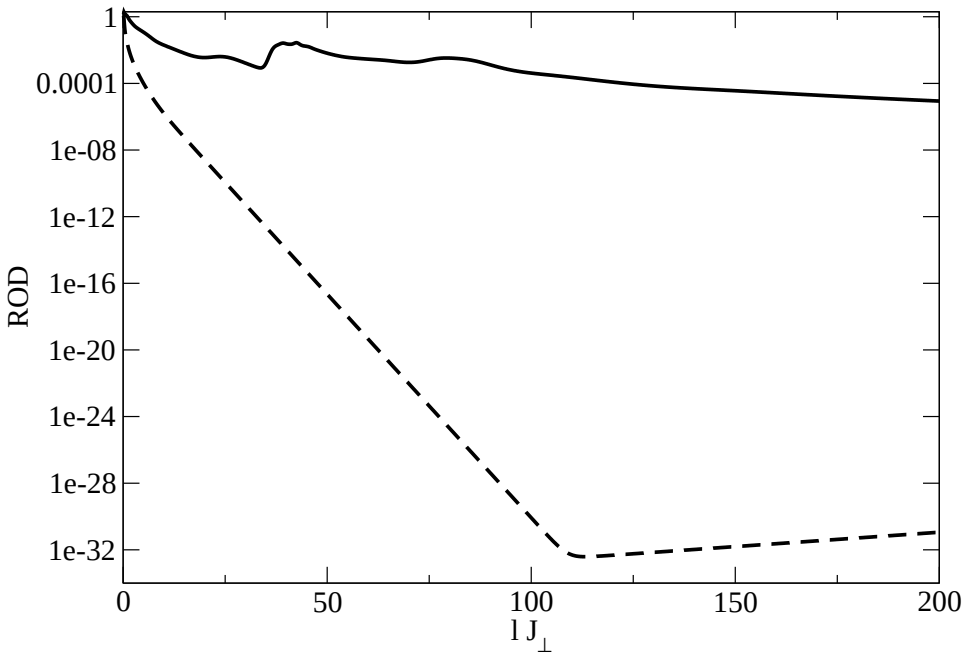

Figure 5.16: ROD for the SCUT for $x = 1$, $x_\square = 0$, $\lambda = 2$ induced by the pc generator (solid line) and by the gs generator (dashed line).

the odd band, which exhibits an overlap with the continuum formed by a triplon and an even hole state.

The behaviour of the ROD (cf. Section 3.6) yields further evidence why the gs results should be preferred to the pc results for this parameter regime. Figure 5.16 depicts the evolution of the ROD during the flow for both generators. Not only that the pc SCUT converges extremely slowly, the shape of the curve for $lJ_\perp < 100$ is an indicator for a problem with respect to the sorting of the eigenenergies. It is a typical behaviour of the ROD that the sorting of the eigenvalues (cf. Equation (2.12)) is reflected by features for small values of l. If the sorting is completed the ROD decreases exponentially with a constant rate henceforward. For the gs generator the decrease of the ROD attains this rate not later than at $lJ_\perp = 5$. Before this point the decrease is slower[6]. The kink of the gs ROD at $lJ_\perp \approx 110$ with the following rise is again most probably due to cumulating numerical inaccuracies (cf. Appendix A). This is no real problem because the gs ROD has already fallen below a value of less than 10^{-32} at $lJ_\perp \approx 110$ and can hence

[6]Even if the ROD exibits a small hump before it decreases with a constant rate, the sorting usually does not pose a problem.

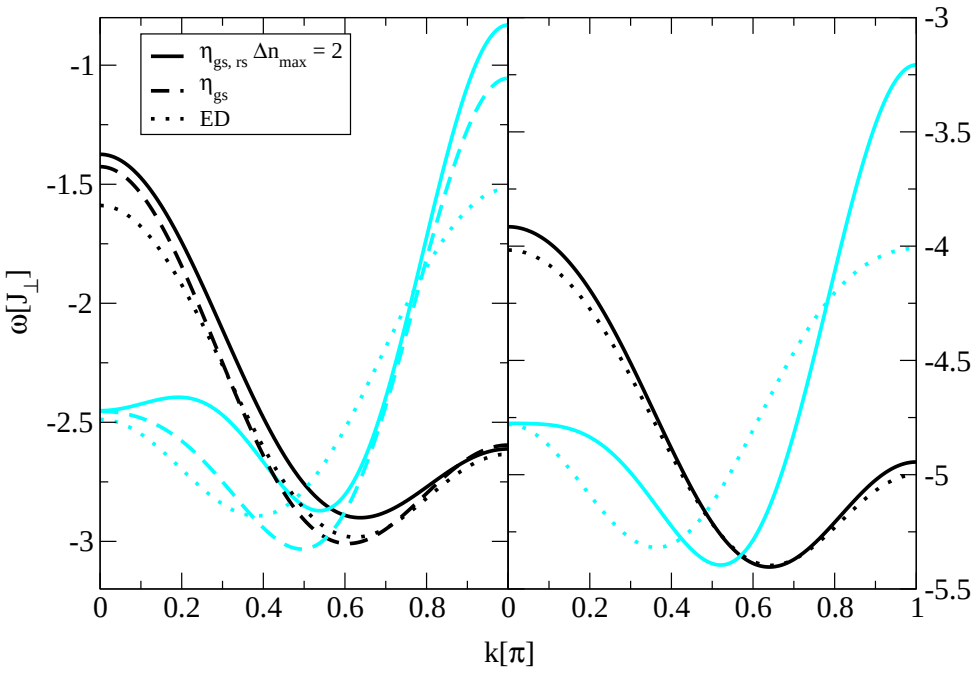

Figure 5.17: Comparison of the one-hole dispersions from the restricted generator with the gs and the exact diagonalisation results. Left panel: $x = 1$, $x_\square = 0$, $\lambda = 2$. Right panel: $x = 1$, $x_\square = 0$, $\lambda = 3$. The black lines represent the even hole dispersion and the cyan lines represent the odd hole dispersion.

be neglected. However, the pc ROD exhibits several humps and a pronounced rise at $lJ_\perp = 34$ before a decrease with a constant rate is achieved. This is a typical indication for a suppressed divergence that would actually occur for a wider truncation. If such a feature is distinct, the transformation is susceptible to errors. These convergence problems are caused by the strong overlap between the one-hole-one-triplon continuua and the one-hole-two-triplon continua (see Figure 5.15).

The exact diagonalisation was also applied for $x = 1$ and $\lambda = 3$ [98], but even the gs generator does not induce convergence for this case. However, if we apply the generator restriction defined in Section 5.3 to the gs generator, it yields convergence for $\Delta n_{\max} \leqslant 2$. Because the Hamiltonian is not diagonalised with respect to the terms that are omitted from the generator, the hole dispersions we obtain from a Fourier transformation are only upper limits for the actual result. Hence we compare the results from the restricted generator for $x = 1$ and $\lambda = 2$ with the gs results before we investigate the results for $x = 1$ and $\lambda = 3$. The left

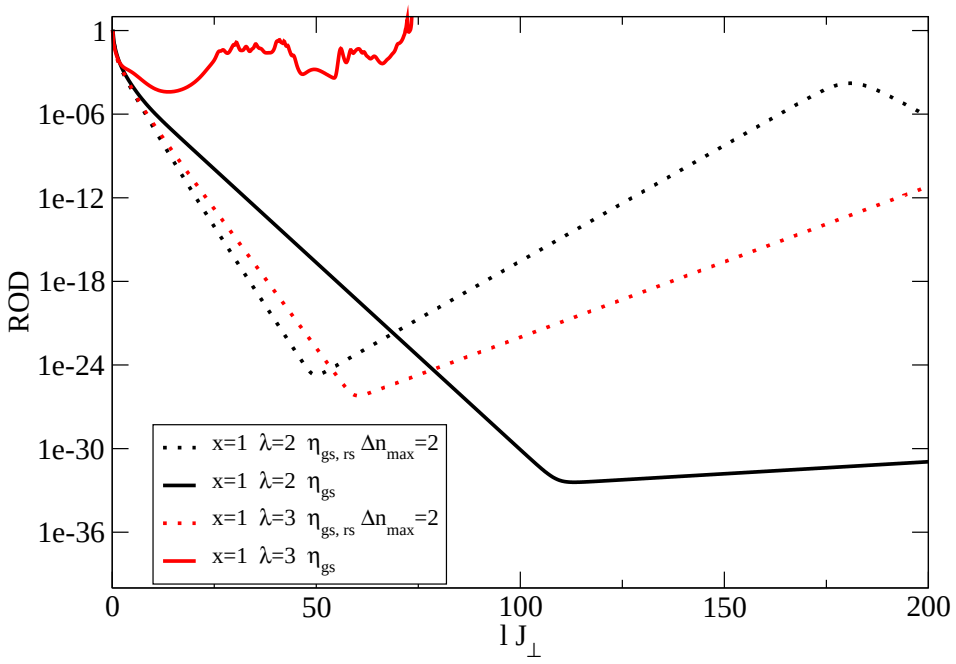

Figure 5.18: ROD for the SCUT calculated with the full gs generator and with the restricted gs generator for different parameters.

panel of Figure 5.17 shows the comparison of the one-hole dispersions for $x = 1$ and $\lambda = 2$. We see that for $\Delta n_{\max} \leqslant 2$ the upper boundary from the restricted gs generator is close to the result from the full gs generator. In the right panel of Figure 5.17 the results from the restricted gs generator are compared to the exact diagonalisation results for $x = 1$ and $\lambda = 3$. For the even hole dispersion the agreement between the result from the restricted gs generator and the exact diagonalisation result is almost perfect. Also the agreement for the odd hole dispersion is good. The deviations are comparable to the deviations of the result by the full gs generator from the exact diagonalisation result for $x = 1$ and $\lambda = 2$.

The investigation of the ROD shows that the restricted gs generator yields a faster convergence than the full gs generator for $x = 1$ and $\lambda = 2$ (see Figure 5.18). For $x = 1$ and 3 the ROD diverges for the full generator, while the restricted generator induces convergence (see also Figure 5.18). Note that the kinks of the RODs in Figure 5.18 with the increase afterwards are again probably due to cumulated numerical inaccuracies (cf. Appendix A). But all the kinks appear at values where the ROD is already smaller than 10^{-24}. So the flow can be considered as converged at the kinks for practical purposes.

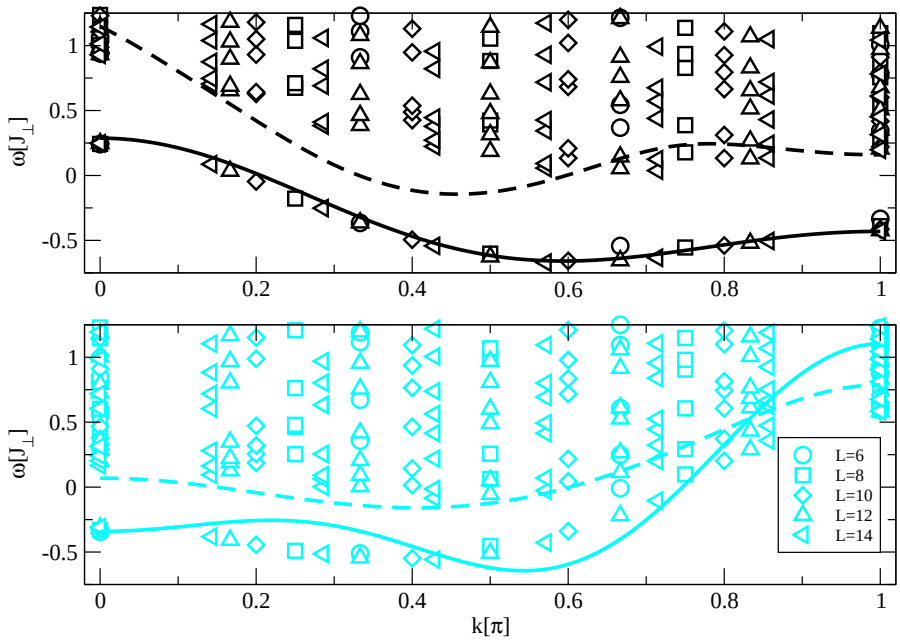

Figure 5.19: Comparison between gs SCUT (solid lines) and exact diagonalisation for various finite ladders with L rungs (discrete points) for $x = 1$, $\lambda = 1$. The lower boundaries of the continua calculated by gs SCUT are shown as dashed lines. The results for the even hole state are black, the results for the odd hole state are cyan.

The terms, which are left out from the generator, still contribute to the Hamiltonian after the transformation. These contributions yield an estimate of the difference between the actual energy and the upper boundary for the energy resulting from the restricted generator. For the 432 terms of the form $a^\dagger_{\tau,\sigma,n} t^\dagger_{\alpha,n+\Delta n} a_{\tau',\sigma',m}$ or $a^\dagger_{\tau,\sigma,m} t_{\alpha,n} a_{\tau',\sigma',n+\Delta n}$ the sum over their squared coefficients is ≈ 0.48. The square root of this value is ≈ 0.69. The largest absolute value of a single coefficient is ≈ 0.16.

To understand the deviations between SCUT and exact diagonalisation we have to investigate the finite size scaling of the exact diagonalisation. In Figure 5.19 the results of the exact diagonalisation for various finite ladders with L rungs are compared to the results from the gs generator for $x = 1$ and $\lambda = 1$. The graph shows the discrete eigenvalues of H calculated by exact diagonalisation. In the case of the even band the lowest lying eigenvalue can be clearly distinguished from the larger eigenvalues, which are the precursor of the continuum. This holds true for all momenta. In the case of the odd band the lowest eigenvalue is very

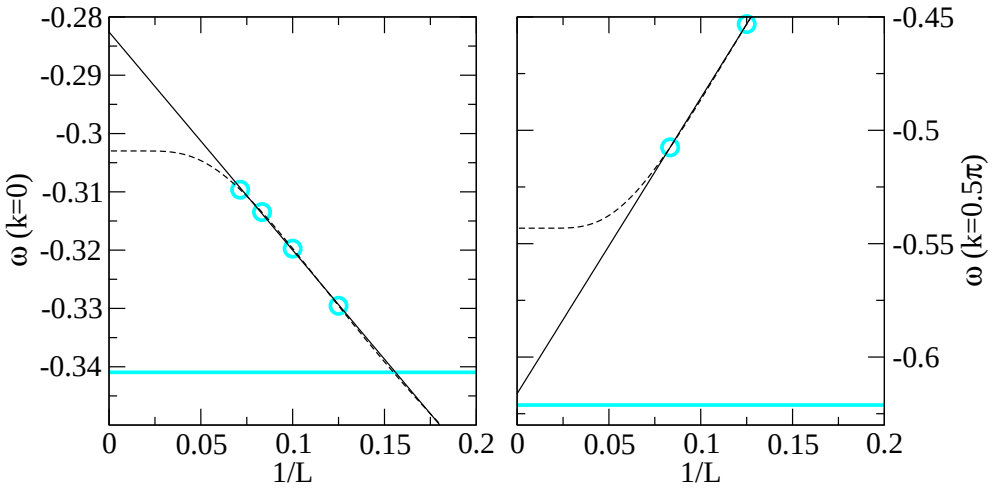

Figure 5.20: Finite size scaling of the exact diagonalisation results for $x = 1$ $\lambda = 1$ in case of the odd band at $k = 0$ and at $k = 0.5\pi$. The cyan circles depict the exact diagonalisation results for finite ladders with various numbers of rungs L. The solid black line is a linear extrapolation with respect to $\frac{1}{L}$ and the dashed line is an extrapolation based on exponential saturation (see Equation (5.11)). For comparison the result from the gs SCUT is also shown (solid cyan).

close to the higher ones for large momenta. Our calculation of the continuum predicts that the dispersion merges with the continuum in this region. Also the quantum Monte Carlo result for the spectral weight [100] exhibits no peak below the continuum around $k \approx \pi$.

Our result for the even band is in excellent agreement with the exact diagonalisation result. Around $k \approx 0.25\pi$ our result for the odd band lies above the exact diagonalisation result, while it lies below the exact diagonalisation result around $k \approx 0.6\pi$. An investigation of the finite size scaling for the exact diagonalisation data in these regions is difficult because we have maximally two points for an extrapolation. Thus at first we consider $k = 0$, where an extrapolation is conclusive. The result of this extrapolation is used to support an extrapolation in the region where the deviations are observed. The left panel of Figure 5.20 shows the finite size scaling for $k = 0$ using two kinds of extrapolation. The first is a simple linear extrapolation with respect to $\frac{1}{L}$, while the second assumes an exponential saturation with increasing L so that

$$\Delta\omega \propto \mathrm{e}^{-\frac{L}{\xi}} \tag{5.11}$$

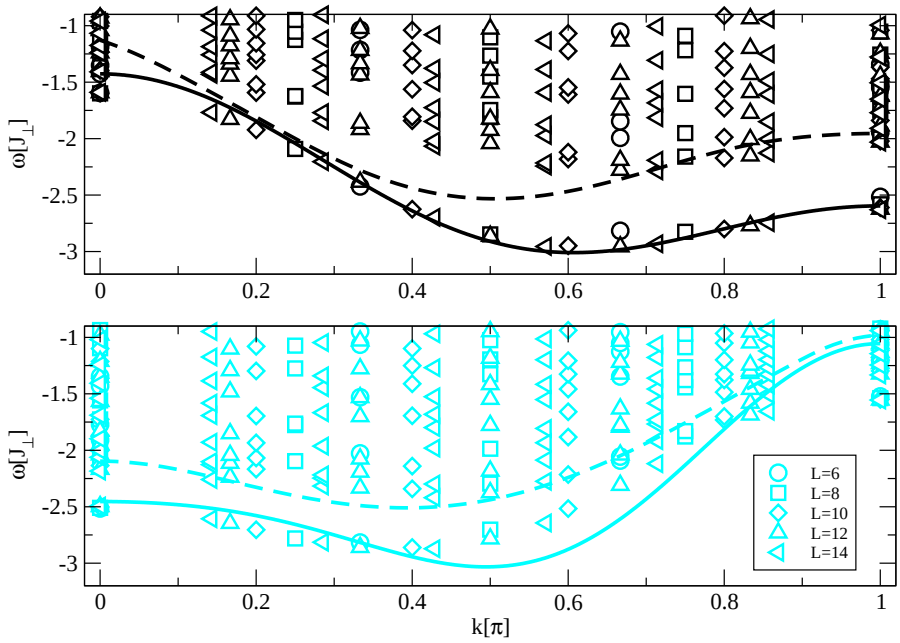

Figure 5.21: Comparison between gs SCUT (solid lines) and exact diagonalisation for various finite ladders with L rungs (discrete points) for $x = 1$, $\lambda = 2$. The lower boundaries of the continua calculated by gs SCUT are shown as dashed lines. The results for the even hole state are black, the results for the odd hole state are cyan.

holds true for the difference $\Delta\omega$ from the limit for $L \to \infty$. The correlation length ξ is determined to be ≈ 4.32 by this extrapolation. The correlation length can be used to apply the second extrapolation also for $k = 0.5\pi$ where only two results are obtained by exact diagonalisation. The finite size scaling for $k = 0.5\pi$ in case of the odd band is investigated by both extrapolations in the right panel of Figure 5.22. The extraploation results at $k = 0$ are still close to the gs SCUT result and the extrapolation results at $k = 0.5\pi$ are in good agreement with the gs SCUT result. The linear extrapolation is even in excellent agreement with our result. Note that the points from the $L = 6$ calculation are omitted for the extrapolations because they deviate from the behaviour of the other points due to the small size of the system.

In Figure 5.21 we compare the results of the exact diagonalisation with the results from the gs generator for $x = 1$ and $\lambda = 2$. In the case of the even band for large momenta the lowest lying eigenvalue is clearly distinguishable from the larger eigenvalues, which are again the precursor of the continuum. The same is true for the odd band for small momenta. But for small momenta in case of the

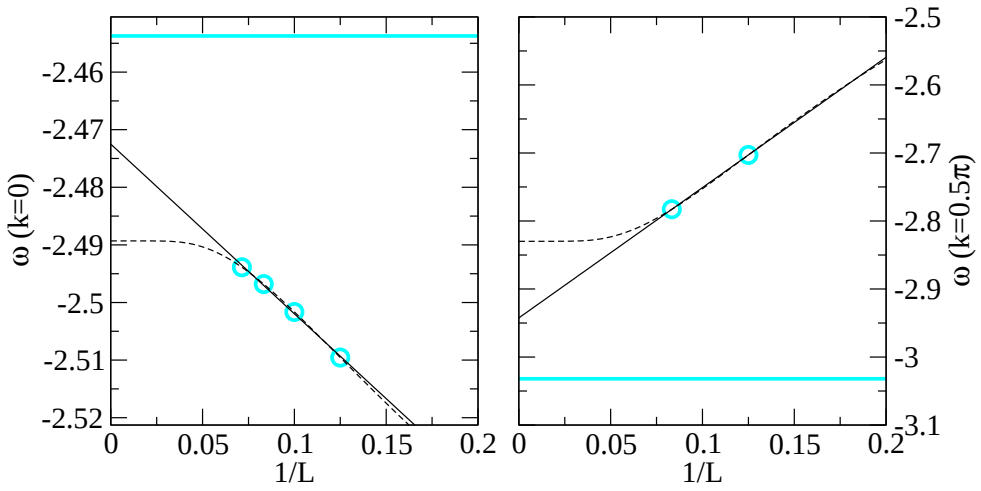

Figure 5.22: Finite size scaling of the exact diagonalisation results for $x = 1$ $\lambda = 2$ in case of the odd band at $k = 0$ and at $k = 0.5\pi$. The cyan circles depict the exact diagonalisation results for finite ladders with various numbers of rungs L. The solid black line is a linear extrapolation with respect to $\frac{1}{L}$ and the dashed line is an extrapolation based on exponential saturation (see Equation (5.11)). For comparison the result from the gs SCUT is also shown (solid cyan).

even band and for large momenta in case of the odd band the lowest eigenvalue is very close to the higher ones. Hence the distinction between hole dispersion and continuum becomes difficult in these regions. It is even questionable if they are actually distinguishable or if the dispersion merges with the continuum. In these regions the deviations between SCUT and exact diagonalisation are the largest. We conclude that the SCUT suffers from truncation errors if the dispersion runs close to continua or even enters them. Also the lower boundary of the continuum that we calculated from the gs result is higher at $k = 0$ for the even band and at $k = \pi$ for the odd band than we would expect from the exact diagonalisation data. However, the interaction between hole and triplon is not included in the calculation of the continua. The consideration of this interaction may lower our result.

In the remaining regions the SCUT result for the dispersions comes close to the extrapolation of exact diagonalisation results. This is most obvious for the odd band at $k = 0$. The left panel of Figure 5.22 shows the finite size scaling for this case using the same extrapolations like for $x = 1$ and $\lambda = 1$. We determine ξ to be ≈ 4.03 by the extrapolation based on exponential saturation. The correlation

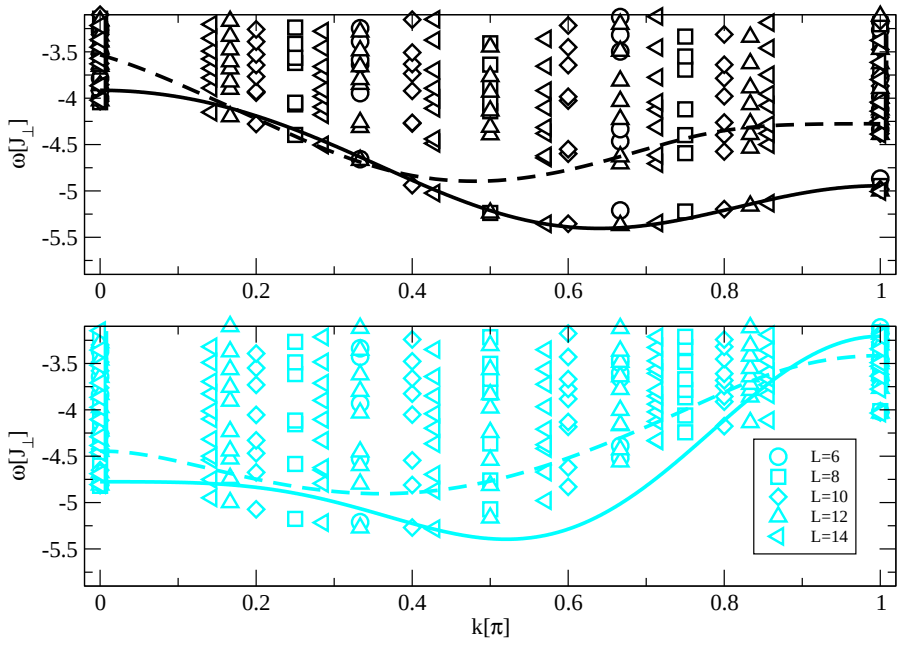

Figure 5.23: Comparison between SCUT from the restricted gs generator with $\Delta n_{\max} = 2$ (solid lines) and exact diagonalisation for various finite ladders with L rungs (discrete points) for $x = 1$, $\lambda = 3$. The dashed lines are estimations for the lower boundaries of the continua based on the result from the restricted gs generator. The results for the even hole state are black, the results for the odd hole state are cyan.

length is again used to apply this kind of extrapolation also for $k = 0.5\pi$. The finite size scaling for $k = 0.5\pi$ in case of the odd band is investigated by both extrapolations in the right panel of Figure 5.22. For both momenta the linear extrapolation comes close to the SCUT result, but also the extrapolation based on exponential saturation does not exhibit large deviations from the SCUT result. The deviation for $k = 0$ is $\approx 2\%$ and the deviation for $k = 0.5\pi$ is $\approx 7\%$. The points from the $L = 6$ calculation are omitted for the extrapolations because they deviate from the behaviour of the other points due to the small size of the system.

For $x = 1$ and $\lambda = 3$ the exact diagonalisation results are shown in Figure 5.23 for various finite ladders with L rungs. The odd hole dispersion is more difficult to distinguish from the continuum than for $x = 1$ and $\lambda = 2$. Also for small momenta the lowest eigenvalue is very close to the higher ones. The upper boundary for the hole dispersions from the restricted gs generator with $\Delta n_{\max} = 2$ is also depicted in Figure 5.23. In the region $0.5\pi \lesssim k \lesssim 0.8\pi$ this upper boundary lies below the exact diagonalisation data. But the tendency of

the finite size scaling at $k = 0.5\pi$ indicates that the exact diagonalisation results overestimate the energy of the odd band in this region so that one can expect that a proper finite size scaling yields a dispersion that lies completely below this upper boundary. However, an extrapolation from the two points ($L = 8$ and $L = 12$) at $k = 0.5\pi$ is not conclusive. We have several points for an extrapolation for $k = 0$ and $k = \pi$, but there the distinction between continuum and dispersion is difficult. Because the gs SCUT diverges without restriction of the generator, we actually expect that a strong overlap is present.

5.4.2 Anisotropic Hopping

We want to consider anisotropic hopping, i.e. $\lambda_\perp \neq \lambda_\parallel$. This is also of interest because at least small differences between the parallel and the perpendicular hopping are expected to be realistic like for the magnetic coupling constants $J_\perp$ and $J_\parallel$. We want to consider three parameter regimes. In each case we start from an isotropic hopping using parameters that yield reliable results. The starting values are $x = 0$, $\lambda_\perp = \lambda_\parallel = 0.5$; $x = 0.5$, $\lambda_\perp = \lambda_\parallel = 0.25$ and $x = 1$, $\lambda_\perp = \lambda_\parallel = 2$. The ring exchange $x_\square$ is always zero. We employ the gs generator in the first two cases and the 0n generation in the latter one because the corresponding results are conclusive for isotropic hopping which was shown in the preceding section. The one-triplon dispersions derived by SCUT for these cases agree well with the results from series expansion [97] and from exact diagonalisation [101] (see Section 5.4.1). Also the ROD converges properly.

The first case starts from $x = x_\square = 0$, $\lambda_\perp = \lambda_\parallel = 0.5$. Increasing the hopping constants separately leads to a lowering of the bands (Figure 5.24(a)), while decreasing them leads to a lifting (Figure 5.24(b)). However, this effect is weak for the odd band in the case of changing $\lambda_\perp$. The constant in the dispersion changes like in the other cases, but the change of the bandwidth is dominant. Hence the odd band for $\lambda_\perp = 0.6$, $\lambda_\parallel = 0.5$ lies above the odd band for $\lambda_\perp = \lambda_\parallel = 0.5$ in the region $k \gtrsim 0.41\pi$; the odd band for $\lambda_\perp = 0.4$, $\lambda_\parallel = 0.5$ lies beneath the odd band for $\lambda_\perp = \lambda_\parallel = 0.5$ in the region $k \gtrsim 0.44\pi$.

The regime around $x = 0.5$, $\lambda_\perp = \lambda_\parallel = 0.25$ and $x = 1$ again exhibits a different behaviour for the odd band in the case of changing $\lambda_\perp$. Figure 5.25(a) shows the separate increase of the hopping constants, Figure 5.25(b) the decrease. The even band is lowered if one hopping constant is increased and raised if one hopping constant is decreased. However, although for $\lambda_\parallel = 0.1$ there is a shift upwards

for the constant of the even dispersion, the bandwidth is decreased by a factor of ≈ 2.5 so that the maximum at $k = 0$ has almost the same value for $\lambda_\parallel = 0.25$ and for $\lambda_\parallel = 0.1$. It is even slightly lower for $\lambda_\parallel = 0.1$. The odd band is also lowered if $\lambda_\parallel$ is increased and raised if $\lambda_\parallel$ is decreased. The different behaviour of the odd band in the case of $\lambda_\perp = 0.4$ consists in the following features: The former local maximum at $k = 0$ for the isotropic case moves to $k \approx 0.33$, the global minimum now lies at $k = 0$ and the global maximum at $k = \pi$ is more pronounced. For $\lambda_\perp = 0.1$ the different behaviour of the odd band consists in the following features: The maxima at $k = 0$ and $k = \pi$ are of almost equal height now and the minimum, which moves from $k \approx 0.41\pi$ (in the isotropic case) to $k \approx 0.52\pi$, is lowered by $\approx 0.03 J_\perp$.

Next, let us start from the isotropic case $\lambda_\perp = \lambda_\parallel = 2$ for $x = 1$ and $x_\Box = 0$. At first we increase the hopping constants separately. Figure 5.26 shows the results for the SCUT induced by the gs generator. The pc results are not examined as they deviate considerably from the results of other methods in this parameter region as shown in the last section.

The increase of one of the hopping constants leads to a lowering of the bands for both the relation $\lambda_\perp > \lambda_\parallel$ and the relation $\lambda_\perp < \lambda_\parallel$. Both bands are decreased in almost equal measure (see Figure 5.26(a)). This effect is almost twice as strong for $\lambda_\perp = 2$, $\lambda_\parallel = 2.5$ as for $\lambda_\perp = 2.5$, $\lambda_\parallel = 2$. The shape of the dispersions is almost conserved, but the locations of the minima change. The crossing point moves to slightly smaller k for increasing $\lambda_\parallel$ and to larger k for increasing $\lambda_\perp$. Although this effect is not pronounced, results for interim values confirm the trend of this movement of the crossing point.

The decrease of one of the hopping constants starting from $\lambda_\perp = \lambda_\parallel = 2$ leads to a lifting of the bands (see Figure 5.26(b)). While for $\lambda_\perp = 1.5$, $\lambda_\parallel = 2$ the shape of the band is again conserved, for $\lambda_\perp = 2$, $\lambda_\parallel = 1.5$ the local maximum moves from $k = 0$ to $k = 0.22\pi$ and a local minimum appears at $k = 0$. The effect of the lifting is approximately twice as strong for the change of $\lambda_\parallel$ than for the change of $\lambda_\perp$. This is in analogy to the effect of the lowering in the case of the increase of one of the hopping constants. The crossing point of the bands moves to larger k with decreasing $\lambda_\parallel$ and to smaller k with decreasing $\lambda_\perp$.

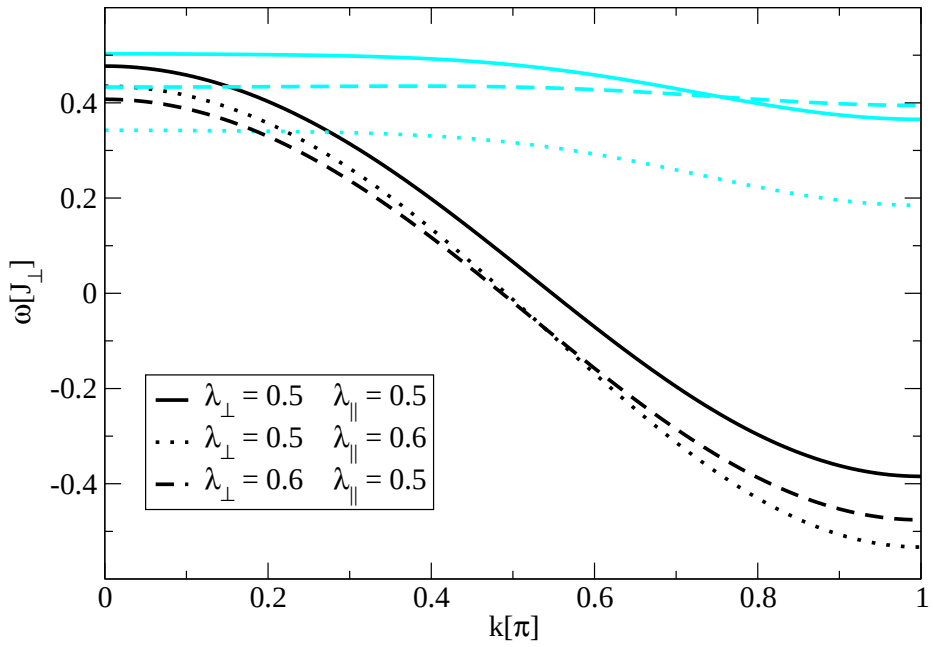

(a) larger hopping constants compared to $\lambda_\perp = \lambda_\parallel = 0.5$.

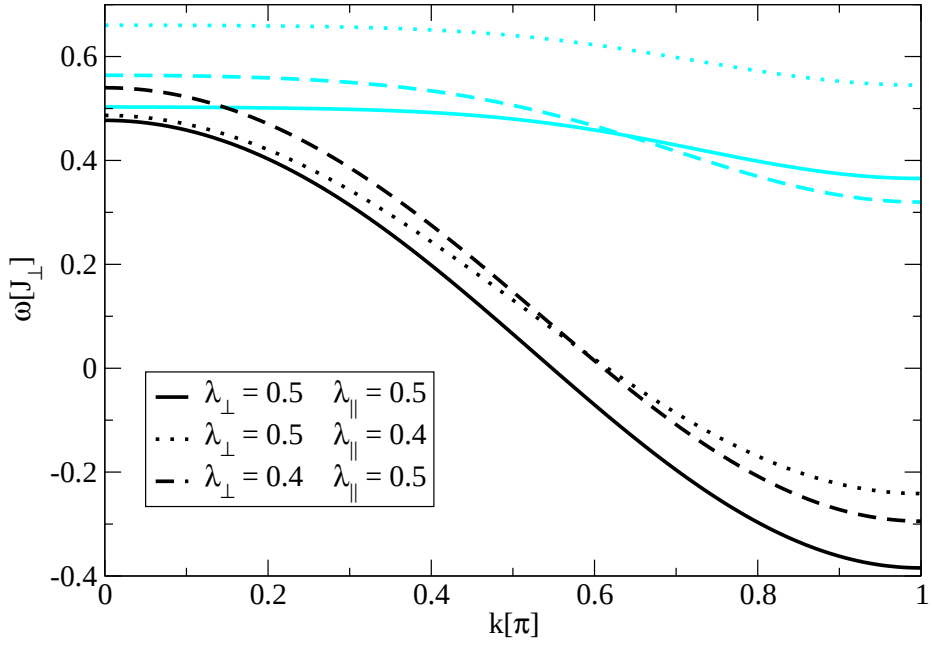

(b) smaller hopping constants compared to $\lambda_\perp = \lambda_\parallel = 0.5$.

Figure 5.24: One-hole dispersions with even parity (black) and odd parity (cyan) for $x = x_\square = 0$ and anisotropic hopping constants.

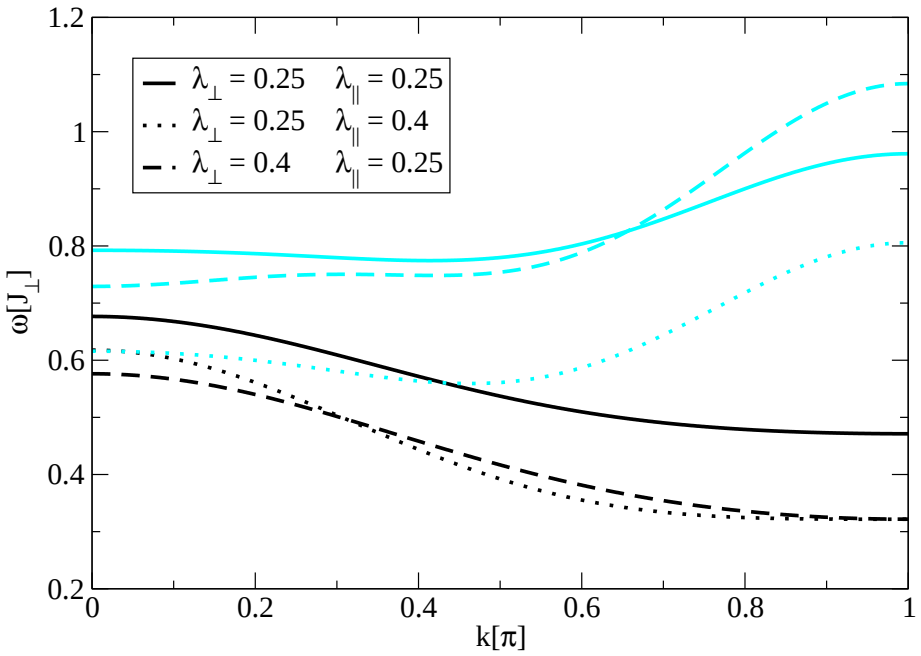

(a) larger hopping constants compared to $\lambda_\perp = \lambda_\parallel = 0.25$.

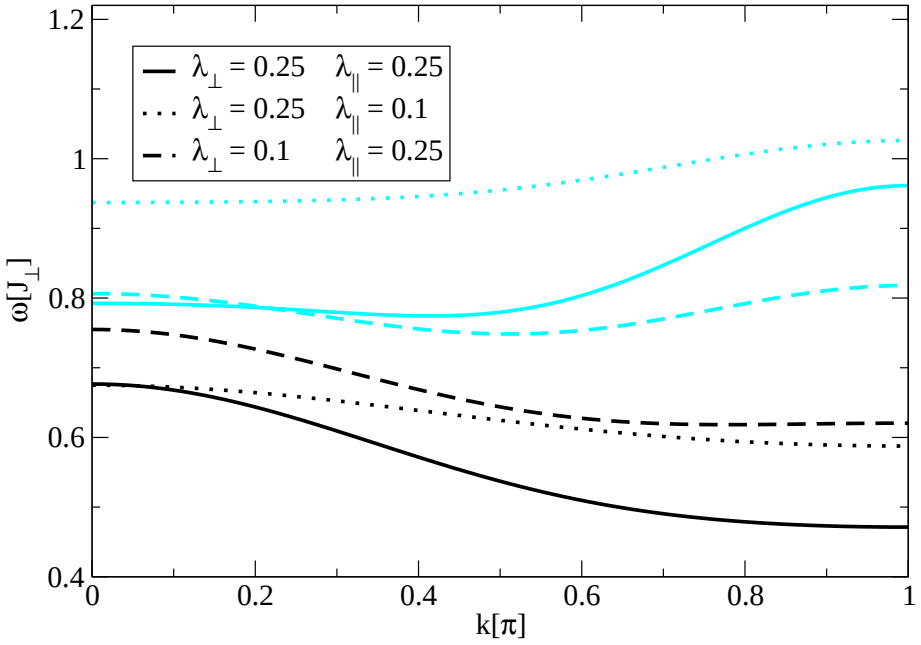

(b) smaller hopping constants compared to $\lambda_\perp = \lambda_\parallel = 0.25$.

Figure 5.25: One-hole dispersions with even parity (black) and odd parity (cyan) for $x = 0.5$, $x_\square = 0$ and anisotropic hopping constants.

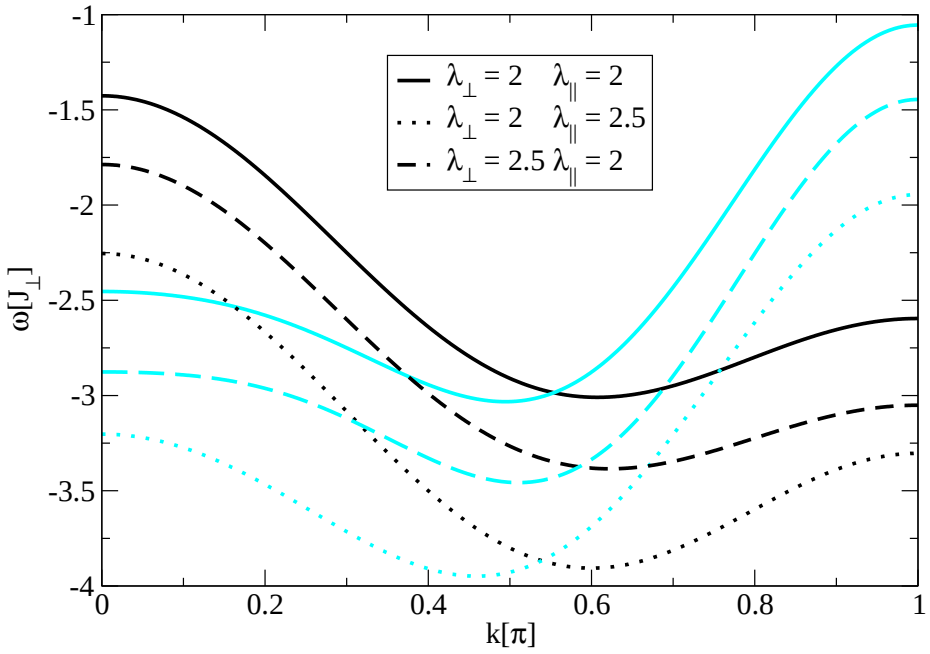

(a) larger hopping constants compared to $\lambda_\perp = \lambda_\parallel = 2$.

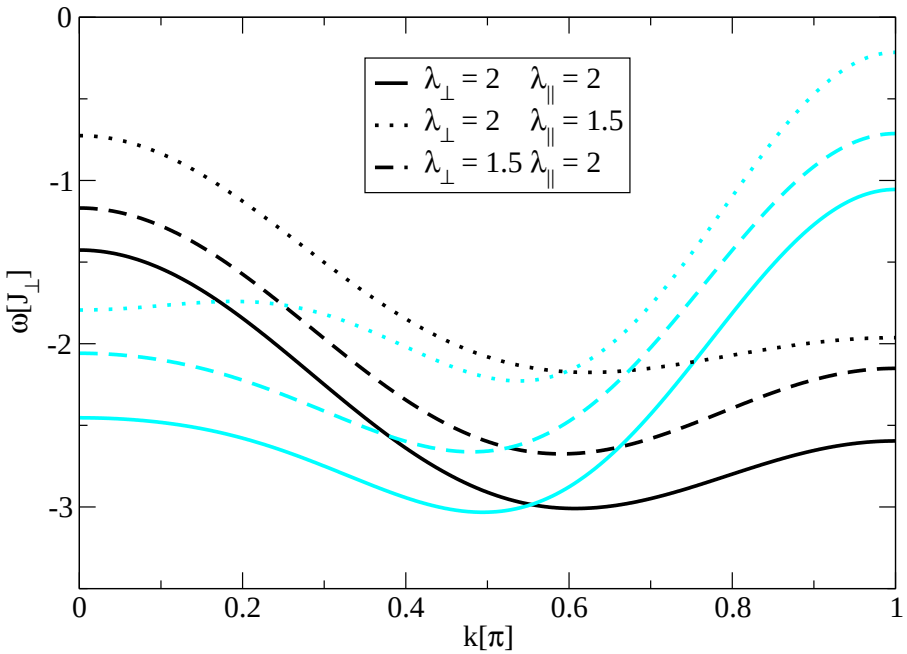

(b) smaller hopping constants compared to $\lambda_\perp = \lambda_\parallel = 2$.

Figure 5.26: One-hole dispersions with even parity (black) and odd parity (cyan) for $x = 1$, $x_\square = 0$ and anisotropic hopping constants.

5.4.3 Influence of the Ring Exchange

Since the ring exchange is needed for an adequate description of the experimentally available systems (see Section 4.1), we also investigate the influence of the ring exchange on the doped ladder which is – to our knowledge – still an open issue. A typical value is $x_\square \approx 0.2$ [75]. Like for the examination of the anisotropic hopping we take the reliable results for $x = 0$, $\lambda_\perp = \lambda_\parallel = 0.5$; $x = 0.5$, $\lambda_\perp = \lambda_\parallel = 0.25$ and $x = 1$, $\lambda_\perp = \lambda_\parallel = 2$ without ring exchange as starting point for our investigation.

For the first case $x = 0$, $\lambda_\perp = \lambda_\parallel = 0.5$ the influence of the ring exchange is the weakest (see Figure 5.27). The odd band hardly changes. It is slightly lowered – only the maximum is decreased more strongly. The even band, however, changes more pronouncedly. It is strongly lowered so that a band crossing occurs and the shape changes. A local miminum appears at $k = 0$ developing into the global minimum with growing $x_\square$.

Figure 5.28 depicts the case $x = 0.5$, $\lambda_\perp = \lambda_\parallel = 0.25$. Both bands are lowered stronger for small k than for large k. Also the shape of both bands changes. While the minimum of the even band moves to $k \approx 0.65\pi$ for $x_\square = 0.2$ and a local maximum at $k = \pi$ occurs, the local maximum at $k = 0$ of the odd band moves to $k \approx 0.55\pi$ and a local minimum at $k = 0$ occurs.

For $\lambda_\perp = \lambda_\parallel = 2$ and $x = 1$ only the gs results are discussed as the pc generator yields no conclusive results for these parameters without ring exchange (see Section 5.4.1). The resulting one-hole dispersions are shown in Figure 5.29. The increase of $x_\square$ yields a lowered dispersion for both bands. The shape of the bands is conserved, but for the odd band the decrease is pronounced around $k = \pi$, while not only a less pronounced decrease, but even an increase of the energy can be observed for the even band around $k = \pi$.

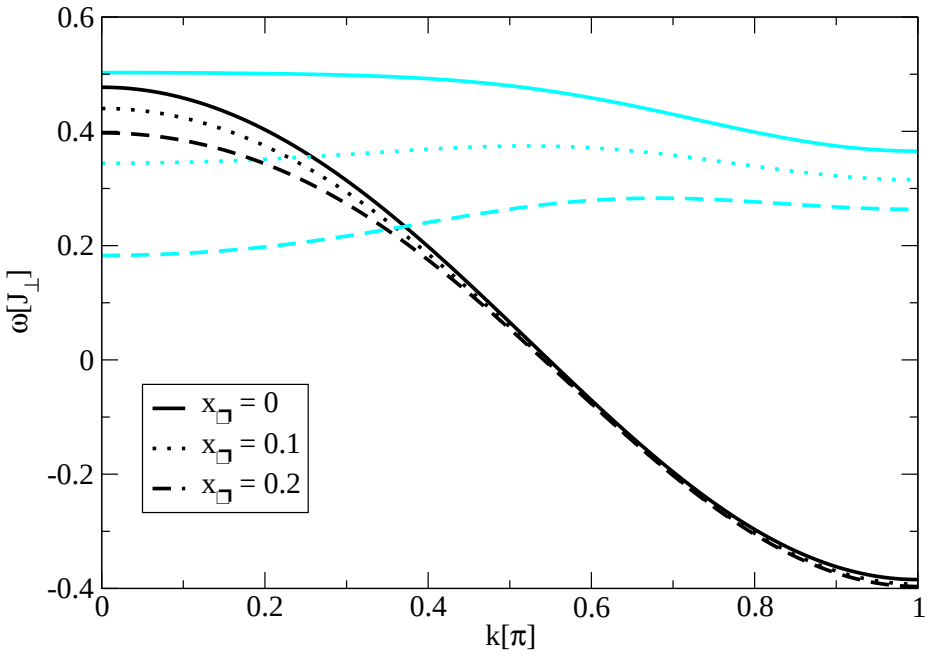

Figure 5.27: One-hole dispersions with even parity (black) and odd parity (cyan) for $x = 0$, $\lambda_\perp = \lambda_\parallel = 0.5$ and various values for $x_\square$.

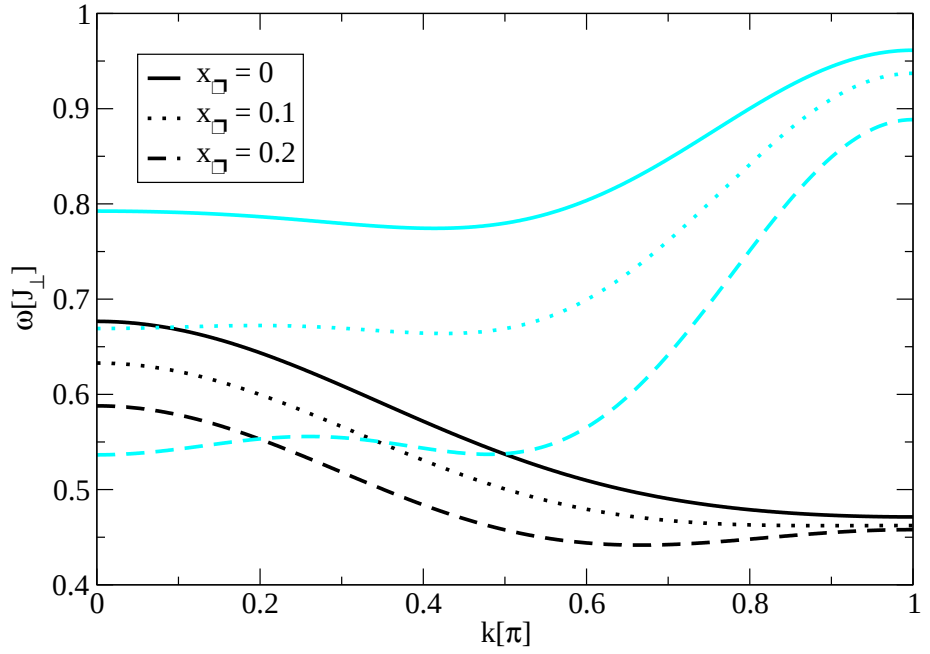

Figure 5.28: One-hole dispersions with even parity (black) and odd parity (cyan) for $x = 0.5$, $\lambda_\perp = \lambda_\parallel = 0.25$ and various values for $x_\square$.

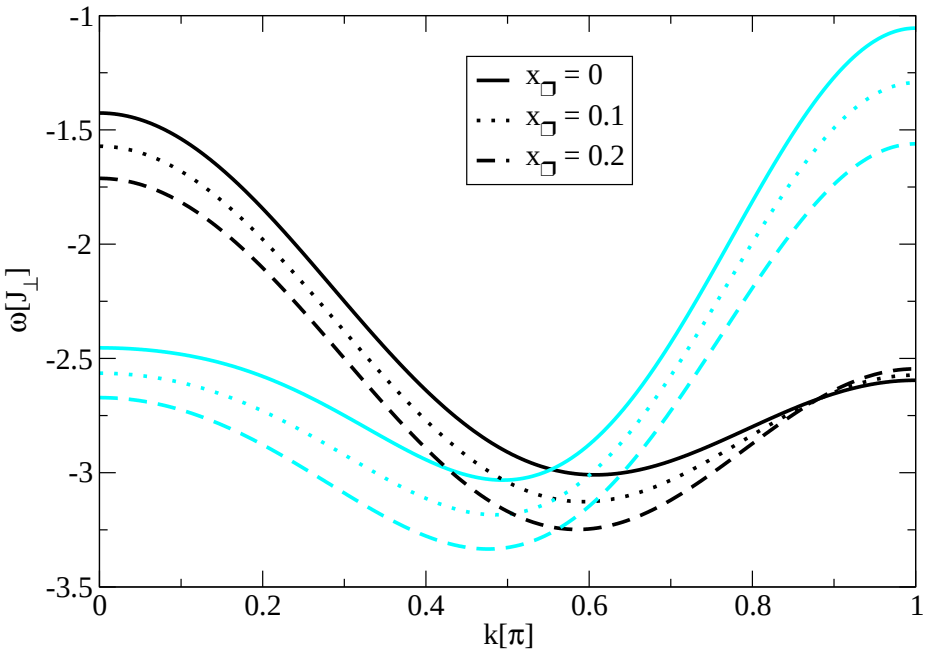

Figure 5.29: One-hole dispersions with even parity (black) and odd parity (cyan) for $x = 1$, $\lambda_\perp = \lambda_\parallel = 2$ and various values for $x_\square$.

5.5 Discussion

We are able to calculate the one-hole dispersions by means of SCUT. The agreement with results from series expansion is very good for small parameters. Even in the regime $x = 1$, $x_\square = 0$, $2 < \lambda < 3$ the agreement with the exact diagonalisation results is still good. The hole dispersions are strongly influenced by the triplons. Because the one-hole dispersion with odd parity has a larger local energy which is influenced more strongly by the continuum above, it changes more explicitly with increasing hopping constants. Hence it is doubtlessly more difficult to calculate, i.e. the influence of the triplons on the odd band is stronger than on the even band. Therefore the deviations from the simple cosine shape are more pronounced for the odd band. These deviations grow if either the magnetic coupling or the strength of the hopping is increased:

- The broadening of the odd band is slowing down, then turned into a narrowing and finally the shape changes totally under the influence of the second harmonic so that the maximum at $k = 0$ is only local, the total maximum occurs at $k = \pi$ and the minimum lies between 0 and π.

- The shift upwards is also slowing down and then turned into a shift downwards due to the influence of the continuum formed by one triplon and one even hole state. In the regime around $x = 1$ and $\lambda_\perp = \lambda_\parallel = 2$ the constant of the odd dispersion is approximately as low as the constant of the even dispersion.

For the even band the deviations from the cosine shaped dispersion consist essentially in the growth of the second harmonic. For $x = 1$ and $\lambda_\perp = \lambda_\parallel = 2$ the minimum has moved from $k = \pi$ into the region $k \approx \frac{\pi}{2}$. A local maximum at $k = \pi$ occurs. But the absolute maximum remains at $k = 0$.

The combination of these effects for $x = 1$ and $\lambda_\perp = \lambda_\parallel = 2$ yield a crossing of the two dispersions. The crossing point lies between the minima of the bands. However, the pc generator is not applicable for the SCUT if the parameters are in this region. This is suggested by the deviations from the series expansion and exact diagonalisation results as well as by the peculiar convergence behaviour of the SCUT.

In the regime $x \approx 1$ and $\lambda_\perp = \lambda_\parallel \gtrsim 1$ the pc generator is no longer suitable because the convergence of the flow is hindered due to the overlap between the one-hole-one-triplon continuua and the one-hole-two-triplon continua. The pc

results are distinct from the series expansion and exact diagonalisation results. Furthermore the convergence is very slow and exhibits features that indicate problems regarding the sorting of the eigenvalues. The remedy is the gs generator which only decouples the zero-triplon space from the rest. Then the hole dispersions are similar to the exact diagonalisation results. Although there are small deviations from the series expansion, the agreement is astonishingly good. Because the exact diagonalisation examines a ladder with fourteen rungs, finite size effects are present so that a part of the deviations are due to constraints of the exact diagonalisation. The remaining deviations are probably due to truncation errors. Another aspect in favour for the SCUT induced by the gs generator is the satisfactory convergence behaviour.

The treatment of the case $\lambda_\perp > 2$ and $\lambda_\parallel > 2$ is problematic for the gs generator because the convergence is hindered by the overlap between the odd one-hole dispersion and the continuum formed by one even hole and one triplon. To achieve convergence in this regime we use the following restriction for the gs generator. A term affecting the hole-triplon continuum is omitted, if the distance between the triplon and the hole state on which the term acts is larger than $\Delta n_{\max}$. The effective Hamiltonian yields an upper boundary for the hole dispersions. The comparison between the results from the full gs generator and from the restricted gs generator for $x = 1$ and $\lambda_\perp = \lambda_\parallel = 2$ shows that the upper boundary given by the result from the restricted generator is already close to the result from the full generator for $\Delta n_{\max} = 2$. For $x = 1$ and $\lambda_\perp = \lambda_\parallel = 3$ this restriction $\Delta n_{\max} = 2$ induces convergence, while the flow diverges for $\Delta n_{\max} > 2$. The estimations we obtain for the hole dispersions are again in good agreement with the exact diagonalisation results. The exact diagonalisation [101] results predict that the situation is qualitatively the same for $\lambda_\perp = \lambda_\parallel = 3$ as for $\lambda_\perp = \lambda_\parallel = 2$ if $x = 1$ and $x_\square = 0$. The bands exhibit a similar shape and relative position to each other so that still a crossing at $k \approx 0.5\pi$ occurs. But the energy is lowered and the bandwith of both bands is increased by a factor of ≈ 1.5. The results from the restricted gs generator yields an estimation for the even band which is in good agreement with the exact diagonalisation result, while the odd hole dispersion exhibits deviations that are very similar to the deviations between the exact diagonalisation and the full gs generator for $\lambda_\perp = \lambda_\parallel = 2$.

The case $x = \lambda_\perp = \lambda_\parallel = 0.5$ is a special one. Both the pc and the gs generator (even with increased maximal extensions) exhibit deviations from the series expansion results for the odd hole state. These deviations stem apparently from

the closeness (or even overlap) of the continuum formed by one even hole and one triplon. If the lowering of the odd band is overestimated by the SCUT or underestimated by the series expansion is not clear.

Anisotropic hopping has the effect that the bands are lowered (raised) if one hopping constant is increased (decreased). But if $\lambda_\perp$ is changed, the odd band exhibits a slightly different behaviour dominated by the first and second harmonic respectively.

The ring exchange leads to a lowering of the hole dispersions. This effect is least pronounced for the even band around $k = \pi$. The deformation of the band shape is most pronounced for the odd band like for the anisotropic hopping.

All in all the odd band is more sensitive to changes of the parameters than the even band.

Ladders doped with more than one hole have not been treated yet. The additional local basis state (the completely empty rung), which is present for at least two holes in the system, increases the number of operator terms to be considered with the calculations. As we have already reached the limits of the computational performance, we expect that this increment is difficult to handle. However, we expect that this state is still negligible for slightly doped ladders because the local energy of this state is larger than the local energies of the remaining states.

The use of the spin symmetry, which reduces the time and memory costs for the undoped ladder by a factor of approximately 6, is still not implemented for the doped ladder. By this implementation also a factor of approximately 6 could be gained concerning the reduction of time and memory. But this implementation is distinctly more difficult for the doped case because the rotation in spin space does not simply convert one local hole state operator into another one like it is the case for the triplet states. A rotation of a hole state operator in spin space yields a linear combination of two operators. This is problematic because linear combinations of operators have to be taken into account for the identification of the representative terms during the setup of the differential equations.

The symmetry utilisation would also allow us to investigate the influence of increasing maximal extensions. Until now we are not able to state whether the results still change if the truncation is made less strict. We expect at least minor changes since the extensions concerning the hole operators are much smaller than the extensions of the pure triplon terms.

6 Summary and Outlook

In the present thesis the technique of self-similar continuous unitary transformations (SCUTs) is used to generate effective Hamiltonians for antiferromagnetic Heisenberg spin-$\frac{1}{2}$ ladders, which are appropriate models for a certain subsystem of $(\mathrm{Sr}, \mathrm{La}, \mathrm{Ca}, \mathrm{Y})_{14}\mathrm{Cu}_{24}\mathrm{O}_{41}$ – the so called telephone number compounds.

A continuous unitary transformation (CUT) is a general method to diagonalise Hamiltonians. The choice of the generator determines the properties of the CUT. The pc generator which creates particle conserving Hamiltonians and adaptions of this generator are used in this thesis. The SCUT uses a truncation scheme that defines which parts of the Hamiltonian shall be omitted. This induces a self-similar transformation. The SCUT is not in need of extrapolation techniques like the perturbative realisation of CUT. However, overlapping energies cause convergence problems[1]. A possible remedy is a generator adaption excluding the terms hindering the convergence.

The doped spin-$\frac{1}{2}$ ladder is a one-dimensional model, which is expected to capture the same qualitative features as the two-dimensional cuprate lattice, which exhibits high-temperature superconductivity. The undoped and the slightly hole-doped case are considered in this thesis. Double occupancy is forbidden for the sites, which is a good model assumption for strong Coulomb repulsion. Because this system is gapful for the considered parameters, the correlations between the excitations decrease exponentially with the distance. Therefore a real space truncation is appropriate.

The performance and the numerical stability of the SCUT are improved decisively for the undoped ladder by utilising the spin symmetries within the bond operator representation. For the undoped ladder the implementation of the gs,1p generator, which decouples only the zero- and one-triplon space from the rest of the Hilbert space, enables the treatment of higher values of x (the ratio between the magnetic coupling parallel and perpendicular to the ladder). Since the

[1] Note that strong overlaps also pose problems for the PCUT on the conceptual level.

two- and the four-triplon continuum overlap becomes stronger with increasing x and therefore hinders the convergence of the transformation, the gs,1p generator avoids the sorting of the corresponding eigenenergies and yields a converging truncation. However, the two-triplon bound states cannot be calculated without an additional diagonalisation. Hence continua with more than two particles cannot be determined easily if the gs,1p generator is used because the two-triplon bound states contribute crucially to these continua. The execution of this decoupling is subject to current research.

We also detect that the one-triplon dispersion enters the three-triplon continuum for $x = 1.5$. Yet the overlap is not too large. Hence it does not hinder the convergence of the gs,1p SCUT.

For the doped ladder we are able to calculate the dispersions for the hole states which include not only a hole but also a spin and therefore interact magnetically with the neighbouring rungs. The hole dispersions, which are degenerate concerning the spin but differ for different parity, are strongly influenced by interactions with the triplons. This influence is stronger on the band with odd parity than on the band with even parity because the local energy of the odd hole state is larger and more sensitive to the continuum above. The agreement with the series expansion results is very good for a large regime of parameters.

If at least one of the continua formed by one hole and one triplon exhibits a pronounced overlap with the higher continua, the pc generator is no longer applicable. The agreement with the results of other methods and the convergence deteriorate. Then the gs generator, which decouples only the zero-triplon state from the remaining states, yields by far more conclusive results. If the parameters are small, the results of the pc and of the gs generator coincide.

In case of strong isotropic hopping constants $\lambda_\perp = \lambda_\parallel \gtrsim 1$ and $x = 1$ the hole dispersions cover approximately the same energies and exhibit a crossing at $k \approx 0.5\pi$. Our results are in good agreement with the exact diagonalisation results for $\lambda_\perp = \lambda_\parallel = 2$. The finite size scaling of the exact diagonalisation explains most of the deviations between both methods. The remaining deviations are probably caused by truncation errors. However, the convergence of the gs generator is lost for even larger hopping constants. Because the restricted gs generator still converges in this regime, the convergence problems must be due to the overlap of the one-hole dispersions with the triplon-hole continua.

The restriction which is applied to the generator omits a term affecting the continuum formed by one hole and one triplon, if the maximal distance $\Delta n_{\max}$

between the triplon and the hole state on which the term acts is exceeded. If we Fourier transform the one-hole subspace of the effective Hamiltonian, we obtain only upper boundaries for the actual hole dispersions. Nevertheless, these results are close to the exact diagonalisation results for $x = 1$ and $\lambda_\perp = \lambda_\parallel = 3$.

We also investigated the influence of anisotropic hopping and magnetic ring exchange on the one-hole dispersions. The odd hole dispersion is more sensitive to changes of the parameters than the even hole dispersion due to the stronger influence of the continuum for the odd band which has a larger local energy.

We conclude with an outlook on future investigations. The next step will be the examination of two-hole states. Especially the two-hole bound states, which are interesting in the context of superconductivity, shall be investigated. The inclusion of the rung state with two holes, i.e. the empty state, which is not needed to be considered for the one-hole dispersions, increases the effort concerning memory and time needed for the calculation incisively. However, we expect that this state is still negligible because it is energetically unfavourable.

Nevertheless, even without the local two-hole state the system of differential equations is larger if all operators acting on global two-hole states are included. The new terms are terms with four hole operators (two creation and two annihilation operators). The utilisation of the spin symmetry for the operators affecting hole states, which is still difficult to implement, would improve the performance of the program significantly. Another approximation that reduces the effort can be made by neglecting all contributions from terms with four hole operators on the right hand side of the flow equation, but not on the left hand side.

A Effects of Utilisation of the Spin Symmetry for the Undoped Ladder

The utilisation of the spin symmetry reduces the terms to be included in the Hamiltonian of the undoped ladder by almost a factor of six. Nearly all terms deal with two or three different spin states. For these terms the application of all possible rotations in spin space to a representative term yields six terms including the representative. These rotations are equivalent to permuting the spin states x, y, z and adding optional signs for the local triplon operators[1]. Therefore these rotations are easy to implement for the triplon operators in the bond operator representation [65].

Together with the utilisation of the Hermiticity and the real space symmetry the memory as well as the time consumed by the calculation can be reduced by almost a factor of 24. But this is only the obvious advantage. The numerical stability of the integration is also improved by utilising the symmetries. Without explicit consideration of the symmetry small numerical deviations between terms that should be equal can increase drastically via feedback. This feedback is due to the coupling of the differential equations. Differences of such terms expected to be zero yield finite numerical values and contribute to the flow equation. These rounding errors link sectors of the Hilbert space which should be decoupled. Hence the SCUT fails at the reordering and the feedback becomes dominant. In Figure A.1 the effect of such a feedback can be observed in the ROD (residual off-diagonality, introduced in Section 3.6). If symmetries are not utilised, the ROD exhibits the typical behaviour for such a numerical instability at $lJ_\perp \approx 70$: The exponential decrease changes into an exponential increase at this point and shows a non-convergent behaviour afterwards, which is characterised by alternating irregular decrease and increase. If the symmetries are

[1] If the parity is conserved, there is always an even number of additional signs.

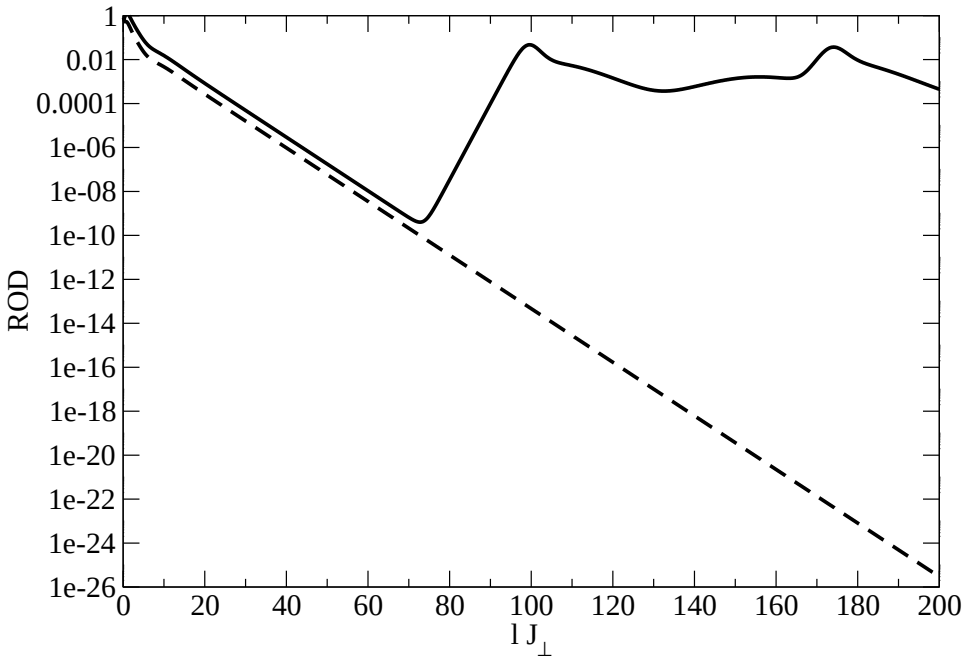

Figure A.1: Comparison of the ROD during the flow for the pc SCUT with (dashed) and without (solid) utilisation of the symmetries; undoped ladder with $x = 1$, $x_\square = 0$; truncation: $N = 4$, $d_2 = 10$, $d_4 = 6$, $d_5 = 5$, $d_2 = 3$.

utilised on the contrary, the ROD decreases exponentially without peculiarities.

The symmetry breaking for the SCUT without utilisation of the symmetries responsible for the feedback is also amplified and distributed via the coupling of the differential equations. Figure A.2 shows this symmetry breaking examplarily for six terms that are actually spin symmetric. The coefficients of these terms should be equal but deviate for $lJ_\perp \gtrsim 100$, i.e. after the kink of the ROD. The convergence seems to be achieved already at $lJ_\perp \approx 12$. Induced by the numerical instability abrupt deviations from the convergence value occur for $lJ_\perp \gtrsim 100$ except for two of the considered coefficients, which, however, finally show small deviations from the convergence value for $lJ_\perp \gtrsim 195$.

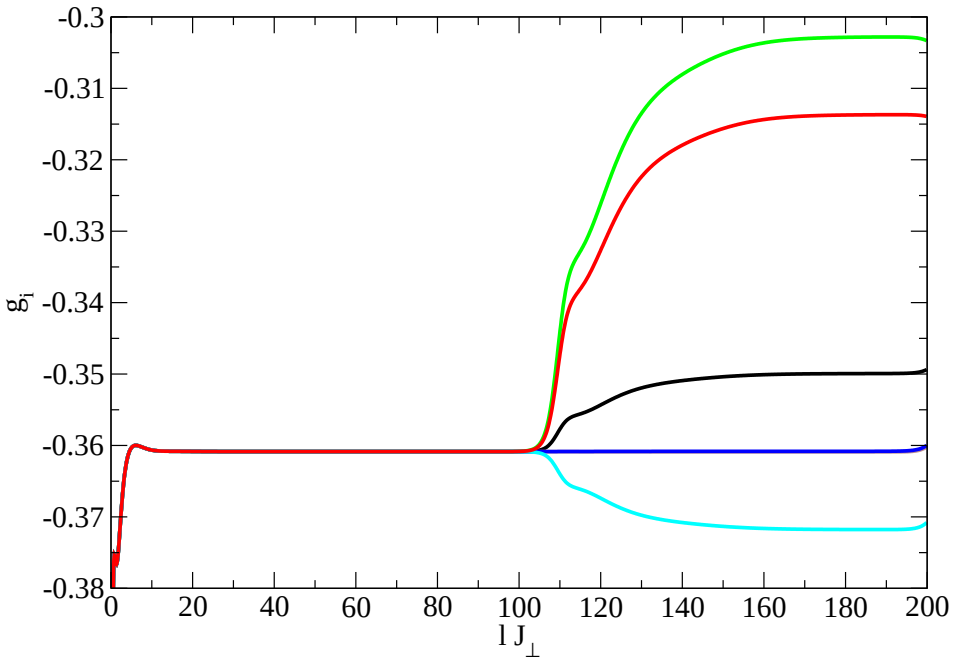

Figure A.2: Comparison of the coefficients g_i of six terms that should be equal due to the spin symmetry during the flow for the pc SCUT without utilisation of the symmetries; undoped ladder with $x = 1$, $x_\square = 0$; truncation: $N = 4$, $d_2 = 10$, $d_4 = 6$, $d_5 = 5$, $d_2 = 3$. The blue curve coincides with the curve of another coefficient.

B Consistency Check for the Doped Ladder Results

A high-level check of the SCUT method for the hole-doped ladder is performed by a systematic comparison with the series expansion results from Ref. [97]. For this purpose a new truncation scheme is introduced that is not based on extensions in real space but on the perturbation parameters instead. This allows us to compare the order of the parameters. In Ref. [97] the ring exchange is not considered and the coupling constants for the hopping are identical. Therefore the only perturbation parameters are x and $\lambda = \lambda_{\parallel} = \lambda_{\perp}$. The ratio $\rho = \frac{x}{\lambda}$ is fixed for each comparison to have actually only one parameter. For the new truncation a new attribute is assigned to each term: the leading order in x for the expansion of the coefficient. Nevertheless, the CUT is still self-similar and the expansions in x are not calculated. This is not necessary to determine the leading order. The leading order for the terms of the starting Hamiltonian is known because all contributions generated by the SCUT are terms of the same or higher order as they originate from commutators and nested commutators of these terms. So the leading order of these terms is the leading order in which x is present for $l = 0$.

The expansion of the coefficients $g_i(l)$ in x has the form

$$g_i(l) = \sum_{m=0}^{\infty} a_{i,n_i+m}(l) x^{n_i+m} \tag{B.1}$$

where n_i is the leading order. As the differential equations for the coefficients have a bilinear form (2.18), the leading order of a $g_i(l)$ which is zero for $l = 0$ is given by the minimal exponent $n_j + n_k$ of all terms $g_j(l)g_k(l)$ on the right hand side of the flow equation.

If the leading order of a term, which occurs during the setup of the flow equation, is higher than a certain $n_{\max}$ defined in advance, this term is omitted. With this truncation we are able to control up to which order the results will be correct.

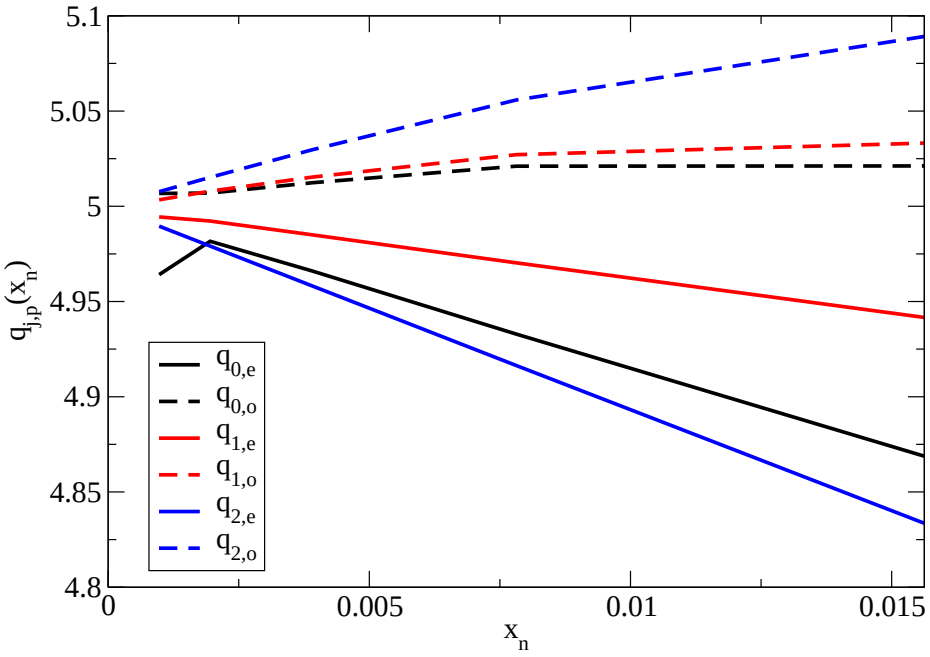

Figure B.1: Consistency check for $n_{\max} = 4$ and $\rho = 0.5$. For all coefficients $c_{j,p}$ the difference quotient $q_{j,p}$ converges against $\alpha = 5$. The difference $\Delta c_{0,e}$ has the smallest value which is already in the order of the numerical precision for $x_n \approx 0.001$. Hence $q_{0,e}$ shows deviations for small x.

The coefficients $c_{j,p}$ of the one-hole dispersions

$$\omega_{1h,p}(k) = c_{0,p} + \sum_{j=1}^{j_{\max}} 2c_{j,p}\cos(jk) \tag{B.2}$$

were compared with the results of the series expansion. The parameter $p \in \{e, o\}$ denotes the parity (even or odd) of the hole state. Because no maximal extension in real space is defined in this truncation scheme, $j_{\max}$ depends on $n_{\max}$. According to the fourth order series from Ref. [97] and using $\lambda = \frac{x}{\rho}$ the leading order for $c_{0,p}$ is zero, one for $c_{1,p}$ and four for $c_{2,p}$, i.e. $j_{\max} = 1$ for $0 < n_{\max} < 4$ and $j_{\max} = 2$ for $n_{\max} = 4$.

If both methods are consistent, the difference between a coefficient calculated by SCUT on the one hand and the corresponding coefficient from the series expansion on the other hand should show power law behaviour $\propto x^{\alpha}$ with $\alpha = n_{\max} + 1$ for $x \to 0$. For the check of the behaviour of this difference $\Delta c_{j,p}(x)$ for $x \to 0$ we analysed several values of x starting with $x_0 = \frac{1}{64}$ and bisecting x consecutively,

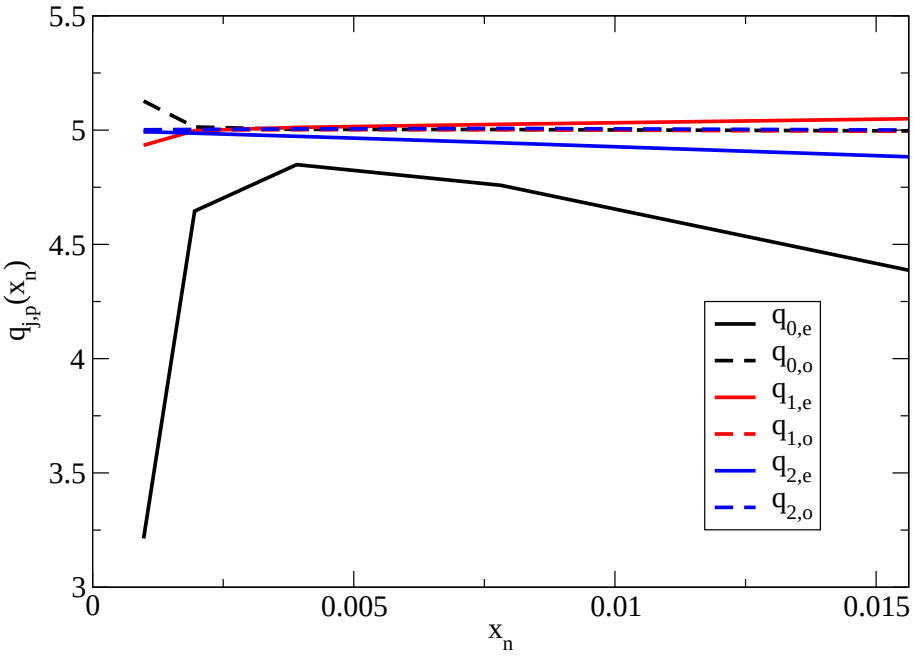

Figure B.2: Consistency check for $n_{\max} = 4$ and $\rho = 1$. For all coefficients $c_{j,p}$ the difference quotient $q_{j,p}$ converges against $\alpha = 5$. Again for $q_{0,e}$ the deviations are the most obvious and larger than for $\rho = 0.5$ but also for $q_{0,o}$ and $q_{1,e}$ deviations are distinguishable.

i.e. $x_{n+1} = \frac{x_n}{2}$. This was done for $\rho = 0.5$, $\rho = 1$ and $\rho = 2$. To show that $\alpha = n_{\max} + 1$ is actually the dominating exponent in $\Delta c_{j,p}(x)$ the ratio of the differences

$$q_{j,p}(x_n) = \frac{\ln\left(\Delta c_{j,p}(x_n)\right) - \ln\left(\Delta c_{j,p}(x_{n+1})\right)}{\ln(x_n) - \ln(x_{n+1})} \tag{B.3}$$

was plotted against x_n. For a function $\Delta c_{j,p}(x)$ dominated by $b\,x^{\alpha}$

$$\lim_{n\to\infty} q_{j,p}(x_n) = \alpha \tag{B.4}$$

holds true. But if x_n becomes too small, $\Delta c_{j,p}$ is reduced to the size of the numerical precision. The difference $\Delta c_{j,p}$ is even numerically zero for very small x_n because the error is smaller than the numerical precision for $x \approx 0$. Therefore the convergence ceases in this region. Nevertheless, in a small region where x_n is neither too small nor too large the convergence is observable.

The figures depicted here (Figures B.1-B.3) show the behaviour of the $q_{j,p}$ for $n_{\max} = 4$. The expected convergence against $\alpha = 5$ is obvious. The deviations for small x can be explained by reaching the limits of the numerical precision. The

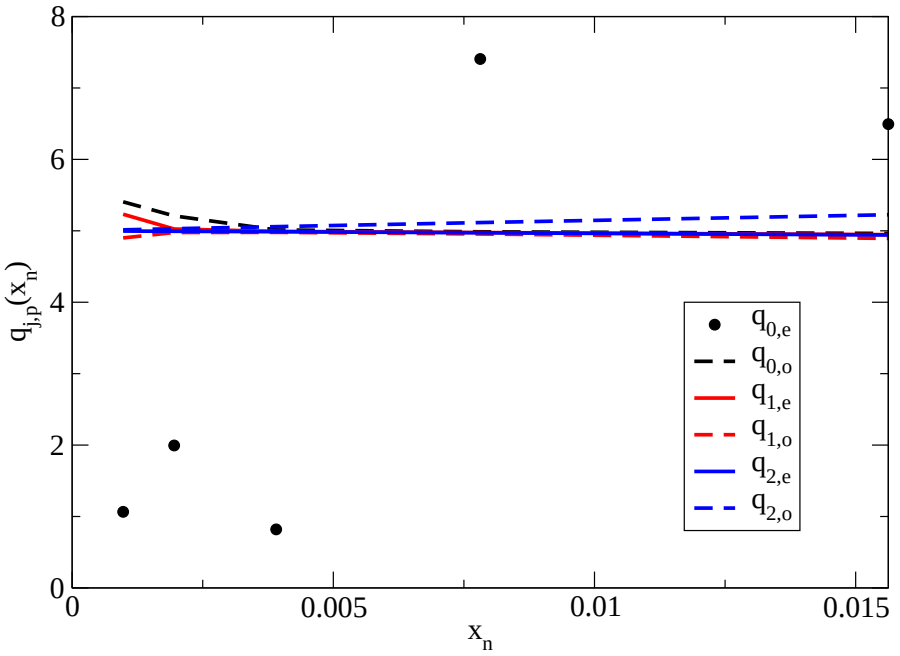

Figure B.3: Consistency check for $n_{\max} = 4$ and $\rho = 2$. For all coefficients $c_{j,p}$ the difference quotient $q_{j,p}$ converges against $\alpha = 5$ except for $q_{0,e}$. For this reason the data points for $q_{0,e}$ were not connected as they do not form a curve. Further explanations can be found in the text.

only remaining discrepancy is the behaviour of $q_{0,e}$ for $\rho = 2$ (see Figure B.3), which does not reveal any kind of convergence. This is due to a zero-crossing of $\Delta c_{0,e}$ in the considered region of x. Thus the ansatz with the ratio $q_{j,p}$ yields no reliable result. However, the proper behaviour of the other $q_{j,p}$ demonstrates the consistency of the SCUT with the series expansion. If $c_{0,e}$ exhibited an error, this error would affect the other coefficients via the flow equations and they would not show a consistent behaviour.

To conclude, we can state that this high-level check supports our method. The results of this check meet our expectations that the SCUT is implemented correctly.

Bibliography

[1] Bardeen, J., Cooper, L. N., and Schrieffer, J. R. *Phys. Rev.* **108**, 1175 (1957).

[2] Bednorz, J. G. and Müller, K. A. *Z. Phys. B* **64**, 189 (1986).

[3] Dai, P. et al. *Physica C: Superconductivity* **243**, 201 (1995).

[4] Anderson, P. W. *Science* **235**, 1196 (1987).

[5] Zhang, F. C. and Rice, T. M. *Phys. Rev. B* **37**, 3759 (1988).

[6] Spałek, J. *Acta Phys. Polon. A* **111**, 409 (2007).

[7] Orenstein, J. and Millis, A. J. *Science* **288**, 468 (2000).

[8] Anderson, P. W. *Science* **288**, 480 (2000).

[9] Lee, D.-H. *Phys. Rev. Lett.* **84**, 2694 (2000).

[10] Bianconi, A., Saini, N. L., Lanzara, A., Missori, M., Rossetti, T., Oyanagi, H., Yamaguchi, H., Oka, K., and Ito, T. *Phys. Rev. Lett.* **76**, 3412 (1996).

[11] Salkola, M. T., Emery, V. J., and Kivelson, S. A. *Phys. Rev. Lett.* **77**, 155 (1996).

[12] Kivelson, S. A., Fradkin, E., and Emery, V. *Nature* **393**, 550 (1998).

[13] Zaanen, J. *Science* **286**, 251 (1999).

[14] Chakravarty, S., Halperin, B. I., and Nelson, D. R. *Phys. Rev. B* **39**, 2344 (1989).

[15] Chakravarty, S., Laughlin, R. B., Morr, D. K., and Nayak, C. *Phys. Rev. B* **63**, 094503 (2001).

[16] Uehara, M. et al. *J. Phys. Soc. Jpn.* **65**, 2764 (1996).

[17] Ueda, Y. and Isobe, M. *J. Magn. Magn. Mater.* **177**, 741 (1998).

[18] Hiroi, Z., Azuma, M., Takano, M., and Bando, Y. *J. Solid State Chem.* **95**, 230 (1991).

[19] Reischl, A. PhD thesis, Universität zu Köln, (2006).

[20] Wegner, F. J. *Ann. Physik* **3**, 77 (1994).

[21] Głazek, S. D. and Wilson, K. G. *Phys. Rev. D* **48**, 5863 (1993).

[22] Głazek, S. D. and Wilson, K. G. *Ann. Physik* **49**, 4214 (1994).

[23] Mielke, A. *Eur. Phys. J. B* **5**, 605 (1998).

[24] Uhrig, G. S. and Normand, B. *Phys. Rev. B* **58**, R14705 (1998).

[25] Knetter, C. and Uhrig, G. S. *Eur. Phys. J. B* **13**, 209 (2000).

[26] Fischer, T., Duffe, S., and Uhrig, G. S. *New Journ. Phys.* **12**, 33048 (2010).

[27] Schmidt, K. P. PhD thesis, Universität zu Köln, (2004).

[28] Windt, M. S. PhD thesis, Universität zu Köln, (2002).

[29] Vuletić, T. et al. *Physics Reports* **428**, 169 (2006).

[30] Anderson, P. W. *Phys. Rev.* **79**, 350 (1950).

[31] Gopalan, S., Rice, T. M., and Sigrist, M. *Phys. Rev. B* **49**, 8901 (1994).

[32] Matsuda, M., Katsumata, K., Eccleston, R. S., Brehmer, S., and Mikeska, H.-J. *Phys. Rev. B* **62**, 8903 (2000).

[33] Schmidt, K. P. and Uhrig, G. S. *Phys. Rev. B* **75**, 224414 (2007).

[34] Barnes, T., Dagotto, E., and Swanson, J. R. E. S. *Phys. Rev. B* **47**, 3196 (1993).

[35] Dagotto, E. and Moreo, A. *Phys. Rev. B* **38**, 5087 (1988).

[36] Dagotto, E., Riera, J., and Scalapino, D. *Phys. Rev. B* **45**, 5744 (1992).

[37] Dagotto, E. and Rice, T. M. *Science* **271**, 618 (1996).

[38] Johnston, D. C. et al. (unpublished) cond-mat/0001147, (2000).

[39] Kato, M., Shiota, K., and Koike, Y. *Physica C* **258**, 284 (1996).

[40] Nücker, N. et al. *Phys. Rev. B* **62**, 14384 (2000).

[41] Mizuno, Y., Tohyama, T., and Maekawa, S. *J. Phys. Soc. Jpn.* **66**, 397 (1997).

[42] Windt, M. et al. *Phys. Rev. Lett.* **87**, 127002 (2001).

[43] Heidbrink, C. P. and Uhrig, G. S. *Eur. Phys. J. B* **30**, 443 (2002).

[44] Knetter, C., Schmidt, K. P., and Uhrig, G. S. *J. Phys. A: Math. Gen.* **36**, 7889 (2003).

[45] Dusuel, S. and Uhrig, G. S. *J. Phys. A: Math. Gen.* **37**, 9275 (2004).

[46] Stein, J. *J. Stat. Phys.* **88**, 487 (1997).

[47] Becker, K. W., Hübsch, A., and Sommer, T. *Phys. Rev. B* **66**, 235115 (2002).

[48] Knetter, C., Schmidt, K. P., and Uhrig, G. S. *Eur. Phys. J. B* **36**, 525 (2004).

[49] Kehrein, S. K. and Mielke, A. *J. Phys. A: Math. Gen.* **27**, 4259 (1994).

[50] Kehrein, S. K. and Mielke, A. *J. Phys. A: Math. Gen.* **27**, 5705 (1994).

[51] Kehrein, S. K. and Mielke, A. *Ann. Phys., NY* **252**, 1 (1996).

[52] Mielke, A. *Ann. Phys., Lpz.* **509**, 215 (1997).

[53] Mielke, A. *Europhys. Lett.* **40**, 195 (1997).

[54] Moca, C. P. and Tifrea, I. *J. Supercond.* **11**, 719 (1998).

[55] Ragwitz, M. and Wegner, F. *Eur. Phys. J. B* **8**, 9 (1999).

[56] A. Reischl, A., Müller-Hartmann, E., and Uhrig, G. S. *Phys. Rev. B* **70**, 245124 (2004).

[57] Wegner, F. *J. Phys. A: Math. Gen.* **39**, 8221 (2006).

[58] Drescher, N. and Uhrig, G. S. in preparation, (2010).

[59] Ashcroft, N. W. and Mermin, N. D. *Solid State Physics*. Saunders College Publishing, (1976).

[60] Sachdev, S. *Quantum Phase Transitions*. Cambridge University Press, (1999).

[61] Kirschner, S. diploma thesis, Universität zu Köln, (2004).

[62] Hamerla, S., Duffe, S., and Uhrig, G. S. in preparation, (2010).

[63] Press, W. H., Teukolsky, S. A., Vetterling, W. T., and Flannery, B. P. *Numerical Recipes in C++: The Art of Scientific Computing*. Cambridge University Press, (2002).

[64] Schmidt, K. P. and Uhrig, G. S. *Phys. Rev. Lett.* **90**, 227204 (2003).

[65] Sachdev, S. and Bhatt, R. N. *Phys. Rev. B* **41**, 9323 (1990).

[66] Coldea, R. et al. *Phys. Rev. Lett.* **86**, 5377 (2001).

[67] Mizuno, Y., Tohyama, T., and Maekawa, S. *J. Low Temp. Ph.* **117**, 389 (1999).

[68] Brehmer, S., Mikeska, H.-J., Müller, M., Nagaosa, N., and Uchida, S. *Phys. Rev. B* **60**, 329 (1999).

[69] Lorenzana, J., Eroles, J., and Sorella, S. *Phys. Rev. Lett.* **83**, 5122 (1999).

[70] Katanin, A. A. and Kampf, A. P. *Phys. Rev. B* **66**, 100403 (2002).

[71] Katanin, A. A. and Kampf, A. P. *Phys. Rev. B* **67**, 100404 (2003).

[72] Eccleston, R. S. et al. *Phys. Rev. Lett.* **81**, 1702 (1998).

[73] Matsuda, M., Katsumata, K., Eccleston, R. S., Brehmer, S., and Mikeska, H. J. *J. Appl. Phys.* **87**, 6271 (2000).

[74] Schmidt, K. P., Knetter, C., and Uhrig, G. S. *Europhys. Lett.* **56**, 877 (2001).

[75] Nunner, T. S. et al. *Phys. Rev. B* **66**, 180404 (2002).

[76] Gößling, A. et al. *Phys. Rev. B* **67**, 052403 (2003).

[77] Schmidt, K. P., Knetter, C., Grüninger, M., and Uhrig, G. S. *Phys. Rev. Lett.* **90**, 167201 (2003).

[78] Notbohm, S. et al. *Phys. Rev. Lett.* **98**, 027403 (2007).

[79] Takahashi, M. *J. Phys. C: Sol. State Phys.* **10**, 1289 (1977).

[80] MacDonald, A. H., Girvin, S. M., and Yoshioka, D. *Phys. Rev. B* **41**, 2565 (1990).

[81] Roger, M. and Delrieu, J. M. *Phys. Rev. B* **39**, 2299 (1989).

[82] Schmidt, H. J. and Kuramotoa, Y. *Physica B* **163**, 443 (1990).

[83] Müller, M., Vekua, T., and Mikeska, H.-J. *Phys. Rev. B* **66**, 134423 (2002).

[84] Shelton, D. G., Nersesyan, A. A., and Tsvelik, A. M. *Phys. Rev. B* **53**, 8521 (1996).

[85] Läuchli, A., Schmid, G., and Troyer, M. *Phys. Rev. B* **67**, 100409(R) (2003).

[86] Schmidt, K. P., Monien, H., and Uhrig, G. S. *Phys. Rev. B* **67**, 184413 (2003).

[87] Oitmaa, J., Singh, R. R. P., and Weihong, Z. *Phys. Rev. B* **54**, 1009 (1996).

[88] Uhrig, G. S. and Schulz, H. J. *Phys. Rev. B* **54**, R9624 (1996).

[89] Uhrig, G. S. and Schulz, H. J. *Phys. Rev. B* **58**, 2900 (1998).

[90] Sushkov, O. P. and Kotov, V. N. *Phys. Rev. Lett.* **81**, 1941 (1998).

[91] Damle, K. and Sachdev, S. *Phys. Rev. B* **57**, 8307 (1998).

[92] Kotov, V. N., Sushkov, O. P., and Eder, R. *Phys. Rev. B* **59**, 6266 (1999).

[93] Trebst, S., Monien, H., Hamer, C. J., Weihong, Z., and Singh, R. R. P. *Phys. Rev. Lett.* **85**, 4373 (2000).

[94] Knetter, C., Schmidt, K. P., Grüninger, M., and Uhrig, G. S. *Phys. Rev. Lett.* **87**, 167204 (2001).

[95] Weihong, Z., Hamer, C. J., Singh, R. R. P., Trebst, S., and Monien, H. *Phys. Rev. B* **63**, 144410 (2001).

[96] Schmidt, K. P. and Uhrig, G. S. *Mod. Phys. Lett. B* **19**, 1179 (2005).

[97] Oitmaa, J., Hamer, C. J., and Weihong, Z. *Phys. Rev. B* **60**, 16364 (1999).

[98] Läuchli, A. private communication, (2010).

[99] Jurecka, C. and Brenig, W. *Phys. Rev. B* **63**, 94409 (2001).

[100] Brunner, M., Capponi, S., Assaad, F. F., and Muramatsu, A. *Phys. Rev. B* **63**, 180511 (2001).

[101] Troyer, M., Tsunetsugu, H., and Rice, T. M. *Phys. Rev. B* **53**, 251 (1996).

[102] Sushkov, O. P. *Phys. Rev. B* **60**, 3289 (1999).

Danksagung

An dieser Stelle möchte ich all denen danken, die zum Gelingen dieser Arbeit beigetragen haben.

Besonders danke ich Prof. Dr. Götz S. Uhrig für das interessante Thema und die hervorragende Betreuung. Seine weitreichenden Fachkenntnisse und sein großer Erfahrungsschatz waren mir eine wichtige Hilfe.

Prof. Dr. Joachim Stolze danke ich dafür, dass er die Zweitkorrektur übernommen hat, als auch für seine Ratschläge und seine Unterstützung.

Dr. Kai. P. Schmidt bin ich für die zahlreichen fruchtbaren Diskussionen besonders dankbar, aus denen stets neue Anregungen und Fortschritte hervorgingen. Dr. Carsten Raas danke ich für die hervorragende Unterstützung bei technischen Problemen und Fragen.

Desweiteren danke ich Tim Fischer für die produktive Zusammenarbeit, der immer ein offenes Ohr für mich hatte. Ebenso danke ich Simone Hamerla für die wertvollen Gespräche und Ideen. Nils Drescher danke ich für die ergiebigen Diskussionen und hilfreichen Vorschläge.

Ich danke Dr. Stefano Pasini für seine Hilfe bei allgemeinen Fragen und die angenehme Atmosphäre im Büro. Jörn Krones danke ich ebenfalls für die angenehme Büroatmosphäre sowie für die vielen interessanten Gespräche, die weit über den Themenbereich der Physik hinausgingen.

Bei Isabelle Exius bedanke ich mich für ihre Unterstützung und Hilfsbereitschaft. Darüber hinaus danke ich allen Mitarbeitern der Lehrstühle T1 und T2 für ihre Kollegialität und die gemeinsamen Aktivitäten.

Dr. Alexander Reischl und Dr. Andreas Läuchli danke ich dafür, dass sie mir ihre Daten zur Verfügung gestellt haben.

Meinen Eltern bin ich dankbar dafür, dass sie mir mein Studium ermöglicht haben und mich stets nach allen Kräften unterstützt haben. Meinem Großvater gilt ein ganz besonderer Dank dafür, dass er mir immer beigestanden hat und einen entscheidenden Beitrag dazu geleistet hat, meine Kritikfähigkeit und meine wissenschaftliche Neugier zu fördern. Meinen Schwiegereltern danke ich für ihr

Interesse an meiner Arbeit und ihre Unterstützung, die von Herzen kam.

Ich danke meiner Frau Stefie dafür, dass sie Höhen und Tiefen mit mir duchgestanden hat und mir liebevoll geholfen hat, wo sie nur konnte. Bei meiner Tochter Sophia bedanke ich mich, weil sie es stets vermag, mich mit ihrem Lächeln alle meine Sorgen vergessen zu lassen.